Design, Modeling, and Optimization of Hybrid LiFi-WiFi Networks for High-Performance Indoor Wireless Communication

Submitted By

Saswati Paramita

under supervision of

Prof. Vivek Ashok Bohara

Prof. Anand Srivastava

INDRAPRASTHA INSTITUTE *of*
INFORMATION TECHNOLOGY DELHI

Department of Electronics and Communication Engineering
Indraprastha Institute of Information Technology - Delhi
New Delhi-110020 (India)

June 2026

Design, Modeling, and Optimization of Hybrid LiFi-WiFi Networks for High-Performance Indoor Wireless Communication

Dissertation submitted to

Indraprastha Insititute of Information Technology-Delhi

in partial fulfillment of the requirements for the award of the degree of

Doctor of Philosophy

Submitted By

Saswati Paramita

Roll No: PhD20101

under supervision of

Prof. Vivek Ashok Bohara

Prof. Anand Srivastava

INDRAPRASTHA INSTITUTE *of*
INFORMATION TECHNOLOGY DELHI

Department of Electronics and Communication Engineering

Indraprastha Institute of Information Technology - Delhi

New Delhi-110020 (India)

June 2026

To Lord Shree Jagannath ...

Indraprastha Institute of Information Technology-Delhi

Okhla Industrial Estate, Phase III

New Delhi-110020, India

June-2026

Certificate

This is to certify that the thesis titled **Design, Modeling, and Optimization of Hybrid LiFi-WiFi Networks for High-Performance Indoor Wireless Communication** being submitted by **Saswati Paramita** to the Indraprastha Institute of Information Technology-Delhi, for the award of the degree of **Doctor of Philosophy**, is an original research work carried out by her under our supervision. In our opinion, the thesis has reached the standards fulfilling the requirements of the regulations relating to the degree. The results contained in this thesis have not been submitted in part or full to any other university or institute for the award of any degree/diploma.

Prof. Vivek Ashok Bohara
Professor
Dept. of Electronics & Communication Eng.
IIIT Delhi, 110020

Prof. Anand Srivastava
Professor
Dept. of Electronics & Communication Eng.
IIIT Delhi, 110020

Place: New Delhi

Date: June 2026

Indraprastha Institute of Information Technology-Delhi

Okhla Industrial Estate, Phase III

New Delhi-110020, India

June-2026

Declaration

This is to be certified that the dissertation entitled **Design, Modeling, and Optimization of Hybrid LiFi-WiFi Networks for High-Performance Indoor Wireless Communication** being submitted by **Saswati Paramita** to the **Indraprastha Institute of Information Technology-Delhi**, for the award of degree of **Doctor of Philosophy**, is a bonafide work carried out by me. This research work has been carried out under the supervision of **Prof. Vivek Ashok Bohara and Prof. Anand Srivastava**.

The study pertains to this dissertation has not been submitted in part or in full, to any other University or Institution for the award of any other degree.

Saswati Paramita

PhD20101

Ph.D. Scholar

IIIT-Delhi, India

Indraprastha Institute of Information Technology-Delhi

Okhla Industrial Estate, Phase III

New Delhi-110020, India

June-2026

Declaration Regarding the Use of AI Tools

I hereby declare that I am fully responsible for the entire content of this thesis. Any use of online tools, including Artificial Intelligence (AI)-based tools, was limited to assistance in language improvement, formatting, proofreading, or enhancing the presentation of the material. The research ideas, methodology, analysis, results, interpretations, and conclusions presented in this thesis are my own work and have been critically reviewed and verified by me.

I acknowledge that I bear full responsibility for the accuracy, originality, and integrity of the content of this thesis, including any sections where AI-assisted tools may have been utilized. I further accept full accountability for ensuring compliance with academic and publication ethics and for any ethical violations arising from the use of such tools.

Saswati Paramita

PhD20101

Ph.D. Scholar

IIIT-Delhi, India

Acknowledgments

I would like to express my heartfelt gratitude to my supervisors, **Prof. Vivek Ashok Bohara and Prof. Anand Srivastava**, for their continuous guidance, encouragement, and support throughout my Ph.D. journey. Their active monitoring, timely feedback, and constructive suggestions greatly helped me refine my work and grow as a researcher. They provided an excellent platform and research ecosystem that allowed me to explore, learn, and showcase my abilities. I feel truly fortunate to have had such inspiring mentors for my doctoral research.

I am also grateful to **Prof. Anand Srivastava and Prof. Vivek Ashok Bohara** for providing me the opportunity to contribute to a MeitY-funded project, which not only enriched my research experience but also supported my Ph.D. through a stipend.

I am grateful to **Prof. Peter Chong** for offering me the opportunity to pursue an research internship at Auckland University of Technology (AUT), New Zealand, which was an enriching experience that greatly enhanced my research. I also sincerely thank my monitoring committee members, **Dr. Arani Bhattacharya and Dr. Rinku Shah**, for their insightful feedback, cooperation, and encouragement. Their guidance and support throughout my Ph.D. journey have been invaluable in improving the quality of my work.

I am sincerely thankful to **Dr. Arani Bhattacharya** for his continuous guidance and collaboration as both a member of my doctoral committee and as a co-author on several of my research publications. His constructive feedback, critical insights, and constant encouragement have been instrumental in shaping my research work and strengthening my research skills. I am deeply grateful for his mentorship, support, and the openness with which he engaged in all aspects of my Ph.D. journey.

I would also like to express my gratitude to my colleagues **Shubham Chaudhary, and Vijay Singh** from the WISE Lab for their continuous support and cooperation. Their assistance in coding development, technical discussions, and collaborative spirit contributed significantly to the progress of my research work.

I am grateful to the **Indraprastha Institute of Information Technology Delhi (IIIT-Delhi)** for providing an excellent research environment, world-class infrastructure, and research-oriented coursework that greatly contributed to my academic and professional growth. I would also like to thank my colleagues from the **Wirocomm Research Group** and the **CoE Li-Fi Lab** at IIIT-Delhi for their collaboration and support. I sincerely acknowledge **Dr. Rizwana Ahmad, Dr. Akshita Gupta, Rahul, Dr. Priyanka Singh, Dr. Saumya Chaturvedi, Dr. Neetu R. R., Dr. Rana Kumar Jana, Dr. Mansi Peer, Dr. Anand Singh, Dr. Parag Agarwal, Dr. Mohd. Hamza Naim Shaikh, Dr. Dil Nashin Anwar, and Dr. Gurinder Singh** for their direct or indirect support as wonderful labmates. My sincere thanks also go to Sonia, Sapna, Hanshita, Anant, Gaurav, Anshu, Jyoti, Najia and Ankit for their cooperation, teamwork and the friendly environment they helped create in our research group and the IIIT-Delhi campus. I would also like to thank the interns **Rajorshi, Manan, and Abhinav** for their valuable assistance in experiments and implementation to my research work.

My gratitude also extends to the **library, IT, academics, examination, stores, technical, student-affairs, and administrative staff of IIIT-Delhi, especially the Ph.D. and IRD administration**, for their timely assistance and efficient handling of academic and administrative matters. I would also like to thank the **Facilities and Management Support (FMS) team, housekeeping staff, and security personnel** of IIIT-Delhi for their constant assistance, which made my stay on campus comfortable and supported me in completing my Ph.D. journey.

I am deeply thankful to my family for their unconditional love, blessings, and constant encouragement, which gave me immense strength and resilience throughout my Ph.D. journey. Finally, I bow in gratitude to Lord Shree Jagannath, whose divine grace has always guided and supported me not only during my Ph.D. but throughout my life.

Saswati Paramita

PhD20101

ABSTRACT

The exponential growth of bandwidth-intensive applications such as ultra-high-definition (UHD) video streaming, cloud computing, augmented and virtual reality (AR/VR), and the Internet of Things (IoT) has pushed existing wireless communication technologies to their limits. Conventional RF-based networks, such as Wi-Fi and LTE, are increasingly strained by spectrum scarcity and escalating user demands. This has spurred interest in alternative or complementary communication paradigms capable of delivering higher data rates, lower latency, improved security, and better energy efficiency.

Light Fidelity (Li-Fi), operating within the visible light spectrum, has emerged as a promising candidate for next-generation indoor wireless systems. Leveraging existing lighting infrastructure, Li-Fi offers vast unlicensed bandwidth, inherent security through confined coverage, and high potential data rates. However, despite these advantages, Li-Fi faces significant deployment challenges—most notably limited coverage, susceptibility to line-of-sight (LoS) blockages, sensitivity to device orientation, and degraded performance in high mobility scenarios. Furthermore, existing MAC-layer protocols in Li-Fi often borrow from Wi-Fi standards, such as CSMA/CA, which are not fully optimized for the unique characteristics of visible light communication (VLC) networks.

The initial stage of this research addressed MAC-layer inefficiencies in heterogeneous Li-Fi environments. A hybrid CSMA/CA–HCCA uplink MAC protocol was developed to

dynamically switch between contention-based and contention-free modes depending on device types and network load, significantly improving throughput, delay, and collision probability in diverse traffic scenarios [1]. While this approach enhanced medium access efficiency, it did not fully address performance degradation caused by user mobility and dynamic channel conditions.

To tackle mobility-induced challenges, an Orientation-Aware Multi-AP Li-Fi Network (OAM-LiFiNet) was proposed [2]. This framework leveraged real-time SINR measurements and channel metrics to dynamically adjust device orientation, thereby mitigating interference and improving throughput under user movement. Although effective, Li-Fi's dependence on LoS links meant that the system remained vulnerable to blockage events caused by static obstacles or transient movement within the environment.

Recognizing the importance of blockage modeling, the research introduced FixOM and SAM [3], two novel approaches for quantifying the impact of obstacles in Li-Fi environments. FixOM modeled stationary obstructions using geometric analysis, while SAM incorporated both complete and partial shadowing effects for a more realistic performance representation. These models provided valuable insights for Li-Fi deployment planning but also highlighted that blockage mitigation within a pure Li-Fi framework could not entirely eliminate service interruptions.

This realization motivated the transition toward hybrid Li-Fi/Wi-Fi networks (HLWNs), which combine Li-Fi's high-speed links with Wi-Fi's broader coverage and robustness. Prototype testbeds were developed [4, 5] to evaluate hybrid systems in realistic indoor scenarios, demonstrating superior throughput, handover performance, and service continuity compared to standalone technologies.

While hybrid networks improved coverage and throughput, modern MU-MIMO Wi-Fi still suffered from one significant drawback—**the high overhead of channel state information (CSI) feedback**. This feedback is essential for spatial multiplexing but consumes substantial wireless resources, reducing spectral efficiency and limiting achievable throughput, especially

in dense multi-user scenarios. In this thesis, this disadvantage is addressed by **utilizing Li-Fi links to carry CSI feedback** through the proposed WiLiConnect and WiLiConnect-Opt systems [6, 7]. By offloading CSI transmission to Li-Fi access points, Wi-Fi capacity is freed for user data, drastically reducing overhead and substantially improving sum-rate performance in hybrid deployments.

Building on this foundation, the research advanced to link aggregation and mobility-aware resource allocation strategies for HLWNs. The final stage of the research focused on advanced link aggregation algorithms—LA-SINR, LA-EQoS, and FLADA [8, 9]—that maximized combined Li-Fi/Wi-Fi throughput while meeting QoS and fairness requirements. These were complemented by a mobility-aware handover optimization strategy [10] that used a two-stage approach: offline linear programming for static users and a search-space pruning mechanism with re-optimization for mobile users near AP borders. Analytical modeling of outage probabilities [11] in LA-enabled HLWNs further validated their superior robustness compared to standalone networks.

Through these interconnected contributions, this thesis presents a holistic, multi-layered framework for high-capacity, mobility-friendly indoor networks. By starting from MAC-layer improvements in standalone Li-Fi, addressing mobility and blockage, overcoming Wi-Fi's CSI feedback bottleneck via Li-Fi, integrating hybrid Li-Fi/WiFi architectures, and culminating in advanced link aggregation and handover optimization, the research provides a comprehensive roadmap for deploying next-generation indoor wireless systems that meet the evolving demands of smart homes, offices, and industrial environments.

Table of contents

List of figures

List of tables

Nomenclature

Abbreviations

ACO-OFDM	asymmetrically clipped OFDM
AP	access point
AR/VR	augmented and virtual reality
BER	bit error rate
BW	bandwidth
CC	central controller
CCDF	complementary cumulative distribution function
CDF	cummulative distribution function
CSI	channel state information
CSMA/CA	carrier sense multiple access with collision avoidance
DCO-OFDM	DC-biased optical OFDM
DMD	digital mirror device
FixOM	Fixed Obstacle Modeling

FLADA	Flow-based Algorithm for Data Allocation
FoV	field of view
HCCA	hybrid-coordination-function-controlled-channel access
HC	hybrid coordinator
HHO	horizontal handover
HLWN	hybrid LiFi-Wi-Fi network
ILP	integer linear programming
IM/DD	intensity modulation with direct detection
IoT	Internet of Things
IR	infrared
LA-EQoS	LA for enhancement of QoS
LA-HLWN	LA-enabled HLWNs
LA-SINR	LA based on SINR
LA	link aggregatione
LED	light emitting diode
LED	light-emitting diode
Li-Fi	light fidelity
LoS	line-of-sight
LP	linear programming
LTE	long term evolution

MAC	medium access control
MAPS-GP	Mobility-Aware Probabilistic Selection-GP
MAPS-LP	Mobility-Aware Probabilistic Selection-LP
MAPS	Mobility-Aware Probabilistic Selection
MCS	modulation and coding schemes
MU-MIMO	multi-user-multiple-input-multiple-output
NAV	Network Allocation Vector
NDP	null data packet
NLoS	non-line-of-sight
OAM-LiFiNet	Orientation-Aware Multi-AP Li-Fi Network
OFDMA	orthogonal frequency division multiple access
OFDM	orthogonal frequency division multiplexing
OIRS	optical intelligent reflecting surfaces
OOK	on-off-keying
OWC	optical wireless communication
PAM	pulse amplitude modulation
PCD	personal computing device
PCF	Point Coordination Function
PD	photodiode
PHY	physical

PSD	power spectral density
QoE	Quality of Experience
QoS	Quality-of-Service
RF	radio frequency
RL	reinforcement learning
RSS	received signal strength
RTS/CTS	Request-to-Send/Clear-to-Send
RWP	random waypoint
SAM	Shadow-Aware Blockage Modeling
SINR	Signal-to-Interference-plus-Noise-Ratio
SNR	signal-to-noise-ratio
TSPEC	traffic specification
TXOP	transmission opportunities
UHD	ultra-high-definition
VHO	vertical handover
VLC	visible light communication
VL	visible light
Wi-Fi	wireless fidelity
WiLiConnect-Opt	WiFi-LiFi Connectivity with CSI sharing-Optimization
WiLiConnect	WiFi-LiFi Connectivity with CSI sharing

Chapter 1

Introduction

This chapter lays the foundation for the research presented in this dissertation. It begins with a discussion of the background and motivation in Section 1.1, followed by Section 1.2, which outlines the limitations of conventional radio frequency (RF) based wireless networks. Section 1.3 introduces light fidelity (Li-Fi) as a complementary technology, while Section 1.4 highlights the key challenges associated with both standalone Li-Fi and hybrid Li-Fi/Wi-Fi networks. Section 1.5 presents the research objectives of this thesis, and Section 1.6 summarizes the major contributions together with the author's relevant publications. The organization of the thesis is described in Section 1.7. Finally, Section 1.8 provides a brief summary to conclude this chapter and transition into the literature review.

1.1 Background and Motivation

The rapid evolution of digital technologies has transformed the way people work, communicate, and consume information. Emerging applications such as ultra-high-definition (UHD) video streaming, cloud-based services, augmented and virtual reality (AR/VR) , and the Internet of Things Internet of Things (IoT) are placing unprecedented demands on wireless communication systems. These applications require very high data rates, ultra-low latency, seamless mobility, and reliable connectivity in order to ensure a satisfactory user experience.

Traditional RF-based systems, including wireless fidelity (Wi-Fi) and cellular networks, have been the primary enablers of wireless connectivity for decades. However, these systems are increasingly strained by spectrum scarcity, interference, and escalating user demands. With indoor environments accounting for the majority of global wireless traffic, addressing these challenges has become a critical priority for the development of next-generation communication networks.

Li-Fi, which operates within the visible light spectrum, has emerged as a promising complementary technology to RF-based systems. By exploiting existing lighting infrastructure, Li-Fi offers several attractive features including abundant unlicensed bandwidth, improved physical-layer security due to confined coverage, and the potential to deliver multi-gigabit data rates. These capabilities position Li-Fi as a strong candidate for supporting the increasing demands of modern indoor wireless networks.

The motivation for this research arises from the recognition that while Li-Fi presents significant opportunities, it also faces critical deployment challenges related to mobility, orientation sensitivity, and blockage effects. These limitations restrict its feasibility as a standalone technology, motivating the need for hybrid Li-Fi/Wi-Fi architectures. Such systems have the potential to combine the strengths of both technologies, high-speed capacity from Li-Fi and wide-area coverage with robustness from Wi-Fi, to meet the requirements of future high-performance indoor wireless communication.

1.2 Limitations of Conventional RF Networks

Despite the widespread adoption of RF-based wireless technologies such as Wi-Fi and long term evolution (LTE) , their ability to sustain next-generation high-capacity applications remains constrained by several fundamental limitations.

Spectrum Scarcity: The RF spectrum is heavily regulated and increasingly congested, especially in the sub-6 GHz bands where most consumer wireless systems operate. This

scarcity limits available bandwidth, restricting achievable data rates and network scalability [16].

Interference and Reliability: RF signals are vulnerable to multipath fading, co-channel interference, and cross-technology interference from neighboring wireless systems. These effects degrade signal quality, increase retransmissions, and reduce effective throughput, particularly in dense deployments [17].

Energy Efficiency: The growing demand for wireless connectivity translates into higher power consumption across access points and user devices. RF-based networks often struggle with balancing throughput and energy efficiency, which becomes critical in IoT and mobile edge computing scenarios [18].

Security Concerns: Since RF signals propagate beyond physical boundaries such as walls and floors, they are inherently more vulnerable to eavesdropping and jamming. Ensuring confidentiality and resilience in RF-based systems typically requires additional cryptographic overhead, further impacting performance [19].

These challenges collectively emphasize the need for alternative or complementary wireless solutions that can provide higher data rates, improved energy efficiency, inherent security, and robustness in dense indoor environments.

1.3 Li-Fi as a Complementary Technology

The exponential rise in data demand, driven by bandwidth-intensive applications such as UHD video streaming, AR/VR, and cloud-based services, has highlighted the limitations of conventional RF-based networks. In this context, Li-Fi, a subset of visible light communication (VLC) , has emerged as a promising complementary wireless technology as depicted in Fig. 1.1. Operating in the unlicensed visible light spectrum, Li-Fi offers an unprecedented amount of available bandwidth compared to the highly congested RF spectrum, thereby enabling multi-gigabit data rates [20].

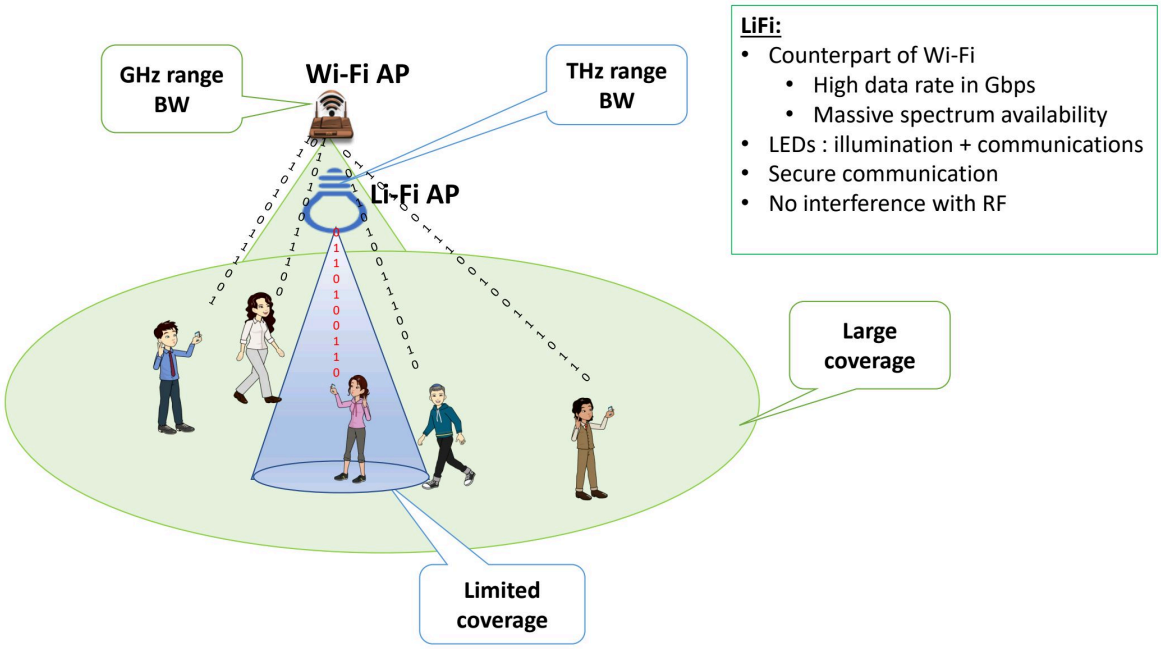

Figure 1.1: Li-Fi vs. Wi-Fi Technology

Beyond capacity enhancement, Li-Fi provides intrinsic security benefits due to the confined nature of light propagation. Since visible light cannot penetrate opaque walls, the spatial confinement of signals significantly reduces the risk of eavesdropping and unauthorized access, which are more prevalent in RF-based networks [21]. This property makes Li-Fi particularly attractive for security-sensitive environments such as financial institutions, healthcare facilities, and defense applications.

Moreover, Li-Fi can leverage existing indoor lighting infrastructure, making it cost-effective to deploy. With the advent of energy-efficient light-emitting diodes (LEDs) , lighting systems can be seamlessly integrated with high-speed data transmission capabilities, thus promoting sustainable and green communication systems. While Li-Fi is unlikely to replace RF technologies such as Wi-Fi entirely, its complementary nature lies in its ability to offload data traffic from congested RF bands, deliver ultra-high-speed links in short-range indoor scenarios, and ensure enhanced security and energy efficiency. Consequently, hybrid LiFi–WiFi architectures are gaining momentum as enablers of next-generation indoor wireless networks, particularly in the context of 6G and beyond [21].

1.4 Challenges in Li-Fi and Hybrid LiFi–WiFi Networks

Despite its significant advantages, Li-Fi faces a number of critical challenges that hinder its widespread adoption as a standalone wireless technology. The foremost issue is its strong dependence on line-of-sight (LoS) communication. Since visible light cannot penetrate opaque obstacles, even minor blockages can cause a complete signal outage, severely degrading user experience [22].

Another important limitation is the sensitivity of Li-Fi performance to device orientation. The optical receiver embedded in mobile devices must maintain a favorable angle relative to the transmitting access point (AP) . Variations in user posture or device handling can result in dramatic fluctuations in received signal strength and throughput [23].

Mobility support also remains a significant challenge. Unlike RF-based systems, where omnidirectional antennas provide broader coverage, Li-Fi's highly directional links make it susceptible to frequent link disruptions during user movement. This not only increases handover frequency but can also cause service interruptions in dynamic environments [24].

Hybrid LiFi–WiFi architectures have been proposed to overcome these limitations, combining the high-speed and secure transmission of Li-Fi with the reliability and extended coverage of Wi-Fi. However, integrating these heterogeneous systems introduces new technical hurdles. Efficient link aggregation, seamless handover management, and resource allocation strategies are necessary to ensure service continuity and maximize performance [25]. Additionally, ensuring fairness among users with diverse channel conditions in hybrid deployments adds another layer of complexity.

Overall, while Li-Fi holds promise as a complementary indoor wireless solution, addressing these challenges is essential to unlock its full potential in next-generation wireless networks.

1.5 Research Objectives

The overarching goal of this dissertation is to design, model, and optimize hybrid LiFi–WiFi networks for high-performance indoor wireless communication. In particular, the research aims to address the inherent limitations of standalone Li-Fi systems, while simultaneously leveraging the complementary strengths of both Li-Fi and Wi-Fi to meet the increasing demands of next-generation applications.

To achieve this goal, the following specific research objectives have been defined:

1. **Enhancement of MAC-Layer Efficiency in Li-Fi Networks:** Develop hybrid and adaptive medium access control (MAC) mechanisms tailored to Li-Fi's unique characteristics, improving throughput, delay, and collision probability compared to conventional RF-inspired protocols.

2. **Mobility and Orientation-Aware Frameworks:** Propose solutions that mitigate the performance degradation caused by user mobility, device orientation, and dynamic channel conditions in multi-AP Li-Fi networks.

3. **Blockage Modeling and Performance Evaluation:** Introduce analytical and simulation-based models to quantify the impact of static and dynamic obstacles, enabling realistic evaluation of Li-Fi system performance under shadowing and blockage events.

4. **Design of Hybrid LiFi–WiFi Architectures:** Develop and experimentally validate hybrid frameworks that integrate Li-Fi and Wi-Fi to ensure seamless connectivity, improved handover performance, and superior user experience in dynamic indoor environments.

5. **CSI Feedback Offloading for MU-MIMO Wi-Fi:** Exploit Li-Fi links for carrying channel state information (CSI) feedback in Wi-Fi networks, thereby reducing overhead, enhancing spectral efficiency, and improving system throughput in dense deployments.

6. **Mobility-Aware Resource Allocation Strategies:** Formulate dynamic rate allocation mechanisms that intelligently distribute traffic across Li-Fi and Wi-Fi links, considering user movement, access point load, and backhaul constraints.

7. **Advanced Link Aggregation and Handover Optimization:** Develop and analyze novel link aggregation schemes and mobility-aware handover strategies that maximize combined throughput, ensure fairness, and minimize outage probability in hybrid LiFi–WiFi networks.

By fulfilling these objectives, this thesis provides a holistic framework that addresses challenges across multiple layers of the communication stack. The outcomes contribute to the realization of reliable, high-capacity, and mobility-resilient indoor wireless systems for smart homes, offices, and industrial environments.

1.6 Major Contributions

This dissertation makes several key contributions toward the design, modeling, and optimization of hybrid LiFi–WiFi networks. The contributions span multiple layers of the communication stack, from MAC-layer protocol design to system-level integration and optimization. The major contributions are summarized as follows:

1. **Hybrid MAC Protocol for Heterogeneous Li-Fi Environments:** Developed a hybrid uplink MAC protocol using carrier sense multiple access with collision avoidance (CSMA/CA) and hybrid-coordination-function-controlled-channel access (HCCA) mechanisms that dynamically adapts between contention-based and contention-free access. This improved medium utilization efficiency, reduced collisions, and enhanced delay performance under heterogeneous traffic loads [1].

    - **S. Paramita**, A. Bhattacharya, A. Srivastava, V. A. Bohara, " Hybrid CSMA/CA and HCCA uplink medium access control protocol for VLC based heterogeneous

users", Computer Communications, Volume 225, 2024, Pages 54-64, ISSN 0140-3664, https://doi.org/10.1016/j.comcom.2024.06.017.

2. **Blockage and Shadowing Modeling:** Introduced two novel models Fixed Obstacle Modeling (FixOM) for stationary obstacles and Shadow-Aware Blockage Modeling (SAM) for shadowing effects (both complete and partial). These models provide accurate performance prediction tools for Li-Fi deployment planning [3].

    - **S. Paramita**, A. Rawat, M. Daderwal and V. A. Bohara, "FixOM-SAM: Blockage Analysis in Indoor Li-Fi Networks," in IEEE Open Journal of the Communications Society, vol. 6, pp. 5746-5758, 2025, doi: 10.1109/OJCOMS.2025.3585614.

3. **Orientation-Aware Multi-AP Li-Fi Network (OAM-LiFiNet) :** Proposed a mobility and orientation-aware Li-Fi framework that leverages Signal-to-Interference-plus-Noise-Ratio (SINR) feedback and real-time channel state information to mitigate orientation sensitivity and improve throughput in dynamic indoor environments [2].

    - **S. Paramita** ,etal. “OAM-LiFiNet: Orientation Aware Multi-AP Li-Fi Network with user mobility”,2025 IEEE Future Networks World Forum (FNWF), Bangalore, India, 2025, pp. 1-6, doi: 10.1109/FNWF66845.2025.11317169.
    - **Saswati Paramita**, A. Rawat and V. A. Bohara, "Adaptive Link Selection and Handover in Orientation-Aware Hybrid Li-Fi/Wi-Fi Networks," in IEEE Networking Letters, doi: 10.1109/LNET.2026.3670370.

4. **Hybrid LiFi–WiFi Network Prototyping:** Designed and implemented testbeds for hybrid LiFi–WiFi systems, demonstrating their superior performance in terms of throughput, service continuity, and seamless handover compared to standalone networks [4, 5].

    - **S. Paramita** et al., "A Proof-of-Concept Demonstration of Hybrid Li-Fi/Wi-Fi Network on a Prototype Testbed," 2023 IEEE International Conference on Ad-

vanced Networks and Telecommunications Systems (ANTS), Jaipur, India, 2023, pp. 509-514, doi: 10.1109/ANTS59832.2023.10468742.

- **S. Paramita** et al., "Demo of Hybrid LiFi/WiFi Network for an Indoor Environment," 2023 15th International Conference on COMmunication Systems & NETworkS (COMSNETS), Bangalore, India, 2023, pp. 213-215, doi: 10.1109/COMSNETS56262.2023.10041414.

5. **CSI Feedback Offloading via Li-Fi:** Proposed the WiLiConnect (WiFi-LiFi Connectivity with CSI sharing) and WiLiConnect-Opt (WiFi-LiFi Connectivity with CSI sharing-Optimization) frameworks, which exploit Li-Fi links to transmit Wi-Fi CSI feedback. This significantly reduces CSI overhead, increases spectral efficiency, and enhances MU-MIMO (multi-user-multiple-input-multiple-output) Wi-Fi capacity [6, 7].

   - **S. Paramita**, A. Bhattacharya, V. A. Bohara and A. Srivastava, "WiLiConnect: A Novel CSI Sharing Technique in Hybrid WiFi/LiFi Networks," 2024 IEEE 99th Vehicular Technology Conference (VTC2024-Spring), Singapore, Singapore, 2024, pp. 1-5, doi: 10.1109/VTC2024-Spring62846.2024.10683067.
   - **S. Paramita**, A. Bhattacharya, V. A. Bohara, A. Srivastava, “Optimizing CSI Overhead in Hybrid WiFi/LiFi Networks Using LiFi-Assisted Feedback", IEEE Transactions on Wireless Communications (TWC). (Submitted)
   - "Utilizing LiFi for sending channel feedback in a hybrid Wi Fi/ Li Fi network" [Inventors: **Saswati Paramita**, Arani Bhattacharya, Vivek Ashok Bohara, Anand Srivastava] (September 11, 2023), application no.202311061031, Indian Patent.

6. **Advanced Link Aggregation Algorithms:** Designed and evaluated novel link aggregation (LA) strategies (LA-SINR, LA-EQoS, and FLADA) that maximize hybrid throughput while satisfying quality-of-service (QoS) and fairness requirements [8, 9, 11].

- **S. Paramita**, A. Bhattacharya, R. Ahmad, V. A. Bohara and A. Srivastava, “Flow-Based Rate Maximization for Link Aggregation Enabled Hybrid LiFi-WiFi Network," in IEEE Transactions on Vehicular Technology, vol. 74, no. 2, pp. 3269-3282, Feb. 2025, doi: 10.1109/TVT.2024.3477310.
- N. M. Karoti, S. Paramita, R. Ahmad, V. A. Bohara and A. Srivastava, “Improving the performance of Heterogeneous LiFi-WiFi network using a novel Link Aggregation Framework," 2022 IEEE Wireless Communications and Networking Conference (WCNC), Austin, TX, USA, 2022, pp. 2322-2327, doi: 10.1109/WCNC51071.2022.9771553.

7. **Mobility-Aware Handover Optimization:** Proposed a two-stage handover optimization framework that integrates offline optimization for static users and online search-space pruning with re-optimization for mobile users near AP borders, reducing handover delay and service interruptions [10].

    - **S. Paramita**, R. Mondal, A. Bhattacharya, V. A. Bohara and A. Srivastava, “MARM-HyLiWi: Mobility-Aware Rate Maximization in Link Aggregation Enabled Hybrid Li-Fi/Wi-Fi Networks," 2025 17th International Conference on COMmunication Systems and NETworks (COMSNETS), Bengaluru, India, 2025, pp. 891-894, doi: 10.1109/COMSNETS63942.2025.10885587.
    - **S. Paramita**, R.Mondal, A. Bhattacharya, V. A. Bohara, A. Srivastava, "Optimizing Handover and Throughput in Heterogeneous LiFi-WiFi Network with User Mobility", IEEE Transactions on Mobile Computing. (Submitted)

Collectively, these contributions form a holistic road-map for the deployment of next-generation indoor wireless systems, ensuring both high-capacity and mobility-resilient connectivity.

1.7 Novelty and Key Contributions Compared to Existing Work

To clearly distinguish this work from prior literature, the key novelties are explicitly highlighted below in comparison with existing approaches. This thesis advances the state-of-the-art in LiFi and hybrid LiFi–WiFi networks through several novel contributions that address key limitations in existing literature. While prior works have explored LiFi systems, hybrid networking, and resource allocation independently [25–27], they often lack a unified cross-layer approach. This thesis provides a comprehensive framework spanning MAC design, channel modeling, mobility management, and system-level optimization.

At the MAC layer, existing LiFi systems largely adopt RF-inspired protocols such as CSMA/CA, which are not well suited for optical wireless communication due to directional transmission and unique interference characteristics [23, 28]. This thesis introduces a hybrid CSMA/CA–HCCA protocol [1], which dynamically switches between contention-based and contention-free access. Unlike static schemes, the proposed approach adapts to traffic heterogeneity, significantly improving throughput, delay, and collision probability.

In terms of blockage modeling, existing studies typically rely on simplified stochastic or geometric models that fail to capture realistic indoor environments [29, 30]. This thesis proposes two novel models, FixOM and SAM [3], that incorporate both static obstacles and dynamic shadowing effects. These models provide a more accurate representation of LiFi channel behavior and enable improved system design and deployment planning.

Mobility and device orientation have been identified as critical challenges in LiFi systems [31, 32], yet most existing works treat them in isolation or with limited adaptability. This thesis introduces the Orientation-Aware Multi-AP LiFi Network (OAM-LiFiNet) [2], which leverages real-time SINR feedback and adaptive link selection to mitigate performance degradation due to mobility and orientation variations.

While prior work on hybrid LiFi–WiFi systems has primarily focused on theoretical analysis and simulations [14, 33], this thesis distinguishes itself by implementing a real-world prototype testbed [4, 5]. The experimental results validate significant improvements in throughput, seamless handover, and service continuity compared to standalone systems.

A key novel contribution of this thesis is addressing the CSI feedback overhead problem in MU-MIMO WiFi systems. Conventional approaches rely entirely on RF links, resulting in reduced spectral efficiency [34, 35]. The proposed WiLiConnect and WiLiConnect-Opt frameworks [6, 7] offload CSI feedback transmission to LiFi links, thereby freeing RF resources for data transmission and improving overall network capacity.

In hybrid network optimization, existing link aggregation techniques are often heuristic-based and do not fully account for fairness or system constraints [36]. This thesis introduces advanced optimization-based algorithms, including LA-SINR, LA-EQoS, and FLADA [8, 9], which formulate the resource allocation problem using linear programming. These approaches achieve near-optimal throughput while ensuring fairness and efficient load balancing.

Furthermore, mobility-aware handover optimization is enhanced through frameworks such as MARM-HyLiWi and related strategies [10, 37]. Unlike conventional static or greedy approaches, the proposed methods incorporate mobility prediction and search-space pruning, significantly reducing handover overhead and improving user experience.

Overall, the novelty of this thesis lies in its holistic, multi-layered design approach, integrating theoretical modeling, algorithmic innovation, and experimental validation. This distinguishes the work from existing literature and provides a comprehensive roadmap for the development of high-capacity, mobility-resilient, and efficient next-generation indoor wireless communication systems.

The key novelties of this thesis, in comparison to existing literature, are summarized in Table 1.1. From Table 1.1, it is evident that the proposed work goes beyond existing studies by not only addressing individual challenges such as MAC inefficiency, blockage, or mobility, but also by providing a unified framework for hybrid LiFi–WiFi networks.

Table 1.1: Comparison of Proposed Contributions with Existing Works

Research Aspect	**Existing Works**	**Proposed Contribution**
MAC Protocol Design	RF-inspired MAC protocols (CSMA/CA, HCCA) with limited adaptation to LiFi characteristics [23, 28]	Hybrid CSMA/CA–HCCA MAC with dynamic switching based on traffic heterogeneity, improving throughput, delay, and collision performance [1]
Blockage Modeling	Simplified stochastic or geometric blockage models with limited realism [29, 30]	FixOM and SAM models capturing both static obstacles and dynamic shadowing for realistic indoor LiFi environments [3]
Mobility & Orientation Awareness	Limited handling of user orientation and mobility; often treated independently [31, 32]	OAM-LiFiNet: SINR-driven orientation-aware multi-AP framework enabling adaptive link selection under mobility [2]
Hybrid LiFi–WiFi Systems	Mostly simulation-based studies with limited real-world validation [26, 33]	Experimental prototype testbed demonstrating throughput gains, seamless handover, and service continuity [4, 5]
CSI Feedback Optimization	High CSI overhead in MU-MIMO WiFi with RF-only feedback mechanisms [34, 35]	WiLiConnect and WiLiConnect-Opt frameworks leveraging LiFi links for CSI feedback, reducing overhead and improving spectral efficiency [6, 7]
Link Aggregation	Heuristic-based aggregation schemes with limited fairness and optimization guarantees [36]	Optimization-driven frameworks (LA-SINR, LA-EQoS, FLADA) using linear programming for throughput maximization and fairness [8, 9]
Mobility-Aware Resource Allocation & Handover	Static or greedy approaches without predictive adaptation [14]	Mobility-aware optimization (MARM-HyLiWi) with search-space pruning and adaptive handover strategies [10, 37]

Unlike prior works that rely on isolated or simulation-based approaches, this thesis combines analytical modeling, optimization-based design, and real-world prototyping. Furthermore, the integration of LiFi for CSI feedback offloading and the development of mobility-aware link aggregation strategies represent key advancements toward practical and scalable next-generation indoor wireless systems.

1.8 Thesis Organization

The remainder of this dissertation is structured as follows:

- **Chapter 2: Background and Related Work** introduces the fundamentals of indoor wireless communication and provides an overview of Li-Fi systems, including phisical (PHY) and MAC layer features, deployment scenarios, and major challenges such as coverage, mobility, orientation sensitivity, and blockage. The concept of hybrid LiFi–WiFi networks (HLWNs) is also reviewed along with their benefits, architectures, and open research gaps. Related work on resource allocation and link aggregation is critically discussed, leading to identified gaps that this dissertation addresses.

- **Chapter 3: MAC-Layer Enhancements for Li-Fi Networks** analyzes the limitations of CSMA/CA in Li-Fi and presents a novel hybrid CSMA/CA–HCCA protocol to enhance uplink performance under heterogeneous traffic. The chapter describes the protocol design, analytical modeling, and performance evaluation through simulations, followed by a detailed discussion of results.

- **Chapter 4: Blockage Modeling in Li-Fi Networks** focuses on the modeling of blockage in indoor Li-Fi systems. Two models are presented: FixOM for static blockages and the SAM for dynamic and partial blockages. Their performance impact is analyzed and validated, providing deployment insights.

- **Chapter 5: Mobility and Orientation-Aware Li-Fi Networks** investigates the impact of user mobility on Li-Fi performance and proposes the OAM-LiFiNet. A SINR-based orientation adjustment scheme and system architecture are introduced. Simulation and experimental results demonstrate improved robustness against mobility and orientation sensitivity.

- **Chapter 6: Hybrid LiFi–WiFi Networks** explores the motivation for integrating Li-Fi and Wi-Fi. A prototype HLWN testbed is developed, including hardware and software setup, and several experimental scenarios are studied. Performance evaluation metrics such as throughput, handover efficiency, and service continuity are presented.

- **Chapter 7: Overcoming CSI Feedback Overhead in HLWNs** addresses the problem of excessive CSI overhead in MU-MIMO Wi-Fi. The WiLiConnect framework is introduced, enabling CSI transmission via Li-Fi links. An optimized version, WiLiConnect-Opt, is also proposed. Analytical and experimental evaluations show significant overhead reduction and spectral efficiency gains.

- **Chapter 8: Link Aggregation in HLWNs** discusses the need for multi-link aggregation in HLWNs and presents algorithms such as LA-SINR (LA based on SINR) , LA-EQoS (LA for enhancement of QoS) , and FLADA (Flow-based Algorithm for Data Allocation). A mobility-aware handover strategy based on offline optimization and re-optimization is proposed.

- **Chapter 9: Mobility-Aware Rate allocation and Handover Optimization in HLWNs** proposes the novel framework for efficient resource allocation in LA-enabled hybrid networks, considering rate distribution, load-aware optimization, and backhaul constraints. Performance analysis highlights improvements in fairness and throughput under dynamic mobility conditions.

- **Chapter 10: Conclusion and Future Work** summarizes the key contributions and findings of the dissertation, highlights the limitations of the current work, and outlines future research directions. Potential avenues include AI/ML-driven hybrid networks, ISAC-based integration, and real-time prototyping for large-scale deployment.

- **References** Provides the complete list of cited works.

1.9 Summary

This chapter introduced the motivation behind exploring Li-Fi as a complementary technology to conventional RF-based wireless networks. It began with the background and limitations of existing RF systems, followed by a discussion on the potential of Li-Fi and the challenges associated with both standalone Li-Fi and hybrid LiFi–WiFi networks. The research objectives were clearly defined, and the major contributions of this dissertation were highlighted along with relevant publications. Finally, the overall structure of the thesis was outlined to provide a road-map for the reader. The next chapter presents the background and related work, establishing the technical foundation for the proposed research.

Chapter 2

Background and Related Work

This chapter presents the theoretical foundations and state of the art relevant to this thesis. It begins with an overview of indoor wireless communication and its evolution beyond conventional RF systems, highlighting the motivation for optical wireless communication (OWC) . The fundamentals of LiFi are then introduced, covering its working principle, modulation techniques, PHY and MAC features, and deployment scenarios. Following this, the limitations of Li-Fi—LoS dependence, blockage sensitivity, and mobility challenges—are discussed in detail. To address these constraints, hybrid LiFi-WiFi networks are explored, emphasizing their architectural approaches, benefits, and shortcomings. The chapter concludes with a survey of related research on resource allocation and link aggregation in HLWNs, leading to the identification of open research gaps that motivate the contributions of this thesis, which are developed in Chapters 3–9.

2.1 Fundamentals of Indoor Wireless Communication

Indoor wireless networks have become increasingly vital with the rapid growth of high-bandwidth applications such as AR/VR, UHD streaming, and IoT. Traditional RF-based technologies like Wi-Fi, while offering broad coverage and mature infrastructure, are now constrained by spectrum congestion, interference, and scalability challenges, as illustrated in

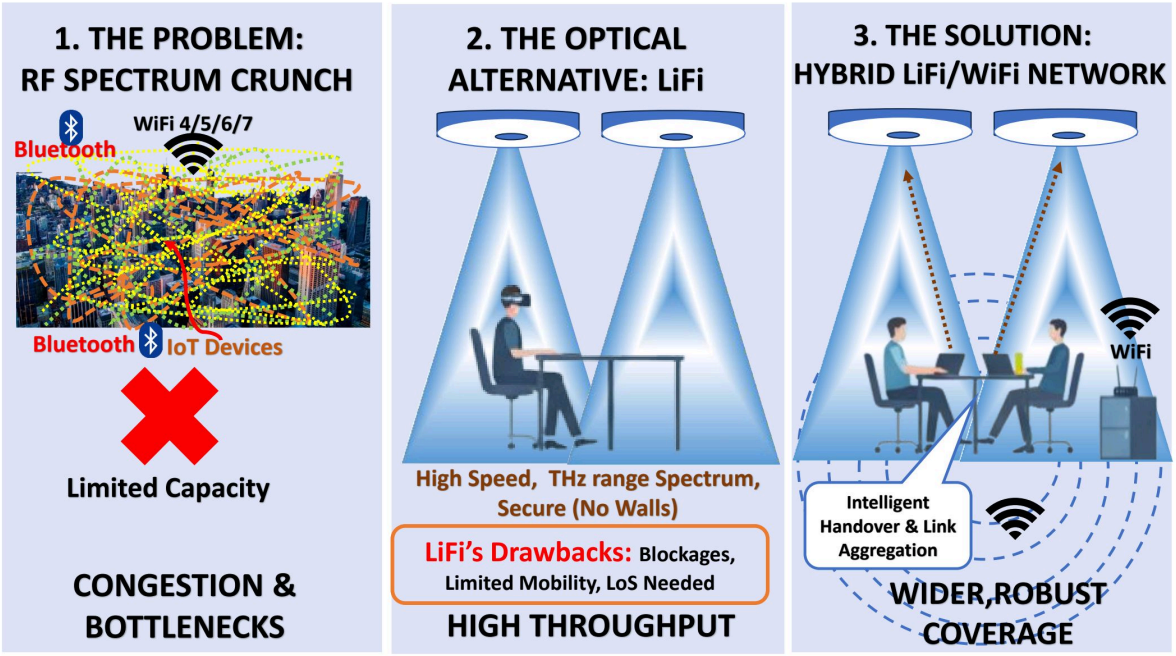

Figure 2.1: Evolution from RF-based networks facing spectrum congestion to hybrid Li-Fi/Wi-Fi architectures combining the capacity of Li-Fi and the coverage of Wi-Fi for seamless indoor connectivity.

Fig. 2.1. In contrast, VLC systems particularly Li-Fi have emerged as promising complementary technologies that utilize the unlicensed visible spectrum to deliver high data rates and enhanced physical-layer security. However, Li-Fi's limited mobility and LoS dependence restrict its standalone applicability. The integration of Li-Fi with Wi-Fi into a hybrid Li-Fi/Wi-Fi network can effectively combine the strengths of both systems, offering improved coverage, capacity, and seamless connectivity. This motivation forms the foundation for the hybrid architectures analyzed in Chapter 6.

2.2 Overview of Li-Fi Systems

Li-Fi is an optical wireless communication technology that employs the visible light (VL) and infrared (IR) spectrum for high-speed data transmission between a transmitter and receiver [38]. Unlike traditional RF systems, Li-Fi leverages the unlicensed and vastly underutilized optical spectrum, thereby enabling data rates much higher than those achievable with RF. The visible

spectrum spans wavelengths from approximately 380 nm (violet, ∼770 THz) to 780 nm (red, ∼430 THz). This broad range allows for a large communication bandwidth, which can be harnessed using standard LEDs as transmitters and photodiodes (PDs) as receivers.

2.2.1 Working Principle

The general architecture of a Li-Fi system is illustrated in Fig. 2.2. At the transmitter side, an LED serves as the optical front-end, driven by an LED driver that modulates the intensity of the emitted light according to the input data stream. Owing to the incoherent nature of LEDs, Li-Fi systems predominantly employ intensity modulation with direct detection (IM/DD) [23]. In this technique, information is encoded in variations of the light intensity, while the PD at the receiver side converts these variations into an electrical signal, which is subsequently demodulated into the original data. Initially, simple modulation techniques such as On-Off Keying (OOK) and Pulse Amplitude Modulation (PAM) were adopted due to their implementation simplicity and low processing requirements. While suitable for low- to medium-rate transmissions, these schemes are limited in spectral efficiency. To enable higher data rates and robust communication under interference and multipath conditions, more advanced schemes such as Orthogonal Frequency Division Multiplexing (OFDM) were later introduced in Li-Fi systems [39]. OFDM allows the optical channel to be divided into multiple orthogonal subcarriers, thereby enhancing throughput, reducing inter-symbol interference, and supporting adaptive resource allocation. Data transmission in Li-Fi is achieved by rapidly switching the LED on and off at imperceptible speeds, with binary ‘1” and 0” encoded into intensity levels. For the uplink, communication can be enabled through infrared or secondary light sources, creating a bidirectional channel. Since photodiodes are highly sensitive in the 430–770 THz range, this portion of the visible spectrum is particularly well-suited for Li-Fi-based communication, though extensions to infrared and ultraviolet bands are also possible.

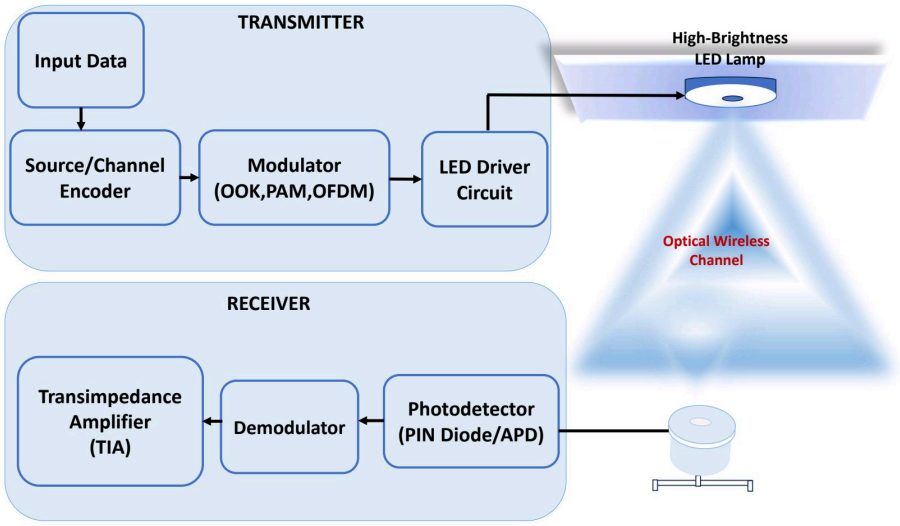

Figure 2.2: System architecture of a Li-Fi network showing APs embedded in LED luminaires and user devices equipped with photodiodes for reception.

2.2.2 Internet Architecture of Li-Fi

Li-Fi networks are organized in a layered architecture similar to Wi-Fi, with PHY and MAC layers adapted to optical wireless communication. At the core, the PHY layer governs modulation schemes such as DC-biased optical OFDM (DCO-OFDM) , asymmetrically clipped OFDM (ACO-OFDM) , or pulse amplitude modulation (PAM) , while the MAC layer coordinates multiple users and APs. At higher layers, Li-Fi integrates seamlessly with IP-based Internet services. The working of end to end Li-Fi communications is illustrated in Fig. 2.3, where Li-Fi access points connect to Ethernet backhaul provide seamless connectivity.

2.2.3 Li-Fi Channel Model

The optical wireless channel in Li-Fi systems is primarily modeled using the LoS propagation between the transmitter (AP) and receiver (user device). The received optical power depends on the geometric alignment, Lambertian emission pattern, and receiver field of view (FoV) .

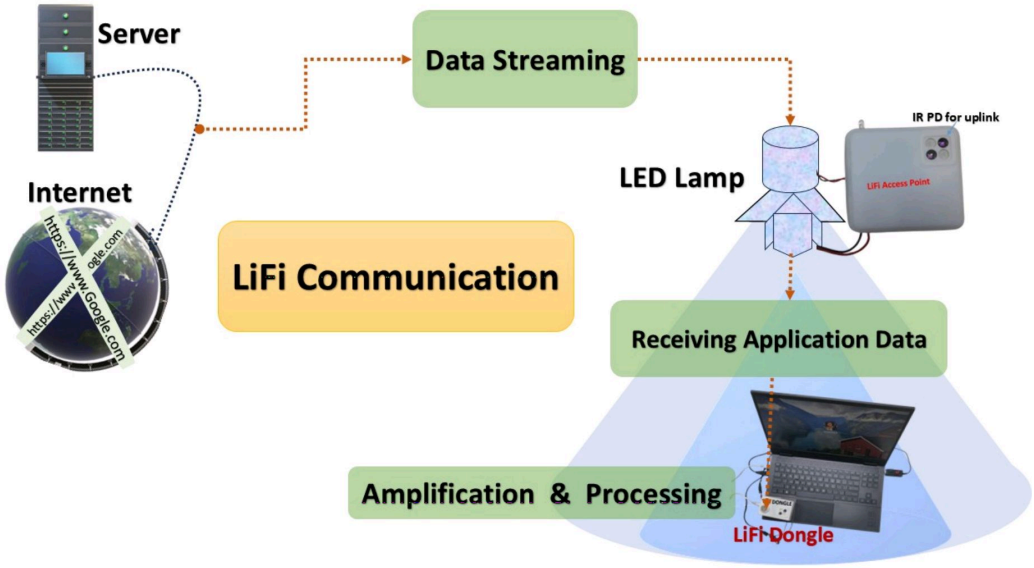

Figure 2.3: Internet architecture of Li-Fi connectivity.

2.2.3.1 LoS Channel

The LoS channel gain between AP i and user j is modeled as [14]:

$$H_{i,j}^{\text{LoS}} = \begin{cases} \frac{(m+1)A}{2\pi d^2}\cos^m(\phi)g_f(\psi)g_c(\psi)\cos(\psi), & 0 \leq \psi \leq \Psi_{\max}, \\ 0, & \psi > \Psi_{max}, \end{cases} \tag{2.1}$$

where m is the Lambertian order, A is the PD area, d is the distance between transmitter and receiver, ϕ is the irradiance angle, ψ is the incidence angle, $g_f(\psi)$ is the optical filter gain, $g_c(\psi)$ is the concentrator gain, and Ψ_{max} is the receiver FoV.

The Lambertian order is given by:

$$m = \frac{-\ln(2)}{\ln(\cos(\Phi_{1/2}))}, \tag{2.2}$$

where $\Phi_{1/2}$ is the LED half-power semi-angle.

The concentrator gain $g_c(\psi)$ depends on the refractive index n of the optical concentrator and the receiver FoV $\Psi_{\max}$ [40]:

$$g_c(\psi) = \begin{cases} \frac{n^2}{\sin^2(\Psi_{\max})}, & 0 \leq \psi \leq \Psi_{\max}, \\ 0, & \psi > \Psi_{\max}. \end{cases} \tag{2.3}$$

2.2.3.2 Non-Line-of-Sight (NLoS) Channel

In addition to direct LoS propagation, indoor Li-Fi systems experience diffuse reflections from walls, ceilings, and objects. The NLoS channel gain can be modeled as the summation of reflected components [40]:

$$H^{\text{NLoS}} = \sum_r \frac{\rho_r (m+1) A}{2\pi^2 d_{tr}^2 d_{rj}^2} \cos^m(\phi_{tr}) \cos(\alpha_r) \cos(\beta_r) T_s(\psi) g_c(\psi) \cos(\psi), \tag{2.4}$$

where ρ_r is the reflection coefficient of surface r, d_{tr} is the distance from transmitter to reflection point r, d_{rj} is the distance from reflection point r to receiver j , and α_r, β_r are the incident and reflection angles at surface r.

2.2.3.3 Discussion

While NLoS reflections contribute to connectivity in obstructed scenarios, their power diminishes significantly after two to three reflections. Therefore, most practical Li-Fi system models primarily consider the LoS path, with at most first-order reflections for robustness.

2.2.4 PHY and MAC layer Features of Li-Fi

At the PHY layer, Li-Fi predominantly employs OFDM-based modulation schemes to support high-speed data rates and robust spectral efficiency. The directional nature of optical signals, combined with LoS requirements, introduces challenges such as sensitivity to user orientation, shadowing, and blockage. To mitigate these effects, Li-Fi systems often rely on multi-AP

Figure 2.4: Li-Fi channel model.

deployments and adaptive modulation schemes. Furthermore, hybrid Li-Fi/Wi-Fi networks can exploit the complementary characteristics of both technologies, where Li-Fi provides high-speed localized coverage and Wi-Fi ensures ubiquitous connectivity. The MAC layer in Li-Fi networks plays a critical role in coordinating medium access and ensuring efficient utilization of resources.

Traditionally, Li-Fi networks adopt Wi-Fi-inspired contention-based MAC protocols, such as CSMA/CA. Several studies have explored modifications to CSMA/CA to handle interference, maximize throughput, and address hidden node and exposed node problems in dense Li-Fi and hybrid networks [27, 41, 42]. Although these studies advanced medium access strategies, they largely overlook MAC mechanisms capable of serving heterogeneous users with diverse throughput requirements, such as high-power personal computing devices (PCDs) and low-power IoT nodes. To address this, recent works have proposed hybrid CSMA/CA–HCCA MAC designs to balance contention-based and contention-free access, thereby improving throughput and latency in heterogeneous Li-Fi environments [2]. The proposed hybrid MAC protocol developed in this thesis is detailed in Chapter 3.

2.2.5 Deployment Scenarios

Li-Fi deployment typically targets indoor dense environments such as offices, classrooms, and industrial setups, where multiple APs provide both illumination and connectivity. Multi-AP deployments enable spatial reuse but also introduce interference, frequent handovers, and mobility challenges. Orientation-aware frameworks have been investigated to enhance signal quality during movement [2]. This thesis extends this line of work with mobility-aware frameworks, which are discussed in Chapter 5.

2.3 Challenges in Li-Fi Networks

Despite its promise, Li-Fi deployment in real-world settings faces several challenges.

2.3.1 Coverage and LoS Issues

Due to its highly directional nature, Li-Fi offers relatively small coverage zones, resulting in frequent handovers when multiple APs are deployed. Moreover, Li-Fi links are heavily dependent on the availability of a LoS path. Obstructions such as human presence, furniture, or user movement can disrupt LoS connectivity, leading to significant throughput degradation. Early studies proposed hybrid Li-Fi–RF architectures as a practical means to maintain reliability during LoS disruptions [40]. More recent works have focused on AP coordination and load balancing to improve coverage, but challenges remain in dynamic environments. This motivates hybrid system architectures, which are further explored in Chapter 6.

2.3.2 Mobility and Orientation Sensitivity

User mobility and device orientation introduce unique challenges in Li-Fi systems. In dynamic indoor settings, mobility often modeled by the Random Waypoint (RWP) model leads to fluctuating channel conditions and frequent handovers. One mitigation strategy explored in the

literature is device orientation control. For example, [32] demonstrated that optimal orientation angles can substantially enhance LoS channel gain and throughput. However, subsequent work revealed that such gains diminish under random user movement. To capture these dynamics, [43] introduced mobility-aware channel models, showing that mobility and orientation jointly influence system reliability and error rates. Similarly, [44] modeled device orientation as a stochastic process and introduced the concept of orientation coherence time, enabling real-time optimization of Li-Fi links. Beyond indoor environments, [45] investigated high-mobility vehicular Li-Fi systems and proposed digital mirror device (DMD) -based receivers to sustain robust connectivity. While these studies highlight the importance of orientation and mobility, they often consider them in isolation. In contrast, this thesis investigates their combined effects in multi-AP scenarios and addresses the open question of when orientation control should be applied under user mobility. Orientation- and mobility-aware strategies such as OAM-LiFiNet [2] serve as the basis for the proposed framework, with extensions presented in Chapter 5.

2.3.3 Blockage and Shadowing Effects

Blockage analysis is a critical aspect of Li-Fi systems, as obstructions from humans, furniture, or devices can significantly reduce link reliability and degrade coverage. Existing studies have examined blockage from different perspectives. For instance, [46] analyzed human-induced blockage and showed that increasing the human–device distance reduces LoS signal-to-noise-ratio (SNR) degradation, while [30] modeled dynamic blockages using the RWP mobility model, capturing the time-varying nature of outage duration. Analytical frameworks such as [47] incorporated field-of-view and random blockers, while mitigation strategies using optical intelligent reflecting surfaces (OIRS) were proposed in [48] to sustain connectivity under dynamic blockage and random orientation. Hybrid Li-Fi/Wi-Fi systems have also been investigated to handle blockages, including adaptive switching [49] and load-balancing approaches [50, 51]. While these studies provide valuable insights, most efforts emphasize mitigation rather than realistic modeling of blockage itself. Simplified assumptions limit their

Table 2.1: Summary of related works on blockage modeling and mitigation in Li-Fi/VLC systems

Reference	**Approach**	**Limitations**
[46]	Human blockage impact on LoS SNR, analytical model	Limited to static blockage distances
[30]	Dynamic blockages modeled with RWP mobility	Time-varying behavior captured but environment simplified
[48]	OIRS-assisted VLC to mitigate blockage	Relies on reconfigurable hardware; not pure modeling
[49]	Hybrid Li-Fi/Wi-Fi adaptive switching	Addresses mitigation, not blockage modeling
Proposed (FixOM)	Geometric modeling of static obstacles	Efficient but less detailed
Proposed (SAM)	Shadow-aware modeling with environmental dynamics	Higher accuracy but computationally intensive

ability to accurately capture environmental and user-driven dynamics in indoor Li-Fi systems. To bridge this gap, this thesis introduces two novel frameworks: **FixOM**, a geometrical model for computationally efficient evaluation of blockage effects, and **SAM**, a shadow-aware modeling approach that accounts for detailed environmental characteristics and dynamic interactions. Together, these models enable realistic analysis of blockage phenomena, providing a foundation for the optimization approaches presented in Chapter 4.

2.4 Hybrid Li-Fi/Wi-Fi Networks (HLWNs)

Hybrid Li-Fi/Wi-Fi networks leverage the broad coverage of Wi-Fi and the high throughput of Li-Fi. Early prototypes demonstrated improved throughput and latency compared to standalone Wi-Fi and standalone Li-Fi, but raised challenges such as AP coordination, interference, and handover management.

2.4.1 Research Directions

Existing works on HLWNs fall broadly into three categories:

- **Load balancing and improving throughput:** Studies [49–53] explored dynamic traffic splitting, adaptive handovers, and load balancing to improve user throughput under blockage.
- **Reducing CSI feedback overhead:** MU-MIMO in Wi-Fi suffers from high CSI reporting cost. Solutions include adaptive quantization [54], OFDMA-based sharing [55], and scalable allocation [56], but none exploited Li-Fi for CSI transport.
- **Learning-based CSI compression:** Neural network-driven approaches such as CsiNet [57] and DeepCMC [58] achieve high-fidelity CSI compression. Hybrid RF–LiFi schemes [59] emerged but lacked blockage resilience and AP-level CSI routing.

Despite progress, open challenges remain. Current HLWN research does not: (i) leverage Li-Fi APs for CSI feedback transmission, (ii) address blockage-aware CSI routing, or (iii) jointly optimize Wi-Fi SINR and Li-Fi reliability. These gaps motivate the **WiLiConnect** and **WiLiConnect-Opt** frameworks proposed in this thesis (Chapters 7), which introduce CSI offloading via Li-Fi and Pareto-optimized resource allocation for hybrid networks.

2.5 Related Work on Resource Allocation and Link Aggregation

Several resource allocation and link aggregation strategies have been proposed to enhance HLWN performance. We classify related works into three categories: (i) Hybrid Li-Fi/Wi-Fi networks without aggregation, (ii) aggregation-enabled HLWNs, and (iii) link aggregation in other networks.

2.5.1 Hybrid Li-Fi/Wi-Fi Networks Without Aggregation

To address spectrum scarcity, several works have explored hybrid Li-Fi/Wi-Fi networks where users connect to either Li-Fi or Wi-Fi based on received signal strength (RSS) [14, 52, 60, 61]. Wang et al. [52] proposed a dynamic load-balancing scheme assigning quasi-static users to Li-Fi and mobile users to Wi-Fi, incorporating fairness and throughput via utility functions. Li et al. [60] introduced centralized and distributed load balancing strategies and evaluated fairness across cell formations. The authors in [14] proposed a two-stage AP selection approach using fuzzy logic for hybrid networks, followed by homogeneous Li-Fi allocation. Kashef et al. [61] focused on maximizing energy efficiency in hybrid systems under power and bandwidth constraints. These works focus on hybrid Li-Fi/Wi-Fi systems but do not support link aggregation.

2.5.2 Link Aggregation Enabled Hybrid Li-Fi/Wi-Fi Networks

Few studies have addressed LA in hybrid networks [53, 62–67]. Jin et al. [53] developed a decentralized scheme for resource allocation in multihome and multimode mobile terminals. However, most studies rely on RSS-based user association without data rate optimization. For example, [68] applied Lyapunov optimization to balance rate and energy, while [62, 63] demonstrated LA feasibility in terms of mobility, multipath TCP, and handover. Implementations of LA at the physical and data link layers were shown in [64, 65, 67]. Pratama et al. [66] also applied Lyapunov-based scheduling for throughput optimization in bandwidth-aggregated systems. These efforts do not address key constraints such as user demand, AP capacity, fairness, or user location.

Reinforcement learning (RL) has recently been applied to hybrid networks. Yang et al. [69] developed an RL-based scheme for energy-efficient resource management considering latency and reliability. Kong et al. [70] used Q-learning for power control. A complex RL-based load balancing approach was proposed in [71]. However, these methods require extensive training

data and lack formal performance guarantees. Furthermore, they ignore link aggregation overheads and fairness–satisfaction trade-offs. Our earlier work [8] considers overhead but uses an exhaustive search for allocation, which is computationally infeasible in real-time.

2.5.3 Flow-Based Optimization in Multipath Transmission

In related domains, flow-based resource coordination has been studied in heterogeneous cellular networks. Works such as [72–75] explore joint optimization of user association, subchannel, and power allocation. However, these methods assume cellular-grade backhaul capacities, unlike indoor HLWNs where Ethernet serves as the backhaul [76]. Recently, MobiFi [77] introduced a mobility-aware framework combining reactive and proactive resource management in hybrid LiFi-Wi-Fi networks. While effective for handover optimization, it does not explicitly model link aggregation overhead or fairness.

In summary, while prior works demonstrate the potential of HLWNs and LA-enabled designs, existing approaches either neglect fairness and user demand, ignore aggregation overheads, or assume unrealistic backhaul conditions. In contrast, this thesis introduces predictive and fairness-aware resource allocation strategies that explicitly account for mobility, link aggregation overhead, user demand, and AP backhaul constraints in Chapter-9.

2.6 Summary and Research Gaps

This chapter presents the theoretical foundations and state of the art relevant to this thesis. It begins with an overview of indoor wireless communication and its evolution beyond conventional RF systems, motivating the exploration of optical wireless communication. The fundamentals of Li-Fi are then introduced, covering its principles of operation, PHY/MAC layer features, and typical deployment scenarios. The discussion then shifts to the key challenges of Li-Fi, including coverage, LoS dependence, blockage, mobility, and orientation sensitivity. To overcome these limitations, hybrid LiFi–WiFi networks (HLWNs) are presented as a promising architec-

tural solution. Finally, this chapter reviews related work on medium access protocols, resource allocation, and link aggregation in HLWNs, leading to the identification of open research gaps that motivate the contributions of this thesis. The research gaps form the foundation for the thesis contributions, which are systematically developed in the subsequent chapters.

Research Roadmap

To bridge the gaps identified in the literature, this thesis proposes targeted solutions. Table 2.2 maps the key research gaps to the corresponding contributions and the chapters where they are addressed.

Table 2.2: Research Gaps, Proposed Solutions, and Corresponding Chapters

Research Gap	**Proposed Solution**	**Chapter**
High delay and collision in Li-Fi MAC protocols with heterogeneous users	Hybrid CSMA/CA–HCCA MAC protocol for adaptive medium access [1]	Chapter 3
Lack of realistic blockage modeling in indoor Li-Fi environments	FixOM and SAM blockage models for static and partial obstructions [3]	Chapter 4
Mobility and orientation sensitivity in Li-Fi systems	OAM-LiFiNet: orientation-aware multi-AP framework with SINR-based optimization [2]	Chapter 5
Coverage limitation of Li-Fi in dynamic indoor environments	Prototype demonstration of hybrid LiFi–WiFi testbed [4, 5]	Chapter 6
High CSI feedback overhead in Wi-Fi MU-MIMO	WiLiConnect and WiLiConnect-Opt frameworks for LiFi-assisted CSI sharing [6, 7]	Chapter 7
Suboptimal throughput and fairness in HLWNs under dynamic conditions	Advanced link aggregation frameworks: LA-SINR, LA-EQoS, FLADA [8, 9]	Chapter 8
Unreliable performance due to mobility and frequent handovers in LA-enabled HLWNs	Mobility-Aware Rate Allocation and Handover Optimization [10, 37]	Chapter 9

Chapter 3

MAC-Layer Enhancements for Li-Fi Networks

This chapter examines the design and performance of MAC-layer protocols for Li-Fi networks, focusing on the suitability of the CSMA/CA and HCCA mechanisms through both analytical modeling and simulation. The comparative analysis reveals the inherent trade-offs between distributed and centralized channel access strategies, motivating the development of an adaptive hybrid MAC framework. The proposed hybrid mechanism aims to dynamically balance scalability and QoS while supporting heterogeneous user types, including high-data-rate personal computing devices and low-power IoT devices.

3.1 Motivation

While Li-Fi offers substantial bandwidth advantages through the use of the optical spectrum, its efficiency critically depends on the design of the MAC layer. Most current Li-Fi implementations adapt Wi-Fi-based MAC schemes such as CSMA/CA. Although simple and decentralized, CSMA/CA suffers from high delay, frequent collisions, and the hidden node problem.

Conversely, the HCCA protocol offers contention-free access with strong QoS guarantees but introduces significant polling overhead and scalability challenges as the number of

connected devices increases. These contrasting characteristics highlight the need for a more adaptive mechanism capable of dynamically balancing throughput and scalability.

This motivates the exploration of a hybrid MAC protocol for Li-Fi that intelligently integrates CSMA/CA and HCCA modes, tailored to environments where heterogeneous users (e.g., IoT and PCDs) coexist.

3.2 Contributions of this Chapter

The main contributions of this chapter are as follows:

- **Analytical model of HCCA in Li-Fi:** The Hybrid Coordination Function Controlled Channel Access (HCCA) protocol, originally developed for IEEE 802.11e WLANs, is analyzed in the Li-Fi context for the first time. An analytical model is developed to capture throughput, busy channel, and collision probabilities under Li-Fi channel characteristics.
- **Comparative evaluation of CSMA/CA and HCCA:** Using simulations and analytical insights, the trade-offs between distributed (CSMA/CA) and centralized (HCCA) MAC mechanisms are quantified in terms of throughput, delay, and overhead.
- **Identification of switching thresholds:** The analysis identifies the user density threshold beyond which HCCA loses efficiency relative to CSMA/CA, providing a foundation for hybrid operation.
- **Proposal of a hybrid MAC mechanism:** A dynamic hybrid scheme is proposed that switches between CSMA/CA and HCCA based on the number and type of users in a Li-Fi cell, ensuring scalability and QoS across heterogeneous devices.

3.3 Fundamentals of MAC Protocols in Li-Fi

The MAC layer in Li-Fi manages access to the shared optical medium while maintaining fairness and QoS among users. Unlike RF-based networks, Li-Fi requires line-of-sight connectivity and uses separate spectral bands for downlink (visible light) and uplink (infrared). Hence, channel access mechanisms from Wi-Fi (e.g., CSMA/CA) are not directly optimized for Li-Fi.

3.3.1 CSMA/CA and Hidden User Problem in Li-Fi

CSMA/CA operates by sensing the channel before transmission. If busy, devices back off for a random interval before retrying. In Wi-Fi, the Request-to-Send/Clear-to-Send (RTS/CTS) handshake alleviates hidden node issues [78, 79].

However, in Li-Fi, users cannot sense each other due to directional optical links and the use of different spectra for uplink and downlink, as shown in Fig. 3.1. This exacerbates the hidden user problem. RTS/CTS is thus essential but introduces significant signaling overhead, reducing overall throughput.

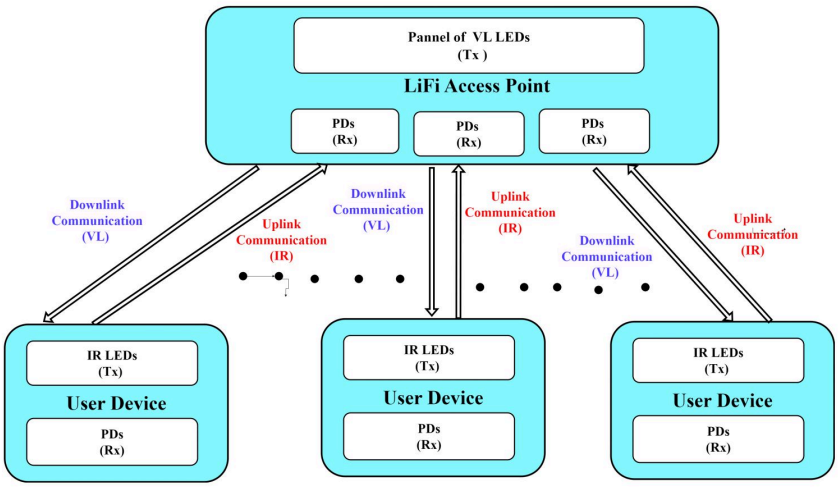

Figure 3.1: Uplink and downlink communication model in Li-Fi using VL and IR channels.

3.3.2 From PCF to HCCA: Toward QoS-Aware Scheduling

To enable deterministic access, IEEE 802.11e introduced HCCA, extending the Point Coordination Function (PCF) to include QoS differentiation through traffic specification (TSPEC) parameters [80, 81]. The AP acts as a Hybrid Coordinator (HC) that polls users and grants Transmission Opportunities (TXOPs) .

While HCCA is rarely used in Wi-Fi due to complex admission control, Li-Fi's confined attocell environment makes it a viable choice. Each Li-Fi AP handles fewer users, allowing efficient centralized scheduling. This observation motivates the study of HCCA for Li-Fi networks.

3.4 System Model and Analytical Framework

This section models the HCCA protocol analytically for Li-Fi uplink communication, capturing key parameters that determine throughput and collision dynamics.

In HCCA, users decrement their backoff counters before sending an association request. The AP grants channel access if the channel is idle; otherwise, users resume their backoff. The user granted a TXOP can transmit multiple packets while others wait. This ensures high throughput at the cost of higher busy channel probability and collisions among association requests.

3.4.1 Key Analytical Expressions

To characterize the performance of HCCA, three key probabilities are derived:

- **Channel sensing probability (ζ):** The *channel sensing probability* ζ is defined as the probability that at least one user senses the channel as free and attempts transmission. Mathematically, it can be expressed as:

$$\zeta = P_r\left(B_{0\geq 1}\right), \tag{3.1}$$

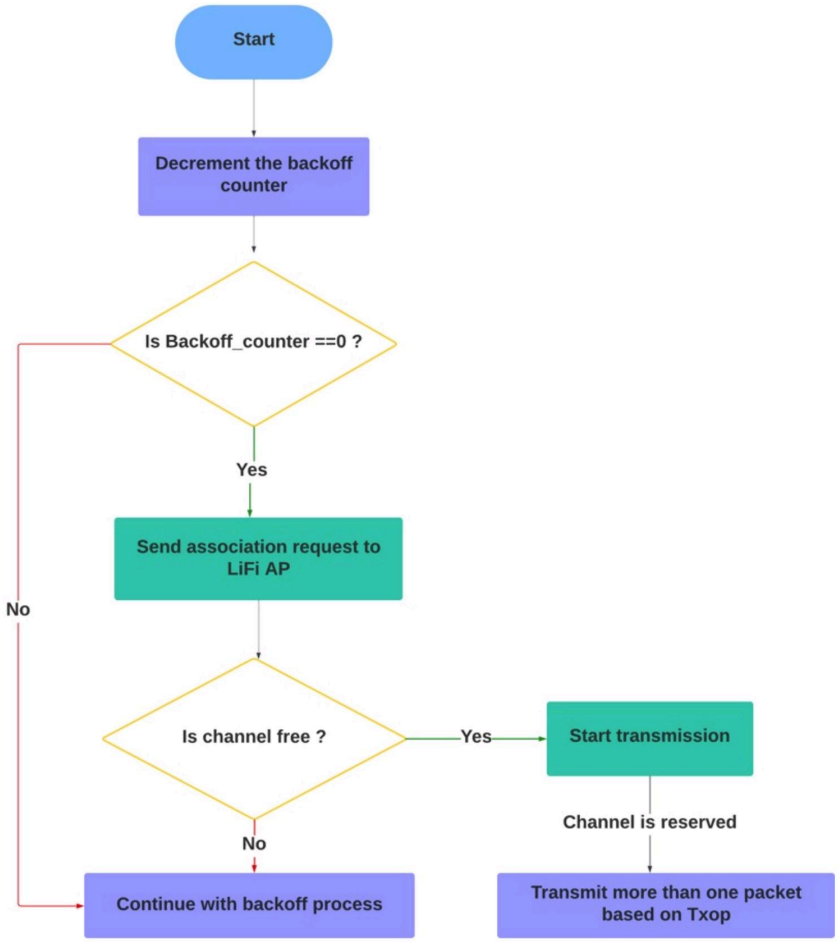

Figure 3.2: Operational flow of HCCA-based uplink MAC protocol in Li-Fi.

where B_0 represents the number of users whose backoff counter has reached zero. Equivalently, ζ can be rewritten as:

$$\zeta = 1 - P_r\left(B_{0\supseteq\{0\}}\right), \tag{3.2}$$

where $P_r\left(B_{0\supseteq\{0\}}\right)$ is the probability that no user has a backoff counter equal to zero.

Since each user's backoff counter is uniformly distributed over $[1, CW_{\max}]$, the probability that no user chooses a backoff value of 1 among N users is $\left(1 - \frac{1}{CW_{\max}}\right)^N$. Therefore, the probability that at least one user attempts to access the channel is:

$$\zeta = 1 - \left(1 - \frac{1}{CW_{\max}}\right)^N. \tag{3.3}$$

Equation (3.3) represents the probability that at least one user attempts to transmit during a backoff interval. In contrast, CSMA/CA relies on carrier sensing and the Network Allocation Vector (NAV) to determine channel availability rather than explicit polling.

- **Busy channel probability (α):** The *busy channel probability*, denoted as α, measures the likelihood that the channel is occupied due to an ongoing transmission. Under the HCCA mechanism, the AP allows only one user to transmit during its TXOP while all other users sense the channel. Thus, α can be formulated as:

$$\alpha = {}^{N}C_1 P_r(Tx_{\supseteq\{1\}}) = NP_r(Tx_{\supseteq\{1\}}), \tag{3.4}$$

where $P_r(Tx_{\supseteq\{1\}})$ is the probability that a single user transmits while others are sensing the channel. This probability is given by:

$$P_r(Tx_{\supseteq\{1\}}) = (1-\alpha)\zeta. \tag{3.5}$$

Substituting (3.5) into (3.4) yields:

$$\alpha = N(1-\alpha)\zeta = N\zeta - N\alpha\zeta. \tag{3.6}$$

Simplifying, we obtain:

$$\alpha = \frac{N\zeta}{1+N\zeta}. \tag{3.7}$$

Equation (3.7) provides the probability that the Li-Fi channel remains busy in the HCCA protocol. For comparison, the corresponding busy channel probability in the conventional CSMA/CA scheme [78, 79] is given as:

$$\gamma = 1-(1-p_t)^N, \tag{3.8}$$

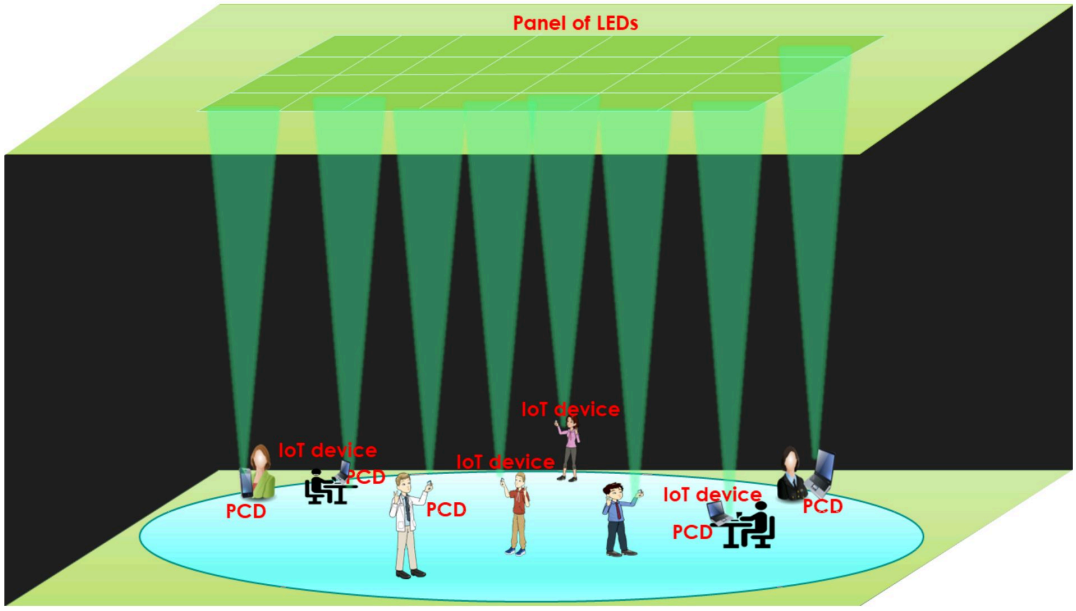

Figure 3.3: Illustration of uplink Li-Fi communication using IR LEDs for heterogeneous devices.

where p_t represents the per-user transmission probability in a given time slot.

3.5 Performance Analysis

The proposed HCCA MAC protocol was evaluated through extensive simulations conducted in a realistic indoor Li-Fi environment, as illustrated in Fig. 3.3. The simulation scenario consists of heterogeneous user devices high-throughput PCDs such as laptops and AR/VR headsets, and low-data-rate IoT nodes such as sensors and smart appliances each exhibiting distinct throughput and latency requirements. To comprehensively assess the system behavior, both HCCA and CSMA/CA configurations were simulated under identical conditions. The objective was to validate the analytical model and to characterize the comparative performance of the two MAC protocols across heterogeneous traffic scenarios. The detailed simulation parameters used for HCCA and CSMA/CA are summarized in Tables 3.1 and 3.2, respectively.

Following this setup, the subsequent subsections present a detailed performance analysis of the proposed HCCA mechanism in terms of key network metrics namely, throughput, collision

probability, busy channel probability, delay, and message overhead. These results form the foundation for developing the hybrid MAC framework that adaptively combines HCCA and CSMA/CA operations based on network conditions.

Table 3.1: Simulation parameters for the HCCA MAC protocol.

Parameters	**PCD-HCCA**	**IoT-HCCA**
Packet length, L_p	400 B (3200 bits)	10 B (80 bits)
ACK duration	40 µs	20 µs
Slot time	20 µs	20 µs
Number of packet sets	8	2
Data rate (per set)	40 Mbps	200 Kbps
Total data rate	320 Mbps	400 Kbps

Table 3.2: Simulation parameters for the CSMA/CA MAC protocol.

Parameters	**PCD-CSMA/CA**	**IoT-CSMA/CA**
Packet length, L_p	400 B	10 B
ACK duration	6 µs	300 µs
Slot time	20 µs	8 µs
Total data rate	40 Mbps	200 Kbps
t_{RTS}	7.2 µs	300 µs
t_{CTS}	6 µs	300 µs
t_{HDR}	10 µs	500 µs
t_{SIFS} / t_{DIFS}	16 µs / 32 µs	16 µs / 32 µs
Number of users, N	14	50

3.5.1 Throughput Analysis

The *average network throughput* represents the fraction of time the Li-Fi channel is successfully used for data transmission, excluding control signaling. For the proposed HCCA MAC protocol, it is analytically expressed as:

$$S = (1-\alpha_{N-1})(1-p_c^{HCCA})(1-\zeta)^{N-1}, \tag{3.9}$$

where ζ is the channel sensing probability, p_c^{HCCA} the collision probability, and $\alpha_{N-1} = \frac{(N-1)\zeta}{1+(N-1)\zeta}$ the busy channel probability with $(N-1)$ users.

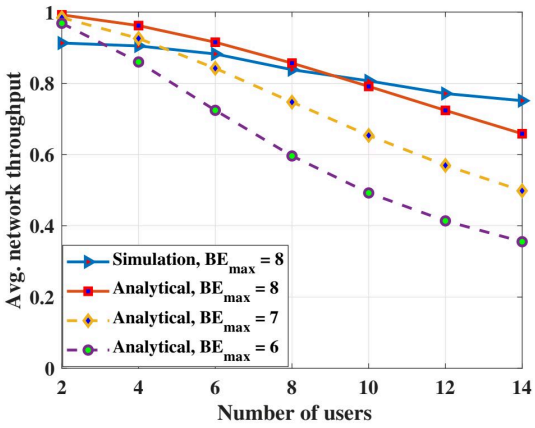

Figure 3.4: Average throughput for different $BE_{\max}$ values using HCCA uplink MAC in Li-Fi.

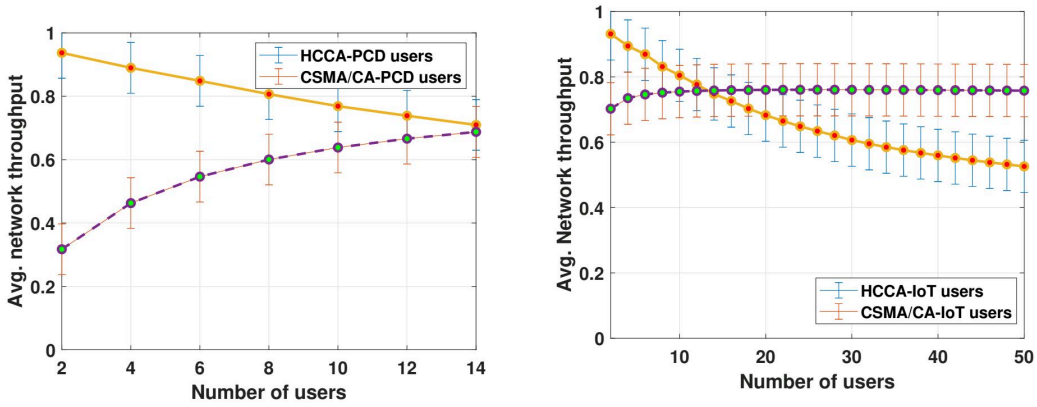

Figure 3.5: Average network throughput for PCD and IoT users using CSMA/CA and HCCA uplink MAC protocols in Li-Fi network.

Figure 3.4 illustrates the average normalized throughput as a function of the number of users for different values of the maximum backoff exponent ($BE_{\max}$). Both analytical and simulation results show a decreasing trend in throughput with increasing number of users due to increased network load and limited transmission opportunities.

It can be observed that higher values of $BE_{\max}$ result in relatively better throughput performance under dense user scenarios. This is because a larger backoff range reduces the probability of contention and scheduling conflicts, thereby improving channel utilization. In contrast, smaller $BE_{\max}$ values lead to higher contention and inefficient use of available transmission opportunities, resulting in a more rapid degradation in throughput.

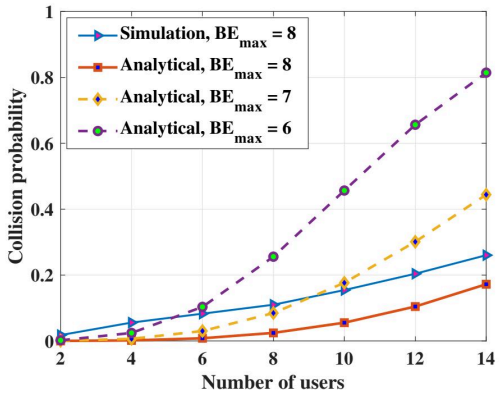

Figure 3.6: Collision probability for different backoff values using HCCA uplink MAC protocol.

The analytical results closely follow the simulation trends for lower user densities. However, as the number of users increases, a noticeable gap appears between analytical and simulation results. This deviation arises due to practical factors such as scheduling overhead, finite transmission durations, and implementation-level inefficiencies that are not fully captured in the analytical model.

Overall, HCCA maintains relatively high throughput compared to contention-based access mechanisms, as the centralized scheduler at the access point allocates transmission opportunities in a controlled manner, thereby minimizing collisions and idle periods.

A comparison with CSMA/CA (Fig. 3.5) shows that CSMA/CA throughput increases initially but saturates under high contention, while HCCA throughput decreases as polling overhead grows. The crossover near $N = 14$ users defines the switching point beyond which CSMA/CA becomes preferable, forming the basis for the hybrid MAC operation described in Section 3.6.

3.5.2 Average Network Collision Probability (p_c)

Collisions occur when multiple users attempt to access the Li-Fi channel simultaneously by sending association requests to the Access Point (AP). The analytical expression for collision probability in the proposed HCCA MAC protocol is given by:

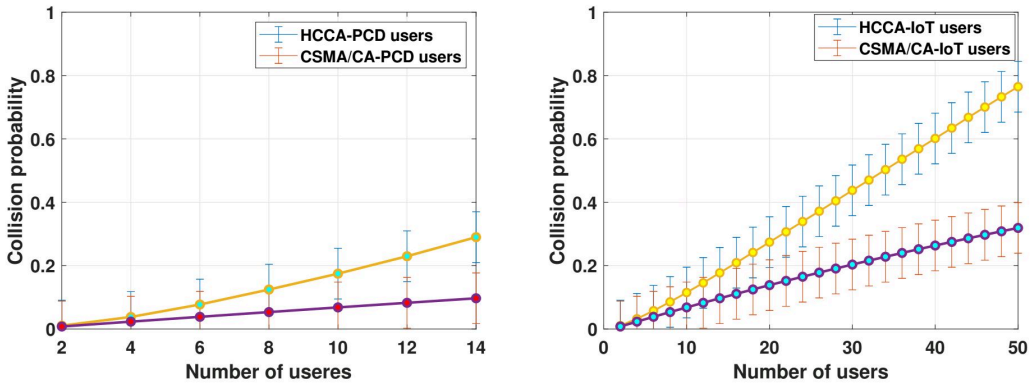

Figure 3.7: Collision probability for PCD and IoT users under CSMA/CA and HCCA.

$$p_c^{HCCA} = 1 - (1-\zeta)^N - N\zeta(1-\zeta)^{N-1}, \tag{3.10}$$

where ζ is the channel sensing probability defined in Eq. (3.3).

Figure 3.6 presents the collision probability for different values of $BE_{\max}$ as the number of users increases. As expected, collision probability increases with the number of users due to a higher likelihood of overlapping transmission attempts.

Lower values of $BE_{\max}$ result in significantly higher collision probability, as the limited backoff range increases the probability that multiple users select similar transmission slots. Conversely, larger $BE_{\max}$ values provide better collision avoidance by spreading transmission attempts over a wider time window.

A gap between analytical and simulation results is observed, particularly for smaller $BE_{\max}$ and higher user counts. The analytical model assumes independent transmission attempts and does not fully capture temporal correlations, retransmission effects, and synchronization issues present in practical systems. In contrast, the simulation accounts for these dynamics, including repeated collisions due to backoff alignment and finite time-slot resolution, leading to higher observed collision probabilities.

This deviation highlights the limitations of the analytical model under dense network conditions, while still validating its effectiveness in capturing the overall system behavior.

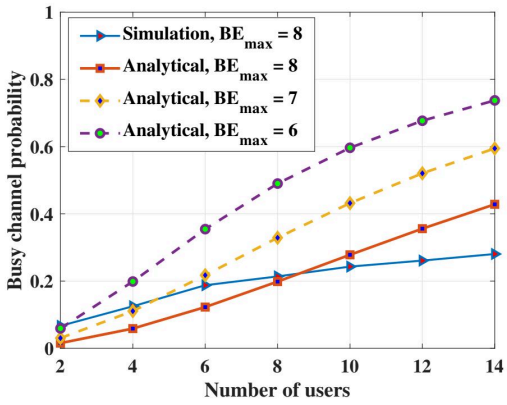

Figure 3.8: Busy channel probability analysis for HCCA uplink MAC protocol with different backoff values.

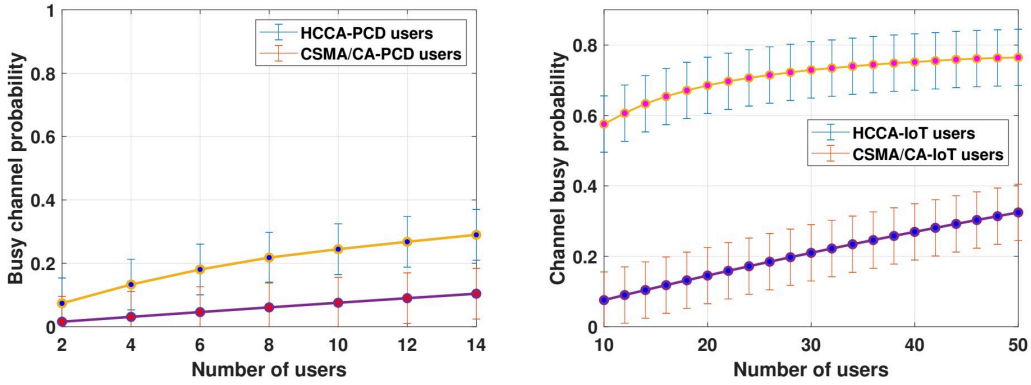

Figure 3.9: Busy channel probability for PCD and IoT users using CSMA/CA and HCCA uplink MAC protocols.

Figure 3.7 compares the collision characteristics of HCCA and CSMA/CA for PCD and IoT users. Due to the RTS/CTS exchange, CSMA/CA experiences lower collision probability, whereas in HCCA, simultaneous association requests during the polling phase can lead to contention. Nevertheless, for smaller user groups (up to $N \leq 14$), HCCA maintains acceptable collision levels while offering higher throughput, reinforcing its suitability for moderate-load Li-Fi scenarios.

3.5.3 Average Network Busy Channel Probability (α)

The busy channel probability (α) represents the fraction of time the Li-Fi medium remains occupied due to ongoing transmissions. In the proposed HCCA MAC protocol, the AP allocates

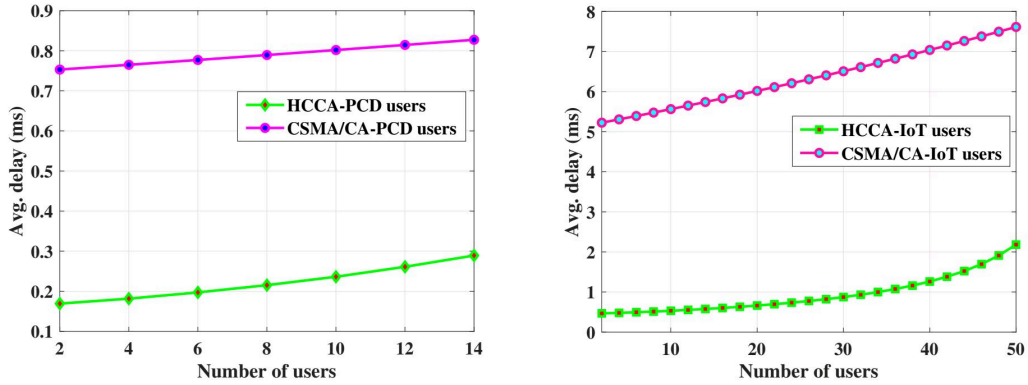

Figure 3.10: Average delay for PCD and IoT users using CSMA/CA and HCCA uplink MAC protocols.

TXOPs sequentially, allowing one user to transmit at a time. Consequently, the probability of the busy channel increases with the number of users and eventually saturates as the AP continuously schedules transmissions.

The analytical expression for α is given by:

$$\alpha = \frac{N\zeta}{1+N\zeta}, \tag{3.11}$$

where ζ is the channel sensing probability.

Figure 3.8 presents the analytical and simulated busy channel probabilities for different $BE_{\max}$ values. Both models show that α approaches saturation for higher user counts, confirming that the channel is effectively utilized under HCCA scheduling.

A comparative analysis between HCCA and CSMA/CA, shown in Fig. 3.9, indicates that HCCA maintains a higher busy channel probability under light-to-moderate load, ensuring efficient medium use for PCD users. In contrast, CSMA/CA exhibits lower α values due to contention backoff, making it more suitable for dense IoT scenarios with frequent idle periods.

3.5.4 Average Delay (τ)

The average delay (τ) is defined as the expected time taken by a user to successfully transmit a packet, including backoff, sensing, transmission, and acknowledgment stages. Considering

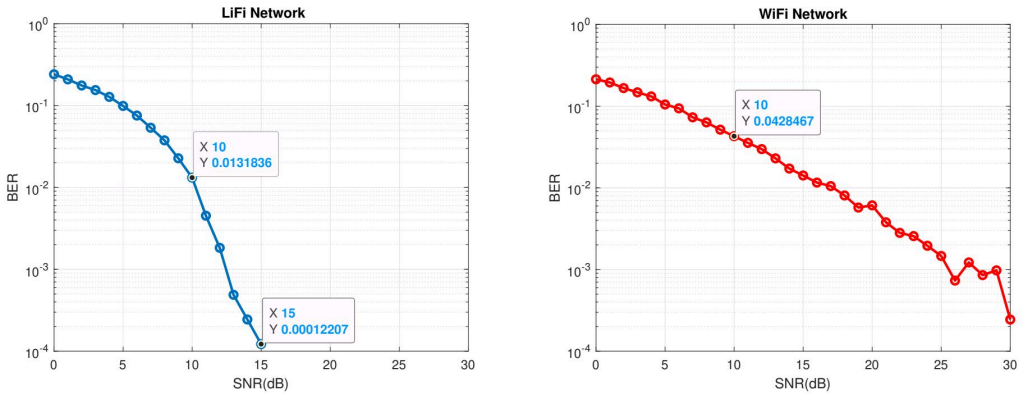

Figure 3.11: BER vs. SNR comparison between Li-Fi and Wi-Fi channels.

possible retransmissions due to collisions, it can be expressed as:

$$\tau = \frac{t_{\text{total}}}{1 - p_c}, \tag{3.12}$$

where t_{total} denotes the total time per transmission attempt, and p_c is the collision probability.

Figure 3.10 compares the delay performance of HCCA and CSMA/CA for both PCD and IoT users. HCCA achieves significantly lower delay under moderate network load due to its centralized scheduling and collision-free access. In contrast, CSMA/CA experiences higher delay because of contention, RTS/CTS exchanges, and random backoffs. However, as the number of users increases, HCCA delay gradually rises owing to polling and queuing overhead at the access point.

3.5.5 Message Overhead (C_m)

Message overhead (C_m) quantifies the additional signaling required for successful channel access. A transmission attempt may fail due to either collision or bit error, with total failure probability given by

$$p_f = p_c + p_e, \tag{3.13}$$

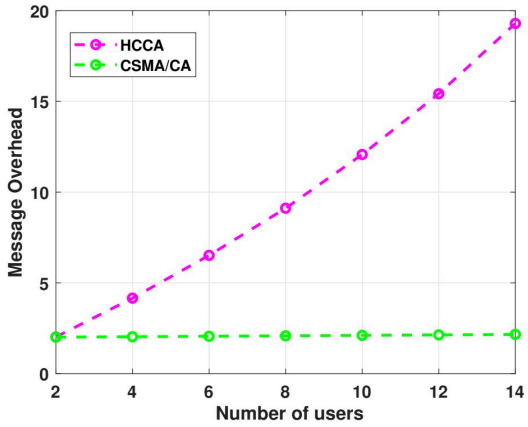

Figure 3.12: Message overhead comparison for HCCA and CSMA/CA protocols.

where p_c is the collision probability and p_e is derived from the bit error rate (BER) as

$$p_e = 1 - (1 - \xi)^N, \tag{3.14}$$

with ξ denoting the BER and N the number of users.

Since LiFi uses directional optical links with limited multipath components, p_e is substantially lower than in Wi-Fi. This is validated in Fig. 3.11, which shows superior BER performance for Li-Fi at the same SNR levels.

The message complexity for the two MAC mechanisms is expressed as [1]:

$$C_m^{HCCA} = \mathcal{O}\left(\frac{N}{1-p_f}\right), \qquad C_m^{CSMA} = \mathcal{O}\left(\frac{p_f}{1-p_f}\right). \tag{3.15}$$

Figure 3.12 illustrates that C_m increases with network size in HCCA due to centralized coordination, while remaining almost constant for CSMA/CA because of its distributed access. Hence, HCCA incurs higher signaling overhead for dense deployments, whereas CSMA/CA offers better scalability for large IoT-oriented networks.

3.6 Hybrid MAC Mechanism

The performance comparison presented in Section 3.5 reveals that the Hybrid Coordination Function HCCA protocol achieves high throughput and low delay under moderate user densities, while CSMA/CA scales better for dense, low-rate IoT environments. To exploit the complementary strengths of these two mechanisms, we propose a **hybrid MAC mechanism** for Li-Fi networks that dynamically switches between HCCA and CSMA/CA based on real-time network conditions.

3.6.1 Design Concept

The proposed hybrid MAC framework operates at the Li-Fi AP, which continuously monitors network parameters such as the number of active users, packet size, and traffic type. An *objective function* is defined to guide the selection of the MAC mode:

$$O_b = \sum_{i=1}^{N} [D_i - \Gamma \tau_i], \tag{3.16}$$

where D_i denotes the achieved data rate (in Mbps) for user i, τ_i represents the corresponding delay (in ms), and Γ is a tunable weighting factor that prioritizes delay-sensitive applications. A higher value of Γ increases the importance of latency reduction, while $\Gamma = 0$ corresponds to throughput-oriented optimization.

The AP evaluates the objective function periodically and selects the most suitable MAC mechanism:

- **HCCA:** selected when the network prioritizes high throughput and low delay (e.g., video streaming, AR/VR, or PCD traffic);
- **CSMA/CA:** selected for dense, low-throughput IoT environments, where distributed access minimizes coordination overhead.

Unlike RF-based systems, where carrier sensing is performed through energy detection of radio signals, Li-Fi systems rely on optical signal detection using photodetectors. In this work, the CSMA/CA mechanism is adapted for Li-Fi environments based on intensity modulation and direct detection (IM/DD). Specifically, each user senses the channel by monitoring the received optical power level at the photodetector. If the detected optical intensity exceeds a predefined threshold, the channel is considered busy; otherwise, it is treated as idle.

Due to the directional nature of optical communication and the dependence on LoS conditions, carrier sensing in Li-Fi is inherently localized and may not detect all ongoing transmissions, unlike omnidirectional RF systems. Therefore, the CSMA/CA mechanism used in this work represents a Li-Fi-adapted version, where sensing is based on received optical intensity within the receiver field-of-view.

3.6.2 Performance-Guided Switching Analysis

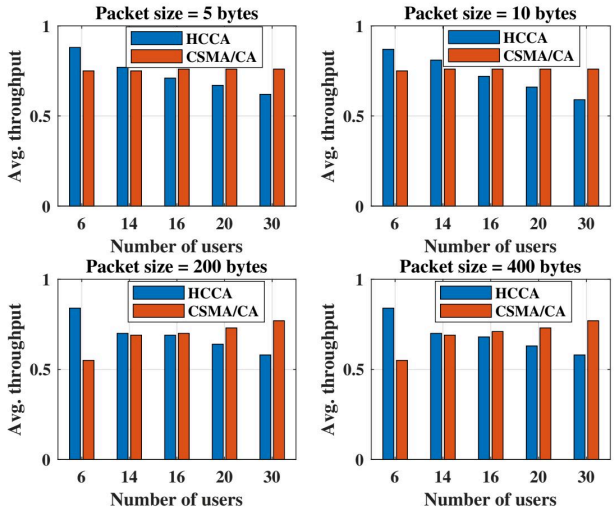

Figure 3.13: Throughput-based switching boundary between CSMA/CA and HCCA in Li-Fi.

To derive the switching threshold between HCCA and CSMA/CA, detailed simulations were performed using the parameters summarized in Tables 3.1 and 3.2. These configurations represent typical Li-Fi uplink scenarios for heterogeneous users.

A comparative summary of the performance results is provided in Table 3.3. It shows that HCCA is more efficient for high-throughput PCD users, while CSMA/CA performs better in dense IoT deployments with smaller packet sizes.

Table 3.3: Comparison of HCCA and CSMA/CA MAC protocols for heterogeneous PCD and IoT users.

Metric	I: HCCA–HCCA		II: HCCA–CSMA/CA		III: CSMA/CA–HCCA		IV: CSMA/CA–CSMA/CA	
	PCD	**IoT**	**PCD**	**IoT**	**PCD**	**IoT**	**PCD**	**IoT**
Average throughput	0.70	0.53	0.70	0.76	0.68	0.53	0.68	0.76
Collision probability	0.29	0.70	0.29	0.32	0.09	0.70	0.09	0.32
Busy channel probability	0.29	0.76	0.29	0.32	0.10	0.76	0.10	0.32
Average delay (ms)	0.28	2.18	0.28	7.6	0.83	2.18	0.83	7.6
Number of users, N	14	50	14	50	14	50	14	50
Data rate	40 Mbps	200 Kbps	40 Mbps	200 Kbps	40 Mbps	200 Kbps	40 Mbps	200 Kbps
Packet size, L_p	400 B	10 B	400 B	10 B	400 B	10 B	400 B	10 B

Figure 3.13 shows the average throughput variation with the number of users for different packet sizes. It can be observed that:

- For smaller packet sizes ($L_p = 5$ B to 10 B) and $N \leq 14$, HCCA yields higher throughput.
- For larger packets ($L_p = 200$ B to 400 B), HCCA remains efficient up to about $N = 16$.
- Beyond these limits, CSMA/CA becomes the more effective mechanism.

Thus, the hybrid MAC operation follows:

$$\text{Use HCCA if } N \leq N_c, \quad \text{Use CSMA/CA if } N > N_c,$$

where N_c is determined empirically based on the packet size and user class composition.

3.6.3 Adaptive Switching Strategy

The adaptive switching process is illustrated in Fig. 3.14. The Li-Fi AP continuously monitors the number of connected users and traffic mix, dynamically switching the MAC operation mode to maintain optimal performance. In practical deployments, this can be realized through multiple optical channels or color bands, e.g., using one wavelength for HCCA-based PCD

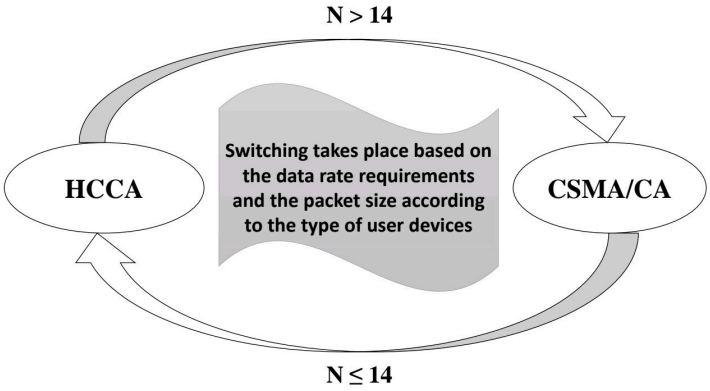

Figure 3.14: Adaptive switching logic for hybrid MAC operation in Li-Fi.

transmissions and another for CSMA/CA-based IoT traffic, to minimize interference and improve coexistence.

Overall, the proposed hybrid MAC mechanism achieves a balance between the deterministic QoS guarantees of HCCA and the scalable, low-overhead nature of CSMA/CA, offering an adaptive and efficient access strategy for heterogeneous Li-Fi networks.

3.7 Summary

This chapter presented a comprehensive analysis of MAC-layer mechanisms for Li-Fi networks, emphasizing the performance trade-offs between the CSMA/CA and HCCA protocols. The analytical and simulation results demonstrated that HCCA achieves superior throughput and lower delay under moderate user densities, whereas CSMA/CA provides better scalability and reduced signaling overhead in dense deployments. Building upon these insights, a hybrid MAC framework was proposed to dynamically switch between HCCA and CSMA/CA, thereby ensuring efficient medium access across heterogeneous Li-Fi environments.

The findings of this chapter form the foundational layer for subsequent investigations in this thesis. In particular, the proposed hybrid MAC framework serves as a precursor to the blockage modeling and mobility-aware enhancements developed in the following chapters,

where link reliability, user orientation, and dynamic resource management are integrated to achieve robust and adaptive Li-Fi communication.

Key Influencing Parameters: It is observed that the performance of the proposed MAC protocol is primarily influenced by the number of users and the maximum backoff exponent ($BE_{\max}$). An increase in user density leads to higher contention and collision probability, thereby degrading throughput. In contrast, appropriate tuning of $BE_{\max}$ helps in mitigating collisions and improving delay performance. Additionally, traffic heterogeneity between IoT and PCD users impacts overall system efficiency by affecting access fairness and channel utilization. These observations highlight the importance of adaptive backoff design and user-aware scheduling for achieving optimal MAC performance in LiFi networks.

Chapter 4

Blockage Modeling in Li-Fi Networks

Building upon the MAC-layer design insights from the previous chapter, where medium access optimization was explored to enhance throughput and QoS in multiuser Li-Fi systems, this chapter focuses on the *physical-layer limitations* arising from **blockage and shadowing effects**. While the hybrid MAC protocol proposed earlier assumed ideal LoS connectivity, real-world indoor environments are often subject to dynamic obstructions caused by users, furniture, or structural elements. These blockages can significantly affect received optical power, SNR, and consequently, the overall link reliability.

To address this challenge, two complementary blockage models are proposed and analyzed: the **Fixed Obstruction Model (FixOM)** and the **Shadowing-Aware Model (SAM)**. The FixOM captures deterministic geometrical blockage scenarios, whereas the SAM extends it to account for probabilistic and partial shadowing effects. The outcomes of this chapter provide an analytical and simulation-based foundation for the mobility and orientation-aware Li-Fi network modeling developed in Chapter 5.

4.1 Impact of Blockage in Li-Fi Networks

Li-Fi communication fundamentally relies on unobstructed optical propagation between an AP and a PD at the user's device. Any obstacle that interrupts this LoS path can severely

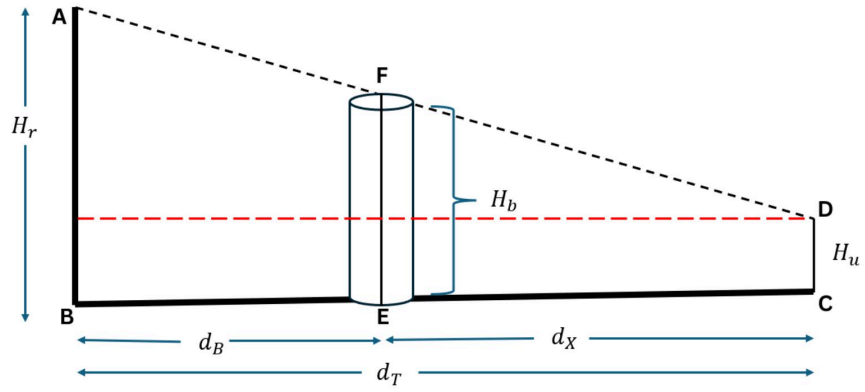

Figure 4.1: Geometric modeling of shadow length calculation.

degrade the received optical power. Blockages in indoor environments arise from static objects such as furniture and walls or from dynamic entities such as humans in motion. Figure 4.1 conceptually illustrates how obstacles between the AP and user create shadow regions that limit optical visibility and degrade the signal. Blockages cause:

1. **Signal attenuation**, reducing received optical power and thereby the achievable data rate.

2. **Temporal link interruptions**, particularly during user mobility or orientation changes.

3. **Spatial variation in channel gain**, resulting in uneven coverage and reduced QoS.

To analyze these effects quantitatively, the following sections develop geometric and probabilistic models that capture both complete and partial shadowing phenomena.

4.2 Fixed Obstruction Model (FixOM)

The **FixOM** provides a deterministic method for quantifying the impact of static obstacles on Li-Fi channel characteristics. Each blockage is represented geometrically as a cylinder defined by its height (H_b) and radius (r_b), positioned at coordinates (x_c, y_c), as shown in Fig. 4.1.

4.2.1 Geometric Modeling and Intersection Criteria

The geometric formulation used in this section is based on standard Euclidean geometry and line-intersection principles commonly adopted in optical wireless communication and blockage modeling studies [23, 24]. These formulations are adapted to model the spatial interaction between LiFi links and blockages in an indoor environment.

For a user located at (x_u, y_u) and a Li-Fi AP projection at (x_{ap}, y_{ap}), the horizontal distance between them is:

$$d_T = \sqrt{(x_u - x_{ap})^2 + (y_u - y_{ap})^2}. \tag{4.1}$$

The LoS between the AP and the user is represented by:

$$y - y_{ap} = m(x - x_{ap}), \tag{4.2}$$

where $m = \frac{y_u - y_{ap}}{x_u - x_{ap}}$ is the slope of the LoS.

The perpendicular distance from a point to a line is computed using the standard point-to-line distance formula [82].

A blockage is assumed to intersect the LoS if the perpendicular distance between the blockage center and the LoS path, denoted by d_p as shown in Fig. 4.2, satisfies:

$$d_p = \frac{|mx_c - y_c + c|}{\sqrt{m^2 + 1}} \leq r_b, \quad c = y_{ap} - mx_{ap}, \tag{4.3}$$

and the blockage lies within the span between the AP and the user as illustrated in Fig. 4.1 and Fig. 4.2:

$$d_B < d_T, \quad d_B = \sqrt{(x_c - x_{ap})^2 + (y_c - y_{ap})^2}. \tag{4.4}$$

The geometric configuration of blockage intersection is illustrated in Fig. 4.2. As shown in Fig. 4.2a, when the blockage radius exceeds the perpendicular distance from its center to

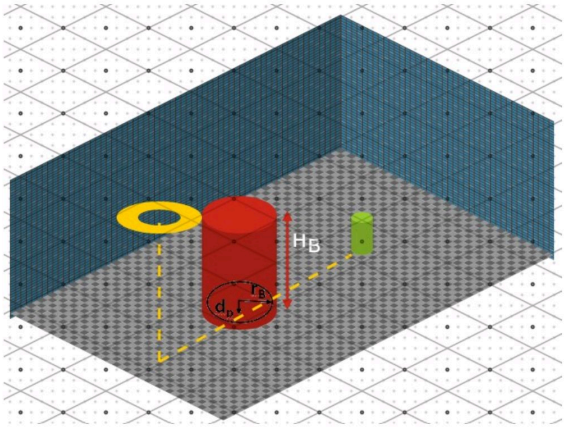

(a) Blockage surface intersecting the LoS.

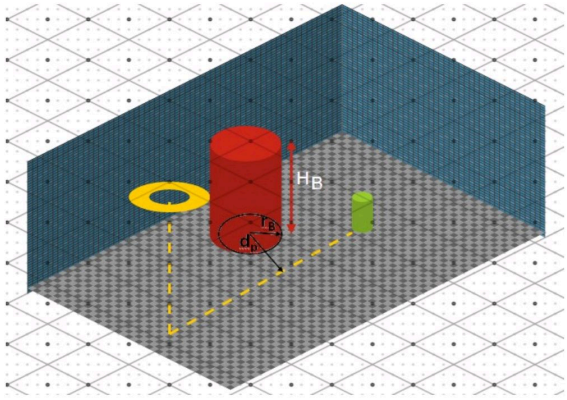

(b) Blockage surface not intersecting the LoS.

Figure 4.2: Illustration of geometric blockage scenarios in the proposed FixOM model: (a) intersecting and (b) non-intersecting cases.

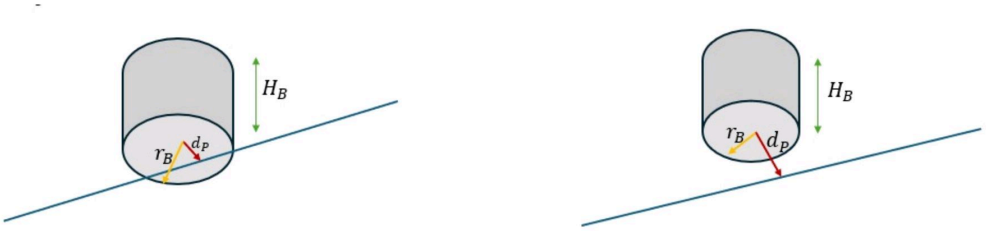

Figure 4.3: Geometric evaluation of blockage intersection along the LoS path.

the LoS ($r_b > d_p$), the blockage surface intersects the LoS path, resulting in a communication obstruction. Conversely, if $r_b < d_p$, the LoS remains unobstructed as shown in Fig. 4.2b.

4.2.2 Shadow Length Estimation

The shadow length estimation is derived using geometric similarity (similar triangles), a commonly used approach in optical propagation and shadow modeling [83].

When an intersection occurs, the shadow length (d_x) on the receiver plane is estimated using geometric similarity shown in Figs. 4.1 and 4.3 as:

$$d_x = \frac{H_b - H_u}{H_r - H_u} \cdot d_T, \tag{4.5}$$

where H_r and H_u denote the ceiling and receiver heights, respectively. A shadow overlaps the receiver if:

$$d_x \geq d_T - d_B. \tag{4.6}$$

The probability of blockage for a single LoS is:

$$P_B = \begin{cases} 1, & \text{if the LoS is obstructed,} \\ 0, & \text{otherwise.} \end{cases} \tag{4.7}$$

A blockage shadows the receiver if $d_x \geq d_T - d_B$. The blockage probability P_B and average blockage probability P_B^{avg} are then calculated over multiple Monte Carlo iterations.

Overall, the FixOM model (as summarized through Figs. 4.1–4.3) offers a deterministic yet efficient way to characterize link blockage in static indoor layouts. For n Monte Carlo iterations, the average blockage probability is:

$$P_B^{avg} = \frac{1}{n} \sum_{i=1}^{n} P_B(i). \tag{4.8}$$

The FixOM model thus offers a deterministic method for evaluating link availability in structured indoor environments and forms the baseline for comparison with the more advanced SAM approach.

4.3 Shadow-Aware Model (SAM)

The **SAM** extends FixOM to capture *partial shadowing*, providing a more realistic representation of light-blocking behavior in populated indoor environments. The SAM geometric relationships are illustrated in Fig. 4.6a, which highlights shadow regions induced by multiple obstacles.

The model defines the obstruction angle θ between the AP and the blockage and estimates the corresponding shadow extent using:

$$d_S = (H_r - H_u)\tan(\theta). \tag{4.9}$$

The resulting partial or full blockage probability, determined using geometric alignment of users and obstacles, allows SAM to predict gradual channel gain reduction instead of abrupt LoS loss, as was the case in FixOM.

4.3.1 Shadow Geometry

The obstruction angle θ between the AP and the blockage is given by:

$$\theta = \cos^{-1}\left(\frac{H_r - H_b}{\sqrt{(x_{ap} - x_b)^2 + (y_{ap} - y_b)^2 + (H_r - H_b)^2}}\right). \tag{4.10}$$

The horizontal distance between the AP and blockage is:

$$d_B = \sqrt{(x_{ap} - x_b)^2 + (y_{ap} - y_b)^2}. \tag{4.11}$$

The corresponding shadow length is:

$$d_S = (H_r - H_u)\tan(\theta). \tag{4.12}$$

The direction of the shadow is derived from the unit vector between the AP and the blockage:

$$B\hat{E}_x = \frac{x_b - x_{ap}}{\sqrt{(x_b - x_{ap})^2 + (y_b - y_{ap})^2}}, \quad B\hat{E}_y = \frac{y_b - y_{ap}}{\sqrt{(x_b - x_{ap})^2 + (y_b - y_{ap})^2}}. \tag{4.13}$$

Finally, the coordinates of the shadow's endpoint are:

$$x_S = x_{ap} + d_S B\hat{E}_x, \quad y_S = y_{ap} + d_S B\hat{E}_y. \tag{4.14}$$

The probability of blockage is defined as:

$$P_B = \begin{cases} 1, & \text{for complete blockage,} \\ 0.5, & \text{for partial blockage,} \\ 0, & \text{otherwise.} \end{cases} \tag{4.15}$$

By combining geometric and probabilistic modeling, SAM captures a finer-grained understanding of how obstacles affect link quality and user connectivity.

4.4 Evaluation and Result Analysis

The FixOM and SAM models are evaluated in realistic indoor scenarios through simulation. The base setup consists of a room of $5\,\text{m} \times 5\,\text{m} \times 3\,\text{m}$ dimensions, with Li-Fi access points mounted on the ceiling and users distributed randomly across the floor. Figure 5.1 shows the simulation layout, including multiple obstacles represented as cylindrical blockages.

The Li-Fi channel parameters are following standard settings from [13, 14]. Simulations consider both small and large room configurations to test scalability and robustness.

User mobility plays a critical role in determining blockage behavior in Li-Fi systems. As the user speed increases, the frequency of changes in user position relative to obstacles also increases, resulting in more frequent line-of-sight interruptions. This leads to a higher occurrence of dynamic blockage events compared to low-mobility scenarios, where users remain in relatively stable positions.

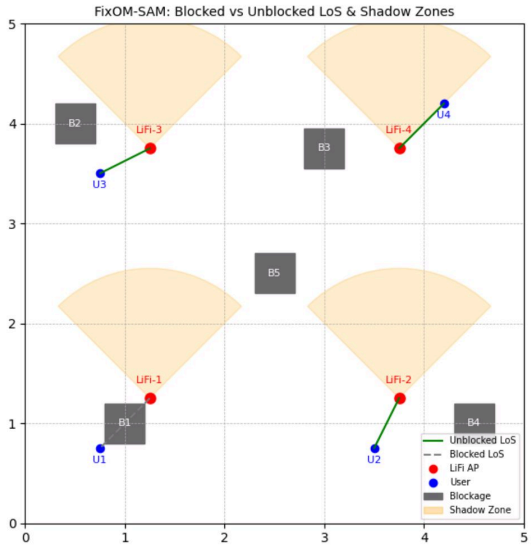

Figure 4.4: Simulation environment for blockage analysis in a $5\,\text{m} \times 5\,\text{m} \times 3\,\text{m}$ indoor Li-Fi setup.

4.4.1 FixOM Evaluation and Analysis

Figure 4.5 presents the FixOM performance. In Fig. 4.5(a), average channel gain declines with increasing obstruction. Figure 4.5(b) shows the cumulative distribution function (CDF) of user rates, where the probability of achieving 30 Mbps drops from 78% (no blockage) to 68% (with blockage). Finally, Fig. 4.5(c) reveals a 10% reduction in average user rate as user count increases.

In FixOM, blockages with radius $r_b \in [0.2, 0.5]\,\text{m}$ and height $H_b = 2.5\,\text{m}$ are placed within the room. Figure 4.5a illustrates the reduction in channel gain due to obstacles, showing a 10–20% degradation depending on blockage placement. CDF analysis in Fig. 4.5b shows that the probability of achieving a threshold rate of 30 Mbps decreases from 78% (no blockage) to 68% (with blockage). The average user rate decreases by approximately 10%, as shown in Fig. 4.5c, confirming the detrimental impact of static obstacles on Li-Fi performance.

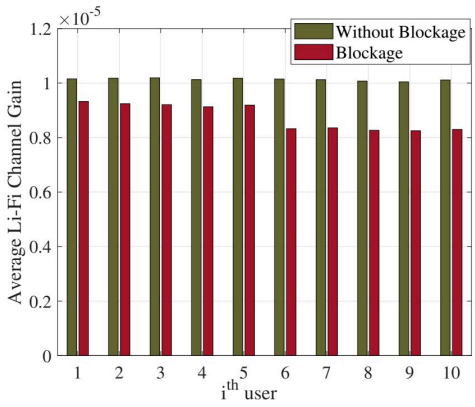

(a) Average channel gain variation.

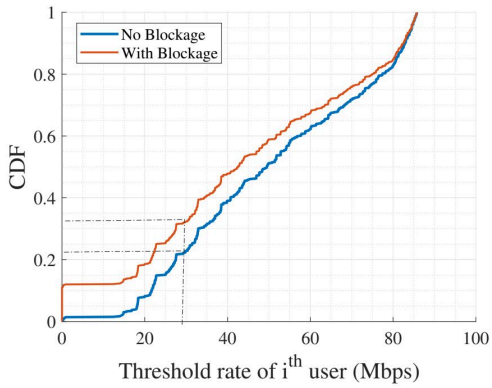

(b) CDF of user rate with/without blockage.

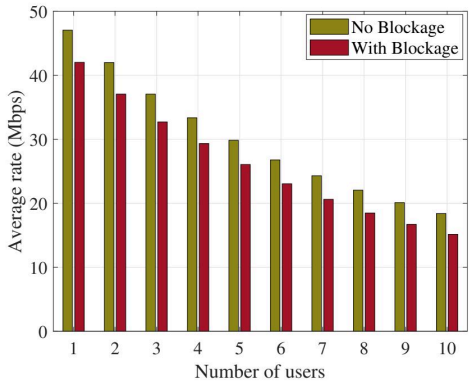

(c) Average rate for varying number of users.

Figure 4.5: Performance evaluation of the FixOM model under blockage and non-blockage scenarios: (a) variation of average channel gain, (b) CDF of achievable user rate, and (c) average rate versus number of users.

4.4.2 SAM Evaluation and Analysis

Figure 4.6 depicts the SAM-based performance. In Fig. 4.6(a), shadow regions are visualized to show partial and complete coverage zones. Figures 4.6(b)–(d) show that channel gain and achievable rate degrade gradually, demonstrating SAM's ability to model partial shadowing. As illustrated in Fig. 4.6(a), the shadow regions clearly demarcate blocked and partially blocked user areas. The channel gain degradation shown in Fig. 4.6(b) and the corresponding CDF and rate performance in Figs. 4.6(c)–(d) demonstrate the effect of both full and partial shadowing on Li-Fi performance.

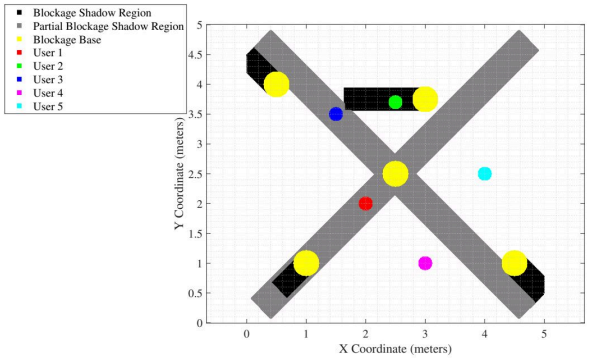

(a) Shadow regions induced by blockages and user locations.

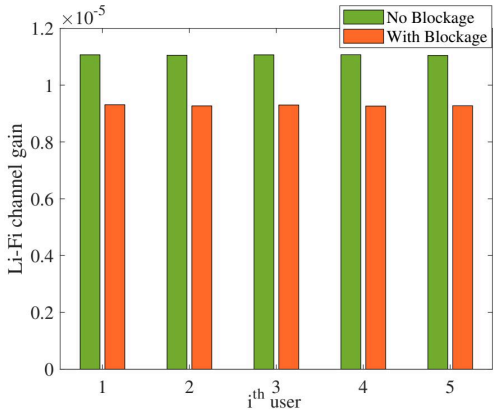

(b) Channel gain performance with and without blockage.

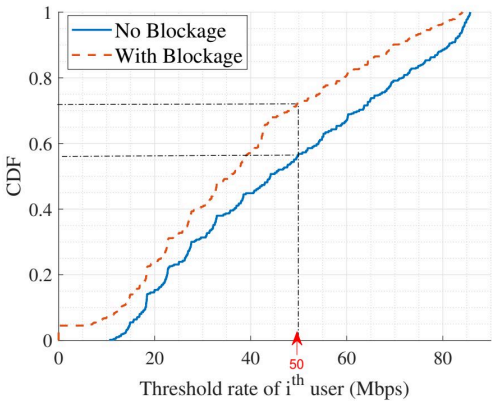

(c) CDF of user rate with and without blockage.

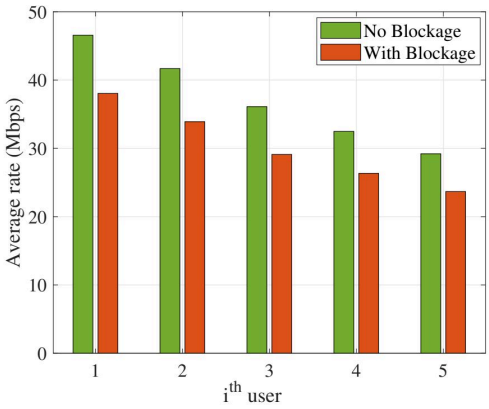

(d) Average user rate under blocked and unblocked scenarios.

Figure 4.6: Performance evaluation of the Shadow-Aware Model (SAM) under blockage and non-blockage conditions: (a) visualization of shadow regions and user locations, (b) channel gain variation, (c) rate distribution (CDF), and (d) average rate performance across users.

CDF plots in Fig. 4.6c show that at a threshold of 50 Mbps, the success probability drops from 72% (no blockage) to 56% (with shadowing). Similarly, Fig. 4.6d demonstrates a 10% drop in average data rate due to partial blockages. These results confirm SAM's ability to model partial shadow effects more accurately than FixOM.

At 50 Mbps threshold, the CDF in Fig. 4.6(c) indicates a drop from 72% to 56% success probability under blockage. This confirms that SAM provides a more realistic performance estimate than the deterministic FixOM.

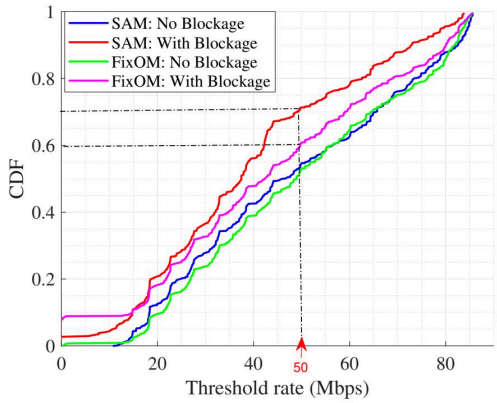

(a) CDF comparison of SAM and FixOM with and without blockage (small room).

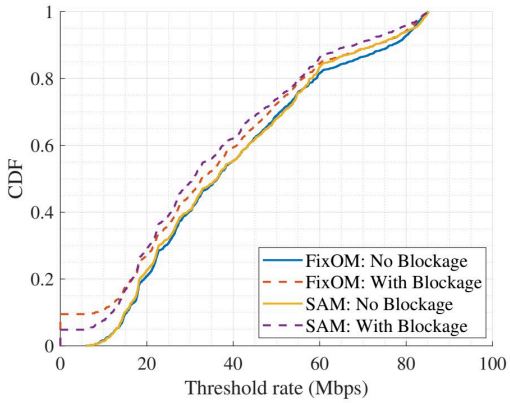

(b) CDF comparison of SAM and FixOM in a larger indoor environment.

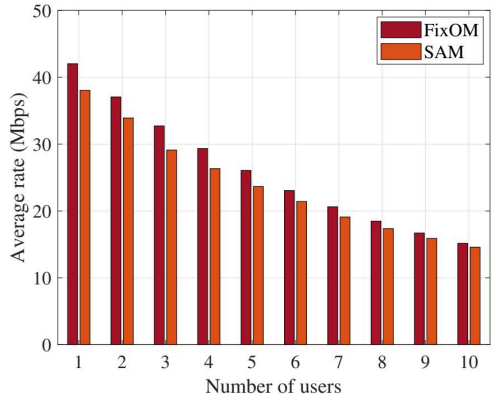

(c) Average rate comparison under blockage for smaller room (4 Li-Fi APs).

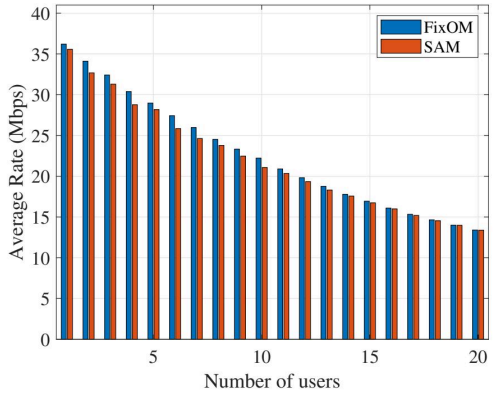

(d) Average rate comparison under blockage for larger room (8 Li-Fi APs).

Figure 4.7: Performance comparison between FixOM and SAM under different blockage conditions: (a) CDF in a small environment, (b) CDF in a large environment, (c) average rate for smaller dimensions, and (d) average rate for larger room dimensions.

4.4.3 Comparative Performance of FixOM and SAM

The comparison between FixOM and SAM is summarized in Fig. 4.7. CDF comparisons in Figs. 4.7(a)–(b) demonstrate that FixOM slightly overestimates achievable rates, while SAM reflects the performance degradation more accurately. Average rate comparisons in Figs. 4.7(c)–(d) further validate this observation.

As shown in Fig. 4.7(a)–(b), SAM demonstrates a higher probability of achieving lower data rates due to more accurate blockage modeling, while FixOM provides an optimistic

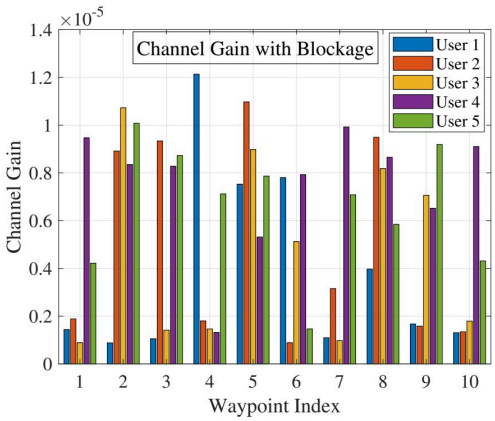

(a) Channel gain degradation under FixOM along user waypoints following the RWP mobility model.

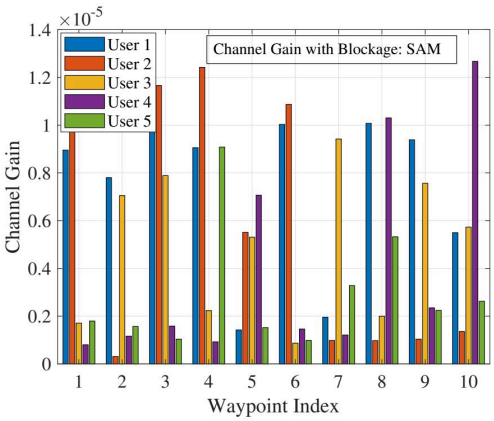

(b) Channel gain degradation under SAM along user waypoints following the RWP mobility model.

Figure 4.8: Comparison of channel gain degradation due to blockage along user trajectories following the RWP mobility model for (a) FixOM and (b) SAM frameworks.

performance estimate. Similarly, Figs. 4.7(c)–(d) illustrate that SAM predicts a slightly reduced average rate but reflects more realistic network behavior in both small and large-scale indoor environments.

4.4.4 Preliminary Evaluation Under Dynamic Blockage Scenarios

Dynamic blockage effects under user movement are illustrated in Fig. 4.8. As users move along trajectories, FixOM shows sharp channel gain drops (Fig. 4.8(a)), whereas SAM provides smoother gain variation (Fig. 4.8(b)) due to partial shadowing. This highlights SAM's advantage for modeling real-world environments.

To examine model robustness under mobility, we introduce dynamic blockage conditions using RWP mobility model. In this work, user mobility is modeled using the RWP model, where users move within a bounded indoor area by selecting random destinations and speeds. The user speed is assumed to be uniformly distributed within the range $v \in [v_{\min}, v_{\max}]$, and the pause time at each waypoint is denoted by T_p. After reaching a destination, the user pauses for T_p seconds before selecting a new random direction and speed. The movement area corresponds to the indoor Li-Fi coverage region considered in the simulation. Figures 4.8a

and 4.8b illustrate channel gain variation for FixOM and SAM respectively as users move along trajectories. FixOM exhibits abrupt gain drops due to its binary obstruction assumption, whereas SAM provides smoother, probabilistic variations corresponding to partial shadowing.

These dynamic analyses confirm that both models can be extended to handle user mobility and moving obstacles, paving the way for adaptive resource allocation strategies explored in the next chapter.

4.5 Summary

This chapter presented two complementary frameworks **FixOM** and **SAM** for modeling blockage and shadowing in Li-Fi networks. FixOM employs deterministic geometry to estimate complete LoS obstruction, providing a computationally efficient baseline for structured environments. SAM, on the other hand, introduces probabilistic modeling to account for partial shadowing, thereby offering more accurate performance prediction in complex and cluttered indoor spaces.

Through detailed simulation and evaluation, it was shown that SAM better captures realistic blockage behavior, while FixOM serves as an efficient worst-case estimator. Preliminary dynamic blockage analysis demonstrated both models' adaptability for user mobility scenarios.

It is observed that blockage performance in LiFi systems is highly sensitive to blockage density, blockage size (r_b), and the relative spatial positioning of users and obstacles. In particular, blockages located close to the LoS path significantly increase the probability of link disruption, thereby reducing link reliability. Additionally, the distance between the user and the AP influences the likelihood of blockage intersection, with longer links being more susceptible to obstruction. These observations indicate that spatial distribution and geometric characteristics of blockages play a dominant role in determining system performance, highlighting the importance of accurate blockage modeling for reliable LiFi network design.

The insights from this chapter form a crucial bridge between static blockage modeling and the **mobility- and orientation-aware Li-Fi framework** developed in Chapter 5, where user motion, device orientation, and adaptive AP selection are jointly considered to enhance link reliability and overall network performance.

Chapter 5

Mobility and Orientation-Aware Li-Fi Networks

Building upon the blockage and shadowing analysis from Chapter 4, this chapter investigates the impact of **user mobility and device orientation** on Li-Fi network performance. A dynamic **Orientation-Aware Mobility (OAM)-LiFiNet** framework is developed to optimize the SINR and throughput in multi-AP environments. Using the RWP mobility model, the framework adaptively adjusts user device orientation based on real-time channel and interference conditions, balancing line-of-sight preservation and interference mitigation. Simulation results demonstrate that OAM-LiFiNet significantly enhances network reliability and achieves up to 100 Mbps average throughput gain over baseline models, establishing a foundation for the cross-layer hybrid Li-Fi/Wi-Fi integration discussed in Chapter 6.

5.1 Challenges of User Mobility in Li-Fi

The Li-Fi system relies on optical LoS communication between the AP and the user's photodiode receiver. As analyzed in Chapter 4, blockages caused by static or dynamic obstacles can attenuate or disrupt the optical signal. However, even when the LoS path is not physically

obstructed, **user mobility and device rotation** can substantially affect channel gain, SINR, and link continuity.

When users move across overlapping AP coverage zones, the following challenges arise:

1. **Variable Channel Gain:** Movement alters the irradiance and incidence angles, changing received optical power.

2. **Interference Fluctuations:** Multi-AP environments introduce co-channel interference as users move closer to multiple transmitters.

3. **Orientation Misalignment:** The user device's FOV may deviate from the AP's beam direction, reducing link quality.

To mitigate these effects, orientation control is proposed as an additional degree of freedom. Adjusting the receiver's orientation dynamically can maintain strong LoS and suppress interference from neighboring APs. This motivates the development of the **OAM-LiFiNet** framework discussed in the next section.

5.2 Orientation-Aware Multi-AP Li-Fi Network (OAM-LiFiNet)

The proposed **OAM-LiFiNet** framework introduces adaptive orientation control for user devices in a mobile multi-AP Li-Fi environment. While traditional systems assume fixed receiver orientation, OAM-LiFiNet continuously evaluates SINR and adjusts device alignment to optimize throughput.

5.2.1 System Model and Motivation

The system setup, illustrated in Fig. 5.1, consists of k Li-Fi APs installed on the ceiling of an indoor area and N_u mobile users distributed on the floor plane. A central controller dynamically assigns each user to the AP offering the highest SINR.

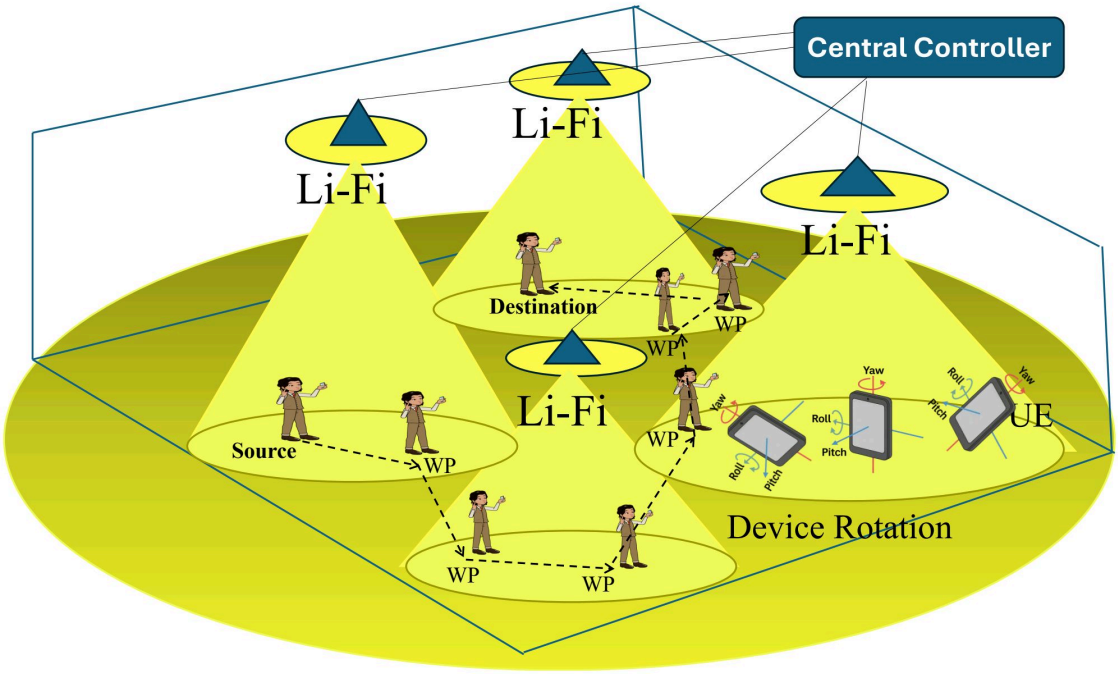

Figure 5.1: System model of a multi-AP Li-Fi network with user mobility and device orientation.

User movement follows the RWP model, which generates realistic trajectories across the indoor environment. Each user device is capable of rotation along yaw, pitch, and roll axes, as depicted in Fig. 5.2, influencing its FOV and the corresponding incidence angle ψ_{ij}.

5.2.2 SINR-Based Orientation Adjustment

The core objective of OAM-LiFiNet is to maximize the SINR at each user waypoint by adjusting device orientation. The instantaneous SINR received from AP j at user i is given by:

$$\gamma_{ij}^{LiFi} = \frac{(\mathbf{R}_{PD} H_{ij}^{LiFi} P_{opt}/\mathbf{K})^2}{N_{LiFi} B_{LiFi} + \sum_{\substack{l_\alpha \in l_j \\ \alpha \neq j}} (\mathbf{R}_{PD} H_{i\alpha}^{LiFi} P_{opt}/\mathbf{K})^2}. \tag{5.1}$$

In Eq. (5.1), $\mathbf{R}_{PD}$ denotes the responsivity of the photodetector (A/W), which converts the received optical power into an electrical signal. H_{ij}^{LiFi} represents the optical channel gain between the j-th AP and the i-th user, which depends on factors such as the distance between

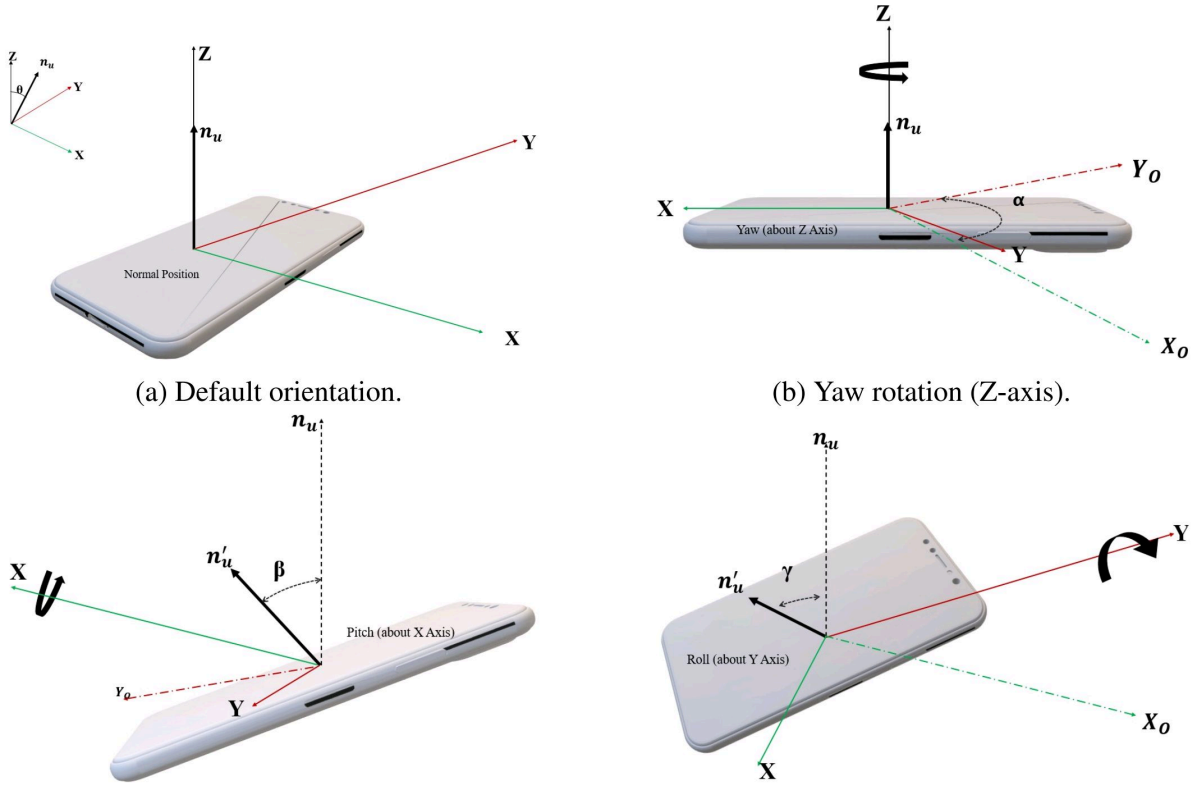

(a) Default orientation.

(b) Yaw rotation (Z-axis).

(c) Pitch rotation (X-axis).

(d) Roll rotation (Y-axis).

Figure 5.2: Orientation of user devices in 3D space.

the AP and the user, the angle of incidence, and the device orientation. P_{opt} is the transmitted optical power from the AP, and **K** is the optical-to-electrical conversion factor.

The numerator corresponds to the squared received electrical signal power from the serving AP j. The denominator consists of two components: thermal and shot noise, represented by $N_{LiFi}B_{LiFi}$, where N_{LiFi} is the noise power spectral density and B_{LiFi} is the system bandwidth; and the interference power from other LiFi APs operating on the same channel, given by the summation term over $l_\alpha \in l_j$, where $\alpha \neq j$.

The interference term captures the impact of neighboring APs whose signals overlap at the receiver, which is particularly significant in dense multi-AP indoor deployments. Since LiFi communication is based on intensity modulation and direct detection (IM/DD), the electrical signal is proportional to the square of the received optical power, leading to the squared terms in both the numerator and denominator.

Algorithm 1 Adaptive UE Orientation Process in OAM-LiFiNet

for each waypoint (WP) **do**
    Generate N_0 random orientations (α, β, γ)
    for each orientation **do**
        Compute γ_{ij}^{LiFi} and H_{ij}^{LiFi}
    end for
    if orientation improves SINR or both SINR and channel gain **then**
        Update device orientation
    else
        Retain current orientation
    end if
end for

This SINR formulation highlights the dependence of link quality on user orientation and position, as both directly influence the channel gain H_{ij}^{LiFi}. Therefore, optimizing device orientation can significantly improve SINR, which forms the basis of the proposed OAM-LiFiNet framework.

At each waypoint, N_0 random orientations are sampled. For each orientation, the SINR and channel gain are computed, and the orientation $\vec{n_u}'^*$ that maximizes SINR is selected:

$$\vec{n_u}'^* = \arg\max_{\vec{n_u}' \in \mathscr{O}} f(\gamma_{ij}^{LiFi}, H_{ij}^{LiFi}), \tag{5.2}$$

where $f(\gamma, H)$ is the joint decision function balancing interference reduction and channel preservation.

Algorithm 1 outlines the adaptive orientation process. This dynamic adjustment enables the device to orient toward APs when interference dominates, and remain fixed when LoS alignment provides sufficient performance.

5.3 Performance under User Mobility and Interference

It is important to note that the performance evaluation presented in this chapter assumes ideal LoS conditions without explicitly incorporating blockage and shadowing effects. While such

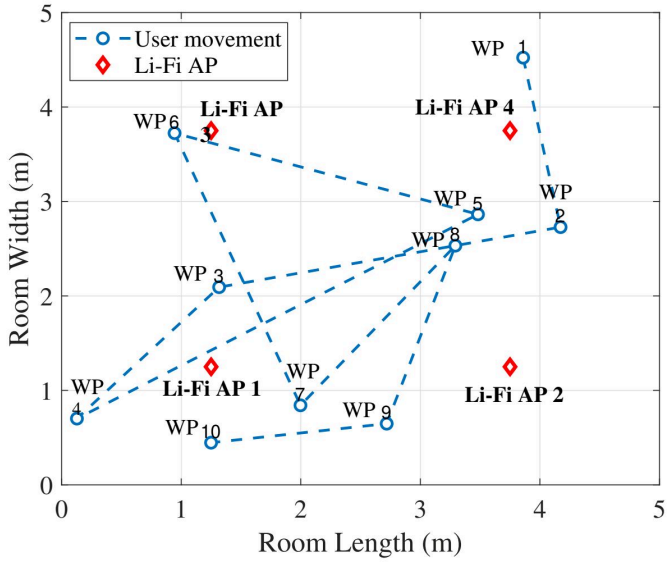

Figure 5.3: User trajectory with waypoints and ceiling-mounted AP locations.

effects are comprehensively modeled in Chapter 4 using the FixOM and SAM frameworks, the focus of this chapter is to isolate and analyze the impact of user mobility and device orientation on LiFi system performance.

Incorporating blockage-aware modeling into the orientation-aware framework is a promising direction for future work and is expected to further enhance the robustness of hybrid LiFi–WiFi systems.

5.3.1 System Architecture

To evaluate OAM-LiFiNet, a $5\,\text{m} \times 5\,\text{m} \times 3\,\text{m}$ indoor environment is simulated with four ceiling-mounted Li-Fi APs. The user moves along predefined waypoints, as shown in Fig. 5.3. Each AP operates at equal power, and interference arises from overlapping coverage zones.

Figure 5.4a shows SINR variations across waypoints with and without orientation. At waypoints such as WP2, WP3, and WP5, where inter-AP interference is significant, orientation improves SINR by up to 5 dB. However, at WP10 (directly under an AP), maintaining the unoriented position yields higher SINR due to stronger LoS gain.

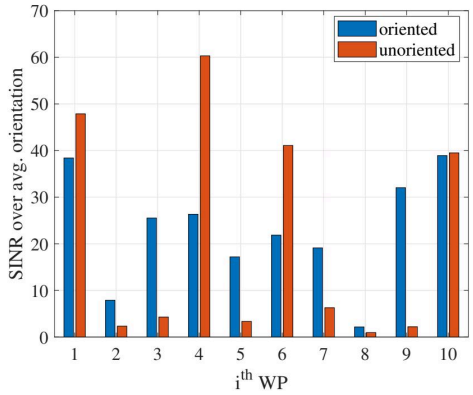

(a) SINR comparison at each waypoint with and without orientation.

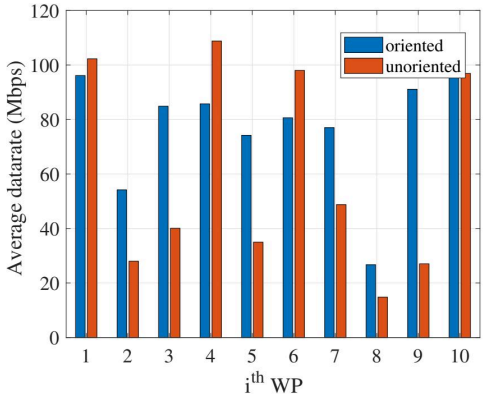

(b) Data rate comparison at each waypoint with and without orientation.

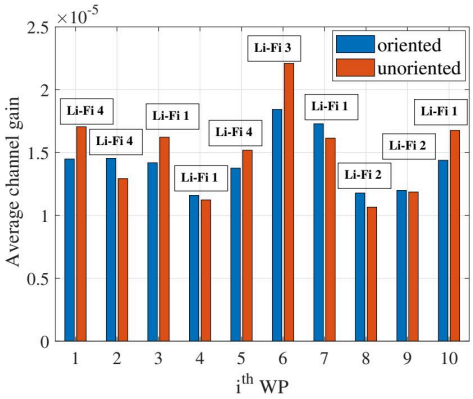

(c) Channel gain comparison under oriented and unoriented conditions.

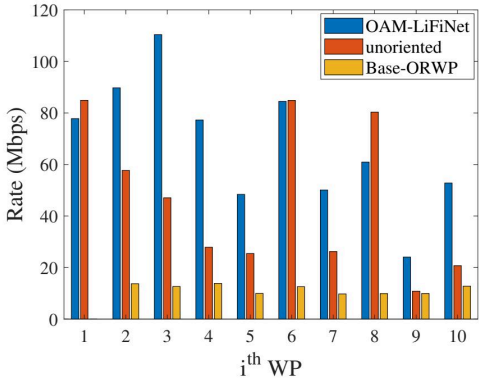

(d) Comparison of OAM-LiFiNet with baseline ORWP-based Li-Fi network.

Figure 5.4: Performance evaluation of OAM-LiFiNet: (a) SINR comparison, (b) Data rate comparison, (c) Channel gain analysis, and (d) Comparison with baseline ORWP-based Li-Fi network.

The resulting data rate comparison is presented in Fig. 5.4b, demonstrating that orientation improves throughput in interference-prone regions while maintaining stability in low-interference areas.

Similarly, Fig. 5.4c illustrates how channel gain varies across waypoints. Orientation can reduce LoS gain in some positions (e.g., WP6, WP10) but increases effective SINR elsewhere by mitigating interference.

Finally, Fig. 5.4d compares the proposed OAM-LiFiNet with baseline orientation models from [43, 44]. OAM-LiFiNet achieves an average throughput gain of up to 100 Mbps, validating the effectiveness of adaptive orientation decisions.

5.4 Discussion and Insights

The results highlight several key observations:

- **Mobility-induced SINR Variability:** As users move between AP coverage zones, SINR fluctuates due to geometric changes and overlapping illumination patterns.
- **Orientation as a Control Mechanism:** Controlled orientation mitigates interference in dense AP regions, yielding consistent data rate gains.
- **Trade-off between LoS and Interference Reduction:** Excessive orientation may weaken LoS reception, indicating the need for adaptive, not static, orientation strategies.

These findings confirm that mobility-aware orientation control is crucial for maintaining link stability in real-world Li-Fi deployments and can complement the blockage modeling approaches discussed in Chapter 4. Furthermore, they motivate the cross-layer adaptation strategies explored in Chapter 6, where Li-Fi and Wi-Fi systems are integrated for seamless coverage and robust throughput under diverse environmental conditions.

Practical Application Contexts: While the proposed orientation-aware framework assumes the ability to adapt device orientation for improved Li-Fi performance, it is important to recognize that such control may not always be feasible in all real-world scenarios. In everyday mobile usage, device orientation is often dynamic and user-driven, limiting the applicability of frequent orientation adjustments.

However, several practical application contexts exist where orientation-aware Li-Fi networking is both realistic and beneficial. These include stationary or semi-static scenarios such as office environments, where devices (e.g., laptops or tablets) are placed on desks; augmented

and virtual reality (AR/VR) applications, where head-mounted displays naturally maintain a stable orientation; and industrial or healthcare environments, where devices are mounted or used in controlled positions. Additionally, autonomous systems such as robots and IoT devices can incorporate orientation-aware optimization more effectively due to predictable movement patterns.

Therefore, the proposed OAM-LiFiNet framework is particularly suited for such controlled or semi-controlled environments, where orientation adaptation can be leveraged to significantly enhance link reliability and throughput.

5.5 Summary

This chapter presented an **Orientation-Aware Mobility (OAM)-LiFiNet** framework for enhancing throughput and reliability in mobile multi-AP Li-Fi networks. By dynamically optimizing user device orientation based on real-time SINR and channel gain, OAM-LiFiNet effectively balances LoS preservation and interference reduction.

Simulation results show up to a 100 Mbps throughput improvement compared to baseline models, highlighting the importance of adaptive orientation in dense indoor Li-Fi systems. The insights gained here establish a direct link between static blockage modeling (Chapter 4) and the **cross-layer hybrid Li-Fi/Wi-Fi coordination** approach detailed in Chapter 6, ensuring robust and flexible connectivity in next-generation indoor wireless environments.

It is further observed that the performance of the proposed OAM-LiFiNet framework is strongly influenced by device orientation, user mobility, and the resulting SINR variations. In particular, misalignment between the transmitter and receiver significantly reduces the optical channel gain, thereby degrading throughput and link reliability. Additionally, user mobility introduces dynamic fluctuations in channel conditions, leading to frequent variations in SINR. These observations highlight that orientation control and mobility-aware adaptation are critical

parameters for maintaining stable and high-performance LiFi communication in dynamic indoor environments.

Chapter 6

Hybrid LiFi–WiFi Networks (HLWNs)

This chapter advances the discussion from Li-Fi-only networks (Chapter 5) to the realization and adaptive enhancement of **Hybrid Li-Fi/Wi-Fi Networks (HLWNs)**. First, a proof-of-concept implementation of a hybrid testbed is presented [4], demonstrating the feasibility of integrating Li-Fi and Wi-Fi to achieve higher throughput, lower latency, and reduced packet loss under user mobility. Subsequently, since Li-Fi's performance is strongly affected by mobility and device orientation, the same effects are investigated within HLWN through analytical and simulation-based modeling. To mitigate these challenges, an **Orientation-Aware Mobility-enabled Hybrid Li-Fi/Wi-Fi Network [12]** is developed, featuring SINR-based link selection and adaptive orientation control. Together, these works validate hybrid optical–RF communication as a practical and adaptable solution for next-generation indoor wireless systems.

6.1 Motivation and Background

In Chapter 5, it was shown that user mobility and receiver orientation significantly influence the performance of Li-Fi networks due to their strong dependence on LoS propagation. While Li-Fi provides high throughput and spatial reuse, its limited coverage area and susceptibility to shadowing restrict practical scalability. Conversely, Wi-Fi offers broad coverage but lower

spectral efficiency. A natural approach is to integrate the two technologies into a **Hybrid Li-Fi/Wi-Fi Network** , enabling users to benefit from both high-speed optical links and reliable RF connectivity.

This hybrid concept, experimentally validated in [4], forms the basis for this chapter. It also motivates the need to analyze how Li-Fi-specific impairments such as mobility and orientation extend to HLWN, leading to the adaptive orientation- and mobility-aware framework proposed in [12].

6.2 HLWN

The exponential growth of mobile and IoT devices has intensified the demand for high-speed indoor wireless communication. However, the finite RF spectrum used by Wi-Fi is increasingly congested, leading to interference, latency, and reduced throughput commonly referred to as the "spectrum crunch." To overcome this limitation, **VLC**, or **Li-Fi**, has emerged as a complementary wireless solution that utilizes the optical spectrum for data transmission [84]. By operating in the visible and infrared bands, Li-Fi offers vast unlicensed bandwidth and the potential for multi-gigabit-per-second data rates, far exceeding the capacity of traditional RF-based systems [85].

A Li-Fi AP typically uses light-emitting diodes (LEDs) for downlink transmission and PDs for reception. At the user end, a Li-Fi dongle equipped with an IR LED and PD enables duplex communication through optical uplink and downlink channels [86]. While Li-Fi can deliver very high throughput, its coverage area is limited due to the directional and LoS nature of visible light propagation. Conversely, Wi-Fi offers broader coverage but suffers from lower spectral efficiency and potential RF interference.

To combine their respective advantages, a **HLWN** has been proposed [87], wherein Li-Fi and Wi-Fi coexist to jointly serve users based on link quality and location. Such integration provides wide coverage through Wi-Fi and high-capacity optical links via Li-Fi, ensuring

improved overall throughput and reliability. Since both operate in non-overlapping frequency domains, their coexistence minimizes interference and allows seamless link switching according to the QoS requirements. Previous studies have demonstrated resource allocation and cooperative link aggregation techniques [36, 52, 53, 60, 88, 89] that significantly enhance user experience in hybrid environments.

The global demand for wireless data is projected to increase several-fold in the coming decade [90], making such hybrid integration a key enabler of future indoor networks. By efficiently utilizing both optical and RF resources, HLWNs offer a practical path toward sustainable high-capacity wireless communication.

6.2.0.1 HLWN System Model

The general architecture of an HLWN is illustrated in Fig. 6.5. The network comprises p Li-Fi and n Wi-Fi APs, all connected via Ethernet to a centralized controller (CC) or network switch that manages user association and traffic flow. The controller receives data from a server or backhaul link and distributes it to the respective APs.

Each Li-Fi AP contains an optical transmitter (LED array) and receiver (PD), while user devices connect through Li-Fi dongles with both transmission (IR) and reception (visible light) capabilities. When a user remains within a Li-Fi AP's FOV, communication occurs entirely through the optical channel. If the user moves beyond the Li-Fi coverage or experiences link blockage, a seamless handover to the Wi-Fi AP ensures uninterrupted service.

For modeling and simulation, we consider an indoor area of size $L \times W \times H$ m^3 (Fig. 6.5). p Li-Fi APs are symmetrically placed at the ceiling of the room, each covering one quadrant, while n Wi-Fi APs are positioned centrally to ensure complete RF coverage. User positions follow a uniform random distribution. A CC [71] coordinates access and manages hybrid handovers between Li-Fi and Wi-Fi APs. The subsequent subsection outlines the analytical channel models for both links, which serve as the basis for hybrid network evaluation.

6.2.1 Channel Modeling in HLWN

To analytically evaluate the performance of the hybrid Li-Fi/Wi-Fi network, the individual link characteristics of both technologies are modeled using well-established channel formulations. The Li-Fi component follows the LoS optical channel model presented in Chapter 2, while the Wi-Fi link is modeled using a standard RF path-loss–based formulation. Together, these channel models allow accurate estimation of received power, SINR, and achievable throughput for hybrid user associations.

6.2.2 Li-Fi Channel Modeling

The impulse response of Li-Fi channel is modeled between the Li-Fi AP j and user i as [14]:

$$H_{i,j}^{Li-Fi} = \frac{(m+1)A_{PD}}{2\pi d_{i,j}^2} \cos^m\left(\phi_{i,j}\right) \cos\left(\psi_{i,j}\right) g_c\left(\psi_{i,j}\right) g_f \tag{6.1}$$

where, $d_{i,j}$ represents the Euclidean distance between the AP j and user i. The irradiance angle is denoted as $\phi_{i,j}$, while the incidence angle is represented by $\psi_{i,j}$. The physical area of the photo-detector is designated as A_{PD}. We use g_f to denote the optical filter gain, and concentrator gain as g_c. Further, we introduce the parameter m to indicate the Lambertian order, as defined in [14].

Further, the received SINR at PD from Li-Fi AP is expressed as [14]:

$$\gamma_{i,j}^{Li-Fi} = \frac{\left(R_{PD} H_{i,j}^{Li-Fi} P_{\text{opt}}/k\right)^2}{N_{\text{Li-Fi}} B_{\text{Li-Fi}} + \sum_{\beta \neq j} \left(R_{PD} H_{i,\beta}^{Li-Fi} P_{opt}/k\right)^2}, \tag{6.2}$$

where R_{PD} represents the PD responsivity, and k signifies optical-to-electrical power conversion coefficient. Furthermore, P_{opt} denotes the transmitted power from Li-Fi AP. We define N_{Li-Fi} as the power spectral density (PSD) of noise, while B_{Li-Fi} stands for the channel bandwidth (BW) associated with each Li-Fi AP.

In Eq. (6.2), the numerator represents the received electrical signal power from the serving Li-Fi AP j. The denominator consists of two components: noise power and inter-cell interference.

The first term, $N_{Li-Fi}B_{Li-Fi}$, represents the total noise power at the receiver, where N_{Li-Fi} is the noise power spectral density (including thermal and shot noise), and B_{Li-Fi} is the system bandwidth.

The second term represents the aggregate interference from all other Li-Fi APs operating on the same channel. The summation term $\sum_{\beta \neq j} \left(R_{PD} H_{i,\beta}^{Li-Fi} P_{opt}/k \right)^2$ accounts for the received electrical interference power from neighboring APs β, excluding the serving AP j.

This interference arises due to overlapping coverage areas in multi-AP indoor deployments, where signals from adjacent APs contribute to degradation in link quality. The impact of this term becomes more significant in dense Li-Fi networks.

Since Li-Fi systems employ intensity modulation and direct detection (IM/DD), the received electrical signal power is proportional to the square of the received optical power. This results in the squared terms appearing in both the desired signal and interference components.

Thus, the SINR formulation captures the combined effect of useful signal power, noise, and interference, and plays a critical role in evaluating link performance in hybrid Li-Fi/Wi-Fi networks.

6.2.3 Wi-Fi Channel Modeling

For indoor RF propagation, the path loss model has a slope of 2 and 3.5 upto and after the breaking-point distance, respectively [91]. The path loss can be written as

$$L(d) = \begin{cases} L_{fs}(d) + X_s, & d \leq d_{BP} \\ L_{fs}(d) + 35log_{10}(d/d_{BP}) + X_s, & d > d_{BP}. \end{cases} \tag{6.3}$$

Here, X_s denotes a Gaussian random variable with zero mean and standard deviation of σ. The free space path loss, denoted as $L_{fs}(.)$, is expressed as follows:

$$L_{fs}(d) = 20log_{10}(d) + 20log_{10}(f_c) - 147.5, \tag{6.4}$$

here f_c signifies the carrier frequency. The Wi-Fi channel multipath propagation is modeled as follows:

$$H_{i,j}^{Wi-Fi} = \sqrt{\frac{K}{K+1}} e^{j\Theta} + \sqrt{\frac{1}{K+1}} X_g, \tag{6.5}$$

where X_g signifies a random variable of complex Gaussian distribution with a mean of zero and variance of 1, and Θ represents the arrival or departure angle of the LOS component. In (6.5), the parameter K denotes the Ricean factor, with K=1 before and K =0 after d_{BP}. The gain of Wi-Fi channel concerning user i is modeled as described in [14]:

$$G_{i,j}^{Wi-Fi} = \left| H_{i,j}^{Wi-Fi} \right|^2 10^{-\frac{PL\left(d_{i,j}\right)}{10}}, \tag{6.6}$$

where $PL(d_{i,j})$ represents pathloss according to the Wi-Fi multipath propagation model. The SNR between user i and Wi-Fi AP j is computed as [14]:

$$\gamma_{i,j}^{Wi-Fi} = \frac{G_{i,j}^{Wi-Fi} P_{Wi-Fi}}{N_{Wi-Fi} B_{Wi-Fi}}. \tag{6.7}$$

Where P_{Wi-Fi} represents the transmit power, N_{Wi-Fi} and B_{Wi-Fi} denote noise PSD and BW of Wi-Fi AP, respectively.

6.2.4 Data rate calculation

The data rate received by the user i from Wi-Fi AP is expressed as:

$$R_{Wi-Fi} = B_{Wi-Fi} \log_2(1 + \gamma_{i,w}^{Wi-Fi}), \tag{6.8}$$

where $\gamma_{i,j}^{Wi-Fi}$ is SNR of i^{th} user connected to Wi-Fi AP j; $j = 1,\ldots,n+p$.
It is important to note that the channel gain $H_{i,j}^{Wi-Fi}$ and the resulting SNR $\gamma_{i,j}^{Wi-Fi}$ are random variables due to small-scale fading effects.

To obtain statistically meaningful results, Monte Carlo simulations are employed. In each iteration, the channel coefficients are randomly generated according to the Rician fading model, and the corresponding SNR and data rate are computed. The final performance metrics are obtained by averaging over 10,000 independent realizations, ensuring convergence and accuracy of the results.

The capacity of the users connected to Li-Fi AP is calculated as follows [92]:

$$R_{Li-Fi} = \frac{B_{Li-Fi}}{2}\log_2(1+\frac{6}{\pi e}\gamma_{i,j}^{Li-Fi}), \tag{6.9}$$

where B_{Li-Fi} denotes the bandwidth of each Li-Fi AP. $\gamma_{i,j}^{Li-Fi}$ is SINR between user i and Li-Fi AP j.

6.2.4.1 Hybrid Link Selection and Throughput Evaluation

In the hybrid system, each user dynamically selects between Li-Fi and Wi-Fi based on instantaneous SINR values:

$$\gamma_i^{HLWN} = \max\left\{\max_{j\in\mathscr{L}}(\gamma_{ij}^{Li-Fi}), \max_{j\in\mathscr{W}}(\gamma_{ij}^{Wi-Fi})\right\}, \tag{6.10}$$

where $\mathscr{L}$ and $\mathscr{W}$ represent the sets of available Li-Fi and Wi-Fi APs, respectively. The achievable data rate for user i is given in (6.8) and (6.9). This formulation provides a unified performance metric for hybrid access selection.

The combined channel model enables the evaluation of both physical and network-level metrics such as average throughput, coverage probability, and handover frequency. When users remain under Li-Fi coverage, the high optical SINR yields higher throughput. However, under mobility or orientation misalignment, the effective optical channel gain decreases, triggering

vertical handover to Wi-Fi. This analytical basis provides the foundation for the performance comparison and experimental validation presented in the next section.

6.3 Proof-of-Concept Demonstration of HLWN

To validate the feasibility of the proposed Hybrid Li-Fi/Wi-Fi Network, a real-time proof-of-concept testbed was implemented at IIIT-Delhi [4, 5]. This section presents the hardware setup, system operation, and experimental performance evaluation of the hybrid network under both static and mobile user conditions. The testbed complements the analytical and simulation-based analyses discussed in earlier sections.

6.3.1 Testbed Design and Implementation

The experimental setup, shown in Fig. 6.1, consists of three ceiling-mounted Li-Fi APs and one Wi-Fi AP interconnected through a Gigabit Ethernet switch and a central server. Each Li-Fi AP operates at 36 V and includes a panel of 24 visible-light LEDs for downlink transmission and an IR LED for uplink. When a user device enters the FOV of a Li-Fi AP, a sync LED on the AP blinks to indicate active communication. The user device connects to the Li-Fi AP via a Li-Fi dongle containing a photodiode for downlink reception and an IR LED for uplink transmission.

The Wi-Fi AP operates in the 2.4 GHz band using a 12 V power adapter and is connected to the same Ethernet switch. All APs communicate with a central controller that manages link selection and handover between Li-Fi and Wi-Fi APs based on the RSS or SNR. When the optical signal strength at the photodiode drops below a predefined threshold, the controller triggers a vertical handover (VHO) from Li-Fi to Wi-Fi, ensuring uninterrupted data transmission.

During testing, live 4K video streaming was transmitted from the server to the client device to assess connectivity continuity. As the user moved across the room, the client experienced smooth switching between Li-Fi and Wi-Fi APs without disruption to video playback or packet

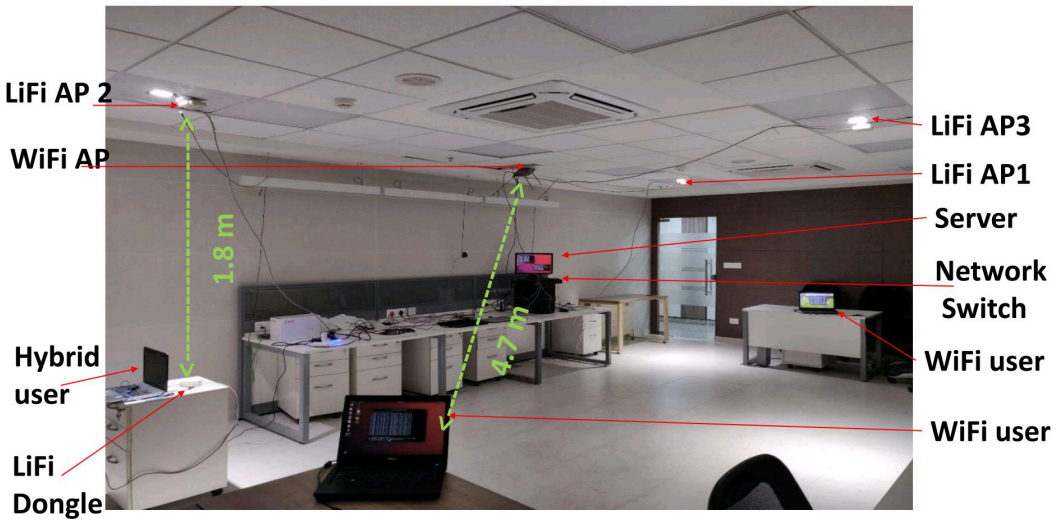

Figure 6.1: Experimental setup of the hybrid Li-Fi/Wi-Fi network testbed [4].

Table 6.1: Testing scenarios for user connection and AP switching status

Scenario	User Connection	AP Status	User Mobility Status
Hybrid Li-Fi/Wi-Fi Network	One user connected to Li-Fi AP, one user connected to Wi-Fi AP	3 Li-Fi APs = ON, Wi-Fi AP = ON	Hybrid user – Mobile; Wi-Fi user – Static
	One user connected to Li-Fi AP, two users connected to Wi-Fi AP		Hybrid user – Mobile; Wi-Fi users – Static
Standalone Wi-Fi Network	Two users connected to Wi-Fi AP	3 Li-Fi APs = OFF, Wi-Fi AP = ON	One Wi-Fi user – Mobile; one – Static
	Three users connected to Wi-Fi AP		One Wi-Fi user – Mobile; two – Static

loss, as illustrated in Fig. 6.2 and 6.3. The transition between the two technologies was verified using ping response logs and network monitoring tools.

6.3.2 Experimental Evaluation

The performance of the hybrid network was evaluated for both static and mobile users. The configuration used three Li-Fi APs ($p = 3$) and one Wi-Fi AP ($n = 1$), all linked to a single server through a Gigabit switch. Users connected dynamically to either Li-Fi or Wi-Fi APs depending on signal conditions, as shown in Fig. 6.1.

The experimental evaluation covered three key performance metrics: throughput, latency, and packet loss, all measured under multiple user configurations as detailed in Table 6.1. In the experiments, one user remained stationary under a Wi-Fi AP, while another moved across Li-Fi coverage zones, switching between Li-Fi and Wi-Fi connections as needed.

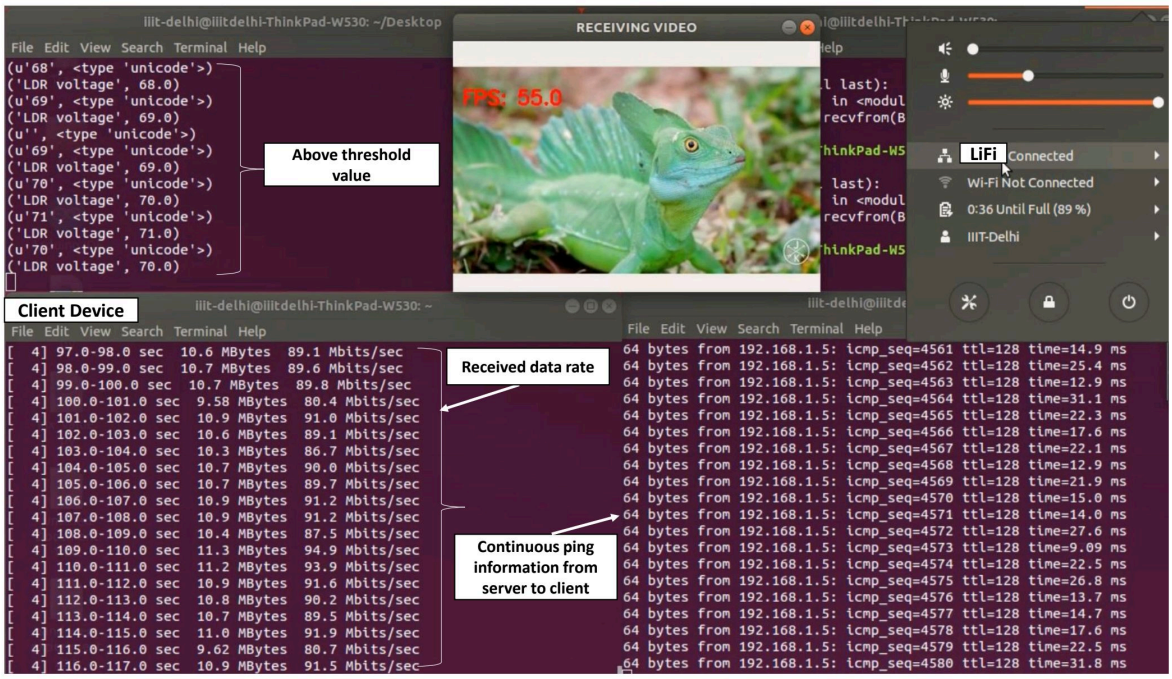

(a) Client-side before handover (Li-Fi active).

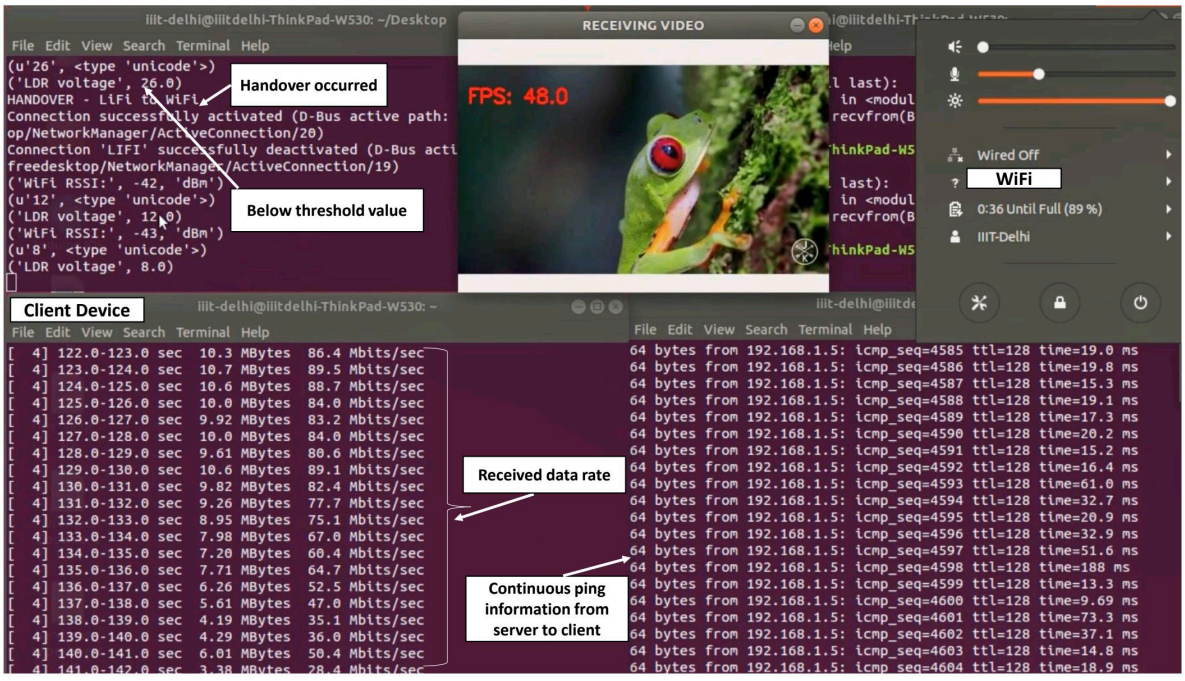

(b) Client-side after handover (Wi-Fi active).

Figure 6.2: Client-side transition from Li-Fi to Wi-Fi during handover.

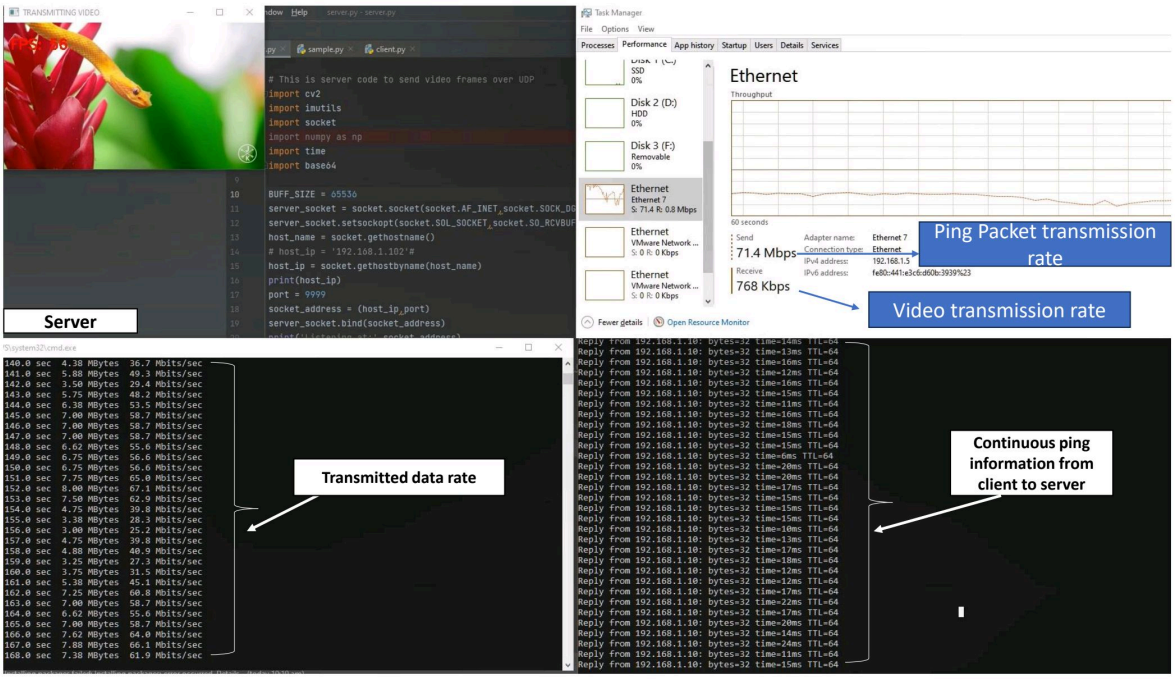

(a) Server-side streaming during hybrid operation.

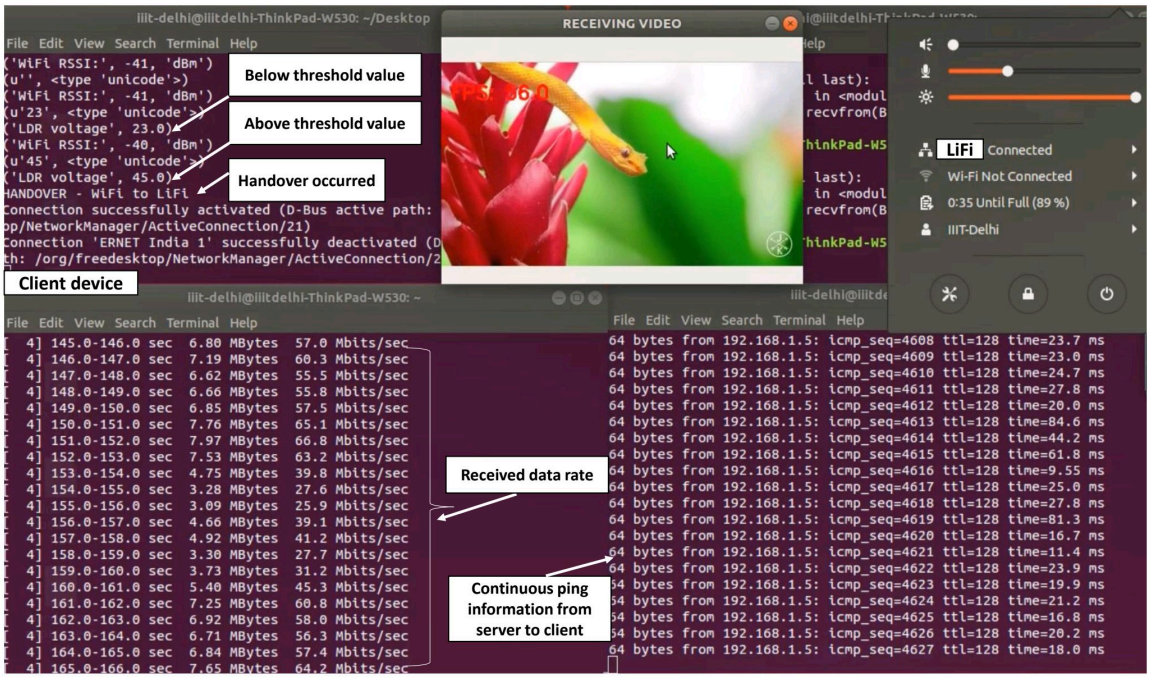

(b) Client-side reception during hybrid operation.

Figure 6.3: Continuous video transmission and reception in hybrid Li-Fi/Wi-Fi network.

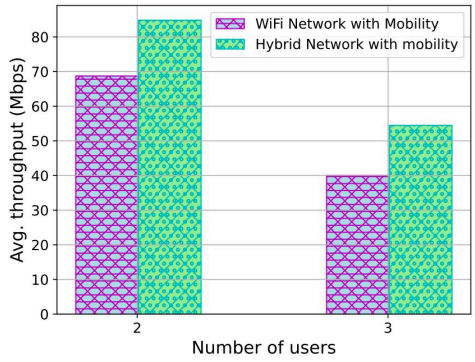

(a) Average throughput performance.

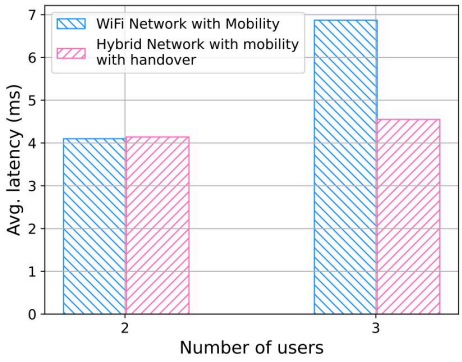

(b) Average latency performance.

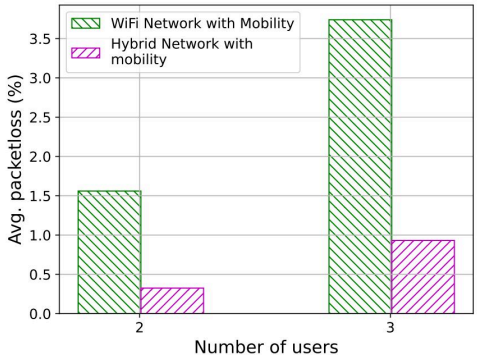

(c) Average packet loss performance.

Figure 6.4: Experimental evaluation of the hybrid Li-Fi/Wi-Fi network showing (a) throughput, (b) latency, and (c) packet loss performance under varying user conditions. The hybrid configuration demonstrates superior throughput and lower latency and packet loss compared to the standalone Wi-Fi network.

6.3.2.1 Average Throughput

The average throughput performance was measured for Wi-Fi-only and hybrid HLWN setups. As illustrated in Fig. 6.4a, the hybrid network achieved throughput improvements of 23.44% and 36.13% for two-user and three-user scenarios, respectively, compared to Wi-Fi-only operation. The gain arises from load distribution between optical and RF channels, allowing users to utilize Li-Fi bandwidth when available and reducing contention on the Wi-Fi link.

6.3.2.2 Average Latency

The average latency results, shown in Fig. 6.4b, reveal that for two-user cases, both hybrid and Wi-Fi-only configurations exhibit similar performance. However, for the three-user scenario, the hybrid HLWN achieves 33.33% lower latency due to offloading part of the data traffic to the Li-Fi APs, thereby reducing contention among Wi-Fi users.

6.3.2.3 Average Packet Loss

Packet loss performance, presented in Fig. 6.4c, demonstrates a substantial reduction in the hybrid configuration compared to the Wi-Fi-only network. The HLWN achieved 73.51% and 74.32% lower packet loss for two-user and three-user cases, respectively. This improvement is primarily attributed to the reduced collision probability due to traffic distribution across Li-Fi and Wi-Fi links.

It is important to note that the results presented in Fig. 6.3 are obtained from experimental measurements on the developed hybrid LiFi–WiFi testbed. The performance metrics, including throughput and latency, are measured using the *iperf* tool under different user scenarios.

For each configuration, multiple measurement runs are conducted, and the reported values represent the average performance, capturing real-time system behavior under practical deployment conditions.

6.3.3 Experimental Observations and Insights

The hybrid testbed successfully demonstrated uninterrupted communication and seamless handover between Li-Fi and Wi-Fi networks during mobility. Continuous 4K video streaming confirmed real-time switching lower packet loss or service interruption. The experimental results validate that HLWN provides:

- Higher throughput due to parallel optical and RF channels.
- Lower latency through distributed data transmission.

- Significantly reduced packet loss and improved reliability.
- Seamless vertical handover maintaining QoS for mobile users.

These outcomes establish the practical viability of hybrid optical–RF networks and form the basis for subsequent simulation-based and mobility-aware optimization studies.

6.3.4 Simulation-Based Evaluation

To complement the experimental results and validate scalability under controlled conditions, a detailed simulation-based evaluation of the proposed HLWN was performed. The same channel models for Li-Fi and Wi-Fi, as discussed in Sections 6.2.1, is used to ensure analytical consistency between experimental and simulated analyses.

6.3.4.1 Simulation Setup

We consider a typical indoor room of dimensions $5 \times 5 \times 3$ m^3, as illustrated in Fig. 6.5. Four Li-Fi APs are symmetrically placed on the ceiling, each positioned at the center of a quadrant, while a single Wi-Fi AP is mounted at the center of the ceiling. User locations are generated following a uniform random spatial distribution to emulate realistic deployment conditions. A central controller or network controller [71] manages link association and handover between Li-Fi and Wi-Fi APs based on the instantaneous SINR and RSS values.

The simulation parameters for both Li-Fi and Wi-Fi links are listed in Tables 6.2 and 6.3, respectively. The primary objective of the simulation is to validate the observed experimental trends by analyzing the average throughput behavior of the hybrid network under varying user densities and comparing it with standalone Li-Fi and Wi-Fi systems.

6.3.4.2 Li-Fi and Wi-Fi Channel Reference Models

The Li-Fi optical channel gain and SINR expressions are derived from the LoS model presented in Chapter 2, while the Wi-Fi channel follows the indoor path-loss and fading model described

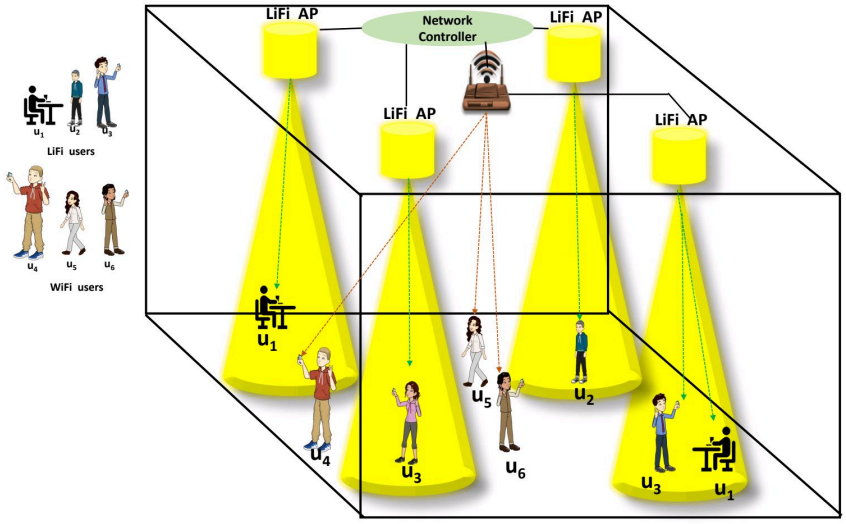

Figure 6.5: System model used for simulation of the hybrid Li-Fi/Wi-Fi network.

earlier in Section 6.2.1. These formulations collectively capture realistic indoor propagation dynamics for both optical and RF links. User association decisions are made based on the maximum instantaneous SINR, ensuring that each user connects to the most favorable access link available.

6.3.4.3 Performance Evaluation

The simulated spatial SNR map for the Li-Fi APs is shown in Fig. 6.6. The SNR peaks near the center of each quadrant, corresponding to the Li-Fi AP locations, and gradually decreases toward the boundaries due to the Lambertian radiation pattern. As users move out of a Li-Fi coverage zone, the central controller seamlessly transitions them to the Wi-Fi AP, maintaining continuous connectivity across the hybrid network.

6.3.4.4 Average Throughput Analysis

The average throughput performance for different user counts in the hybrid, Li-Fi-only, and Wi-Fi-only networks is depicted in Fig. 6.7a. The throughput gradually decreases with increasing user density due to bandwidth sharing, as expected. However, the hybrid configuration consistently outperforms both standalone systems because users dynamically exploit both optical and

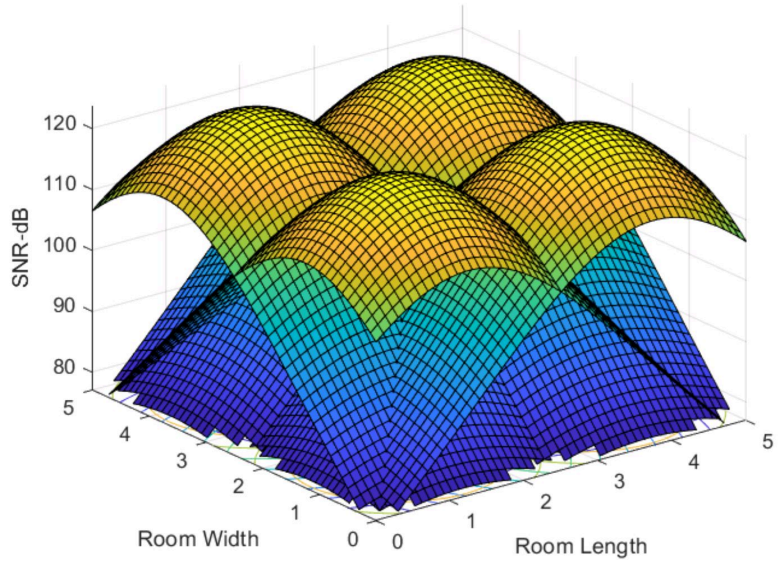

Figure 6.6: Simulated SNR distribution for four Li-Fi APs on the ceiling in the hybrid network.

RF resources. For the three-user case shown in Fig. 6.7b, the hybrid network demonstrates significantly higher aggregate throughput, corroborating experimental observations.

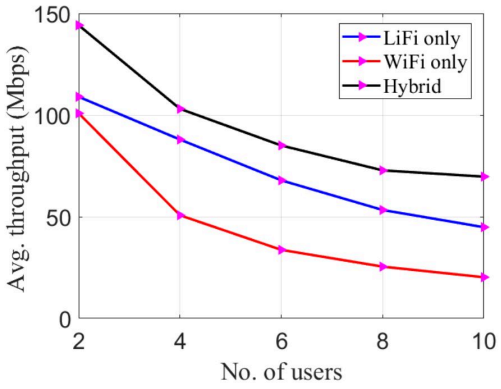

(a) Average throughput performance for varying numbers of users in hybrid and standalone networks.

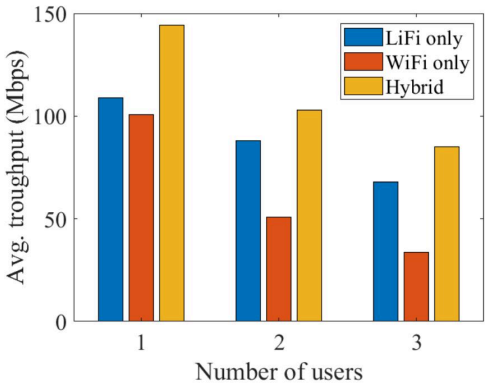

(b) Average throughput performance for a three-user hybrid Li-Fi/Wi-Fi system.

Figure 6.7: Simulated average throughput performance of the hybrid Li-Fi/Wi-Fi network: (a) variation with increasing number of users and (b) performance illustration for a three-user configuration.

6.3.4.5 Discussion and Correlation with Experimental Results

The simulation results closely align with the testbed observations discussed in Section 6.3.2. The hybrid configuration consistently achieves higher throughput and improved reliability compared to Wi-Fi-only operation. As user density increases, throughput declines in all setups due to shared bandwidth, but the HLWN maintains superior performance due to dynamic link adaptation and distributed traffic management. These results confirm the practical benefits of hybrid optical–RF integration under both static and mobile conditions.

Furthermore, the simulated throughput trend validates the experimental gains of approximately 23–36% improvement in throughput, 33% lower latency, and over 70% reduction in packet loss. Hence, the combined experimental–simulation study provides a robust verification of the proposed HLWN architecture and its efficiency in heterogeneous indoor environments.

6.3.4.6 Parameter Summary

The Li-Fi and Wi-Fi simulation parameters used are summarized below for reference.

Table 6.2: Parameters of Li-Fi channel model [13, 14]

Channel Parameter	**Symbol**	**Value**
Height of AP from user level	h	2.15 m
Area of photodiode	A_{PD}	1 cm^2
Optical filter gain	g_{filter}	1
Half-intensity angle	$\theta_{1/2}$	30°
Field of view (FOV)	ϕ_{max}	60°
Optical–electrical conversion factor	k	1
PD responsivity	R_{PD}	0.53 A/W
Li-Fi AP optical power	P_{opt}	3 W
Bandwidth	$B_{\text{Li-Fi}}$	40 MHz
Noise PSD	$N_{\text{Li-Fi}}$	-210 dBm/MHz

The simulation study verifies that HLWN effectively combines the high throughput of Li-Fi with the wide coverage of Wi-Fi, achieving improved overall system performance and robustness against user mobility. These findings substantiate the real-time testbed outcomes and establish a foundation for the mobility- and orientation-aware optimization framework

Table 6.3: Parameters of Wi-Fi channel model [13, 14]

Channel Parameter	**Symbol**	**Value**
Carrier frequency	f_c	2.4 GHz
Transmit power	$P_{\text{Wi-Fi}}$	20 dBm
Bandwidth	$B_{\text{Wi-Fi}}$	20 MHz
Noise PSD	$N_{\text{Wi-Fi}}$	-75 dBm/MHz

developed in Chapter 7, where adaptive link selection strategies are explored to further enhance hybrid network efficiency.

6.4 Orientation-Aware Mobility-Enabled Hybrid Li-Fi/Wi-Fi Network

6.4.1 System Model

Building upon the proof-of-concept demonstration of the Hybrid Li-Fi/Wi-Fi Network presented in the previous section, this work extends the analysis toward mobility- and orientation-aware operation. While the HLWN validated the feasibility of seamless vertical handover between Li-Fi and Wi-Fi domains, its performance was evaluated under predominantly static or slow-moving user conditions. To capture more realistic dynamics, the **Orientation-Aware Mobility-Enabled Hybrid Li-Fi/Wi-Fi Network (OAM-LiFiNet)** framework [12] models a multi-AP hybrid environment in which each user adaptively adjusts the receiver orientation toward the Li-Fi AP offering the highest SINR. When the Li-Fi SINR drops below a predefined threshold γ_{th}, a vertical handover to Wi-Fi is triggered to sustain connectivity. User movement follows the RWP mobility model, effectively representing natural indoor mobility patterns.

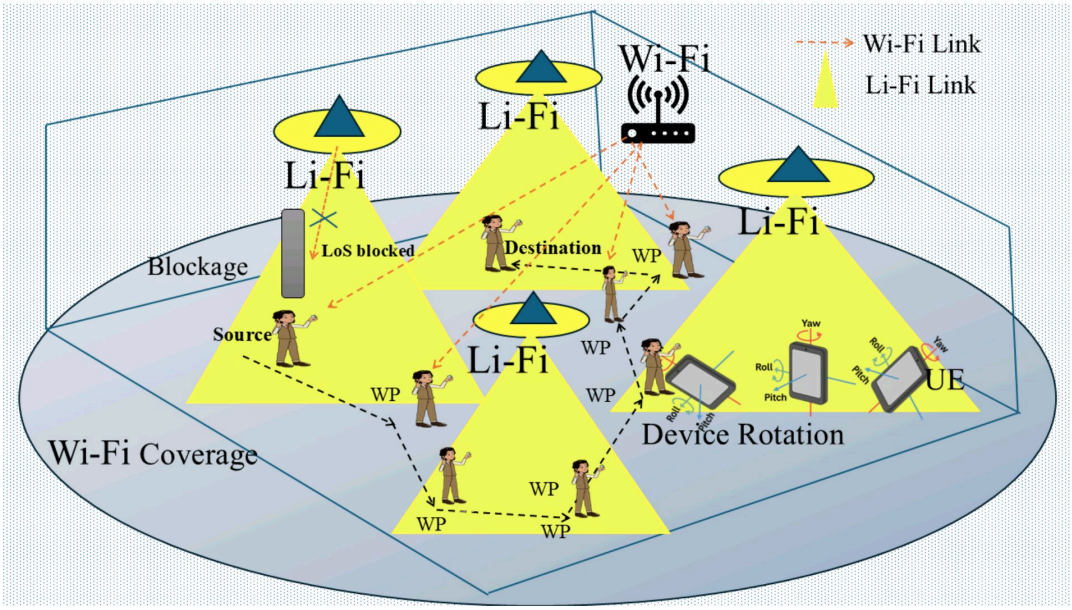

Figure 6.8: System model of Orientation-Aware Mobility-Enabled Hybrid Li-Fi/Wi-Fi Network showing user mobility, orientation, and hybrid AP associations [12].

6.4.2 Adaptive Link Selection Algorithm

At each waypoint, the user evaluates SINR for all available APs:

$$\gamma_{u,k} = \begin{cases} \gamma_{i,j}^{Li-Fi}, & \text{if Li-Fi link is within FOV and } \psi_{i,j} \leq \psi_c, \\ \gamma_{i,j}^{Wi-Fi}, & \text{otherwise.} \end{cases}$$

The user associates with the AP offering the maximum SINR, applying orientation correction if required. Algorithm 2 summarizes this adaptive decision process.

6.5 Evaluation and Result Analysis

This section presents a comprehensive evaluation of the proposed OAM-LiFiNet, extending its applicability from a Li-Fi-only setup to a hybrid Li-Fi/Wi-Fi environment under realistic indoor conditions ($5\,\text{m} \times 5\,\text{m} \times 3\,\text{m}$). The results capture the combined effects of user mobility, device orientation, blockage, and interference on network performance.

Algorithm 2 Adaptive SINR-Based Link Selection for OAM-LiFiNet

Initialize user positions, orientations, and SINR threshold γ_{th}.
for each user u_i at waypoint w_p **do**
    Compute γ_{ij}^{Li-Fi} and γ_{ij}^{Wi-Fi}.
    if $\max(\gamma_{ij}^{Li-Fi}) \geq \gamma_{th}$ **then**
        Adjust orientation to maximize γ_{ij}^{Li-Fi}.
        Connect to Li-Fi AP j^*.
    else
        Connect to Wi-Fi AP with $\max(\gamma_{ij}^{Wi-Fi})$.
    end if
    Move to next waypoint under RWP mobility model.
end for

6.5.1 Performance of OAM-LiFiNet: Orientation-Aware Li-Fi-Only Network

The performance of OAM-LiFiNet in a Li-Fi-only environment has been analyzed in detail in Chapter 5, where the influence of user orientation and mobility on link quality and throughput was extensively studied. In particular, orientation-aware adaptation was shown to significantly improve SINR and achievable data rates in dense, interference-prone Li-Fi deployments.

In summary, those results demonstrated that OAM-LiFiNet:

- Dynamically adjusts receiver orientation to maintain LoS connectivity,
- Achieves up to **84% higher throughput** compared to unoriented Li-Fi baselines, and
- Reduces link fluctuations caused by user movement and random receiver misalignment.

These findings establish a strong foundation for the hybrid network evaluation, confirming that orientation-awareness substantially enhances Li-Fi performance even before integrating Wi-Fi as a complementary fallback link.

6.5.2 Performance of OAM-LiFiNet-Assisted Hybrid Li-Fi/Wi-Fi Network

Building on the orientation-aware Li-Fi-only analysis, we now evaluate OAM-LiFiNet within a hybrid Li-Fi/Wi-Fi environment that includes multiple Li-Fi APs, one Wi-Fi AP, and a central controller managing handover decisions. The simulation captures realistic indoor conditions involving user movement, AP overlap, and occasional blockage.

6.5.2.1 Impact of Orientation and Blockage

Fig. 6.9 illustrates the average user data rate versus the number of users for four different scenarios: with/without orientation and with/without blockage. The results indicate that the orientation-aware configuration achieves the highest throughput across all cases. While blockage events substantially degrade performance particularly when orientation control is disabled OAM-LiFiNet mitigates this effect by reorienting user devices toward available Li-Fi APs or offloading sessions to Wi-Fi links as needed.

6.5.2.2 Handover Rate Analysis

Fig. 6.10 compares horizontal handovers (HHO , between Li-Fi APs) and vertical handovers (VHO, between Li-Fi and Wi-Fi). In conventional systems, VHO frequency tends to be higher due to link loss under blockage or mobility. However, OAM-LiFiNet's orientation adaptation reduces the VHO rate significantly, implying more stable Li-Fi connectivity and longer session retention within the optical domain. This stability enhances user Quality of Experience (QoE) by reducing interruptions and unnecessary transitions.

6.5.2.3 Impact of SINR Thresholding on Rate and Handover

To further analyze the adaptability of OAM-LiFiNet in hybrid Li-Fi/Wi-Fi environment, the system is evaluated for SINR thresholds $\gamma_{\text{th}} = 5$ dB and 10 dB.

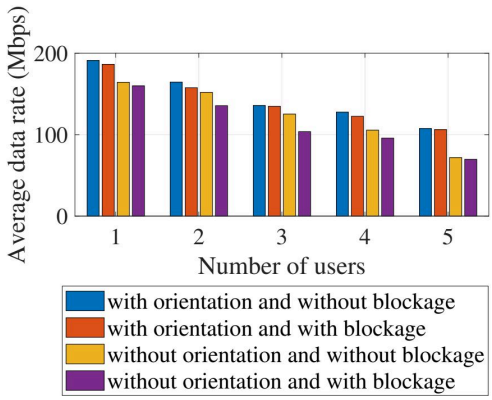

Figure 6.9: Average user rate versus number of users under various hybrid Li-Fi/Wi-Fi scenarios.

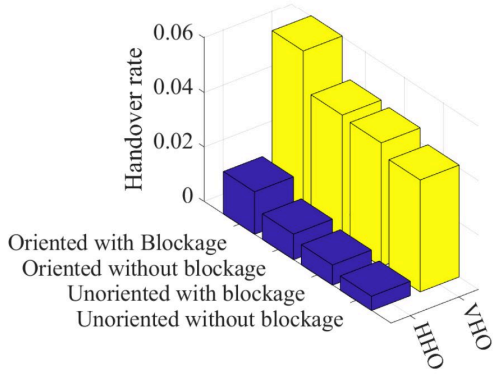

Figure 6.10: Comparison of horizontal and vertical handover rates across different hybrid configurations.

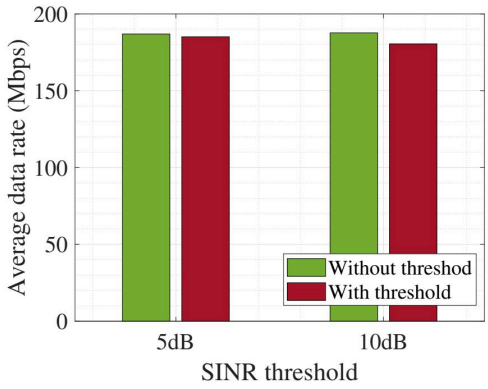

Figure 6.11: Variation in average achievable rate with changing SINR threshold.

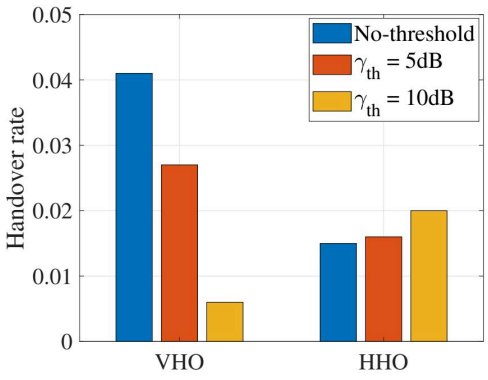

Figure 6.12: Effect of SINR threshold on handover rate.

(a) Rate Performance under SINR Thresholding: As shown in Fig. 6.11, increasing γ_{th} slightly decreases the average achievable rate, since higher thresholds limit the number of available Li-Fi APs that satisfy the condition. At $\gamma_{\text{th}} = 5$ dB, most APs remain usable, causing minimal impact on throughput, whereas $\gamma_{\text{th}} = 10$ dB leads to noticeable rate reduction.

(b) Handover Behavior under Thresholding: Fig. 6.12 illustrates the effect of SINR thresholds on handover rates. Higher γ_{th} values lower the frequency of vertical handovers by prioritizing high-quality Li-Fi connections. However, horizontal handovers become more frequent, as users switch between Li-Fi APs to maintain SINR above the threshold. This highlights a trade-off between link reliability and handover overhead, which must be optimized based on network conditions.

Overall, the hybrid network evaluation verifies that OAM-LiFiNet effectively balances link reliability and connectivity continuity. Orientation-aware control enhances throughput in interference-heavy and partially blocked conditions, while intelligent SINR thresholding manages handover dynamics efficiently. These capabilities make OAM-LiFiNet a robust framework for hybrid Li-Fi/Wi-Fi networks under realistic user mobility.

6.6 Discussion and Insights

The integrated insights from both the experimental testbed and simulation-based studies reveal that:

- The **testbed (HLWN)** confirms the feasibility of hybrid Li-Fi/Wi-Fi coexistence, achieving measurable improvements in throughput and latency.
- The **OAM-LiFiNet framework** extends this feasibility study by analytically incorporating user orientation and mobility dynamics for adaptive link selection.
- Orientation-aware adaptation enhances stability and user QoE without requiring hardware modifications, providing a scalable design for next-generation indoor networks.

This synthesis bridges real-world implementation and analytical modeling, laying the groundwork for intelligent hybrid communication systems.

6.7 Summary

This chapter presented two complementary contributions: (i) a **proof-of-concept hybrid Li-Fi/Wi-Fi testbed** demonstrating the baseline feasibility and performance of HLWN [4], and (ii) a **mobility- and orientation-aware analytical framework (OAM-LiFiNet)** [12], which extended the testbed to account for dynamic user movement, interference, and adaptive link selection. The combined insights from experimental and simulation studies revealed that

integrating optical and RF technologies offers both high-capacity and robust indoor connectivity, especially under realistic mobility conditions.

However, as HLWNs evolve to include multi-antenna Wi-Fi systems and dense Li-Fi deployments, maintaining such adaptivity demands accurate and timely CSI across all access points. Frequent CSI estimation and feedback introduce substantial communication overhead, which can degrade throughput and limit scalabilityparticularly in MU-MIMO Wi-Fi environments. Addressing this emerging bottleneck forms the focus of the next chapter, which addresses this limitation by introducing a novel LiFi-assisted CSI feedback framework, termed WiLiConnect, and its optimized extension WiLiConnect-Opt, which together aim to overcome CSI feedback overhead in Hybrid Li-Fi/Wi-Fi Networks.

It is further observed that the performance of hybrid Li-Fi/Wi-Fi networks is strongly influenced by the quality of Li-Fi and Wi-Fi links, user mobility, and the effectiveness of link selection and load distribution strategies. In particular, Li-Fi link quality, which depends on line-of-sight conditions and user orientation, plays a critical role in achieving high data rates, while Wi-Fi provides robustness under mobility and blockage conditions. Additionally, the efficiency of traffic distribution between Li-Fi and Wi-Fi significantly impacts overall throughput and service continuity. These observations highlight the importance of intelligent hybrid coordination and adaptive link selection for achieving reliable and high-capacity indoor wireless communication.

Chapter 7

Overcoming CSI Feedback Overhead in HLWNs

7.1 Introduction

Building upon the orientation- and mobility-aware HLWN framework developed in Chapter 6, this chapter focuses on another fundamental limitation in hybrid Li-Fi/Wi-Fi systems, the **CSI feedback overhead** in Wi-Fi MU-MIMO systems. While OAM-LiFiNet improved throughput and reliability through orientation and mobility adaptation, these benefits rely on timely and accurate CSI acquisition. In dense multi-AP environments, Wi-Fi's CSI feedback process introduces significant signaling delays and bandwidth consumption, thereby constraining MU-MIMO efficiency and hybrid performance.

To address this issue, we introduce the **WiLiConnect** framework, which utilizes Li-Fi APs to offload CSI feedback from Wi-Fi uplinks. By exploiting Li-Fi's dedicated infrared uplink channels, WiLiConnect enables parallel, interference-free CSI transmission. An enhanced variant, **WiLiConnect-Opt**, incorporates **blockage awareness** and a **Pareto-optimized feedback allocation** mechanism to ensure robust CSI sharing even under dynamic indoor conditions.

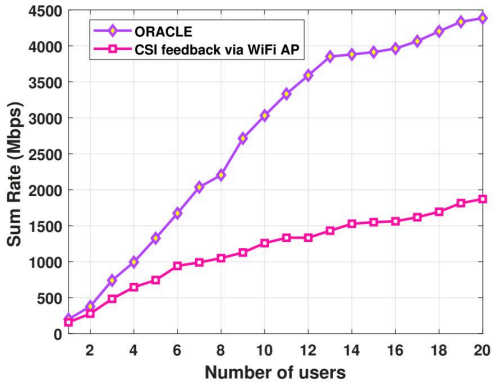

Figure 7.1: Impact of CSI feedback overhead on hybrid Wi-Fi/Li-Fi networks: comparison between ideal CSI availability (ORACLE) and practical Wi-Fi CSI polling. ORACLE represents a theoretical upper bound with perfect CSI and zero feedback overhead.

7.2 Motivation

To highlight the severity of CSI feedback overhead, we evaluate the sum rate performance of a typical indoor hybrid Li-Fi/Wi-Fi setup using Wi-Fi MU-MIMO deployment. Figure 7.1 compares two cases: (i) an *ideal case* (**ORACLE**) where perfect and instantaneous CSI is assumed, and (ii) a *practical case* where CSI is obtained through conventional Wi-Fi polling.

The ORACLE model represents the theoretical upper bound (no feedback overhead), while the practical model reflects real-world feedback latency. Results reveal that realistic CSI polling reduces achievable throughput by nearly **65% for 10 users** and **56% for 20 users**, consistent with prior studies [54, 93]. This demonstrates that the overhead from Wi-Fi's CSI feedback process critically limits system efficiency, particularly in dense hybrid deployments.

To overcome this, we propose **WiLiConnect**, which enables users to transmit CSI via Li-Fi APs using infrared uplinks, significantly reducing Wi-Fi uplink congestion. An advanced version, **WiLiConnect-Opt**, incorporates blockage-aware optimization for robust CSI delivery under dynamic or obstructed scenarios.

7.3 Background

Working of MU-MIMO in Wi-Fi: Since the IEEE 802.11ac (Wi-Fi 5) standard, Wi-Fi APs can utilize multiple antennas to serve multiple users simultaneously through MU-MIMO. This technique requires accurate CSI knowledge and multiple uncorrelated channels. Wi-Fi 6 and Wi-Fi 7 APs support up to 4 and 8 antennas respectively, but as the number of users grows, the demand for CSI feedback also increases, creating significant uplink congestion.

Hybrid Wi-Fi/Li-Fi Network: Li-Fi operates in the optical domain using visible light for downlink and infrared for uplink communication [86]. In contrast, Wi-Fi uses the same RF channel for both directions, which leads to contention during control and feedback signaling. Because Li-Fi's coverage is small, hybrid deployments combine multiple Li-Fi APs with one or more Wi-Fi APs to ensure continuous coverage, enabling the high-speed, interference-free benefits of Li-Fi to complement the range of Wi-Fi.

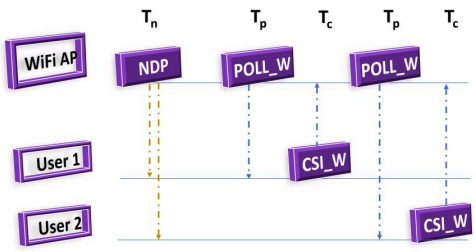

(a) Conventional Wi-Fi CSI feedback: sequential polling and CSI response.

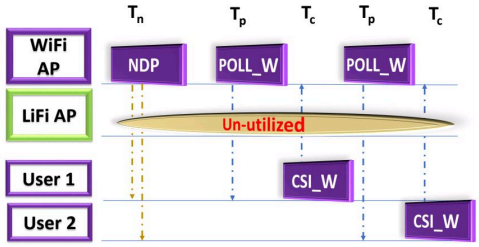

(b) Hybrid system with unutilized Li-Fi uplinks during CSI collection.

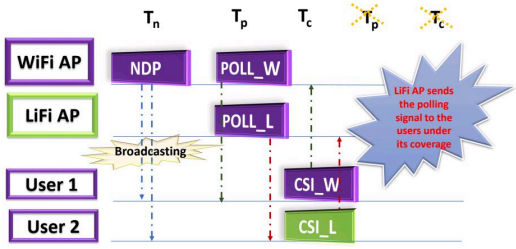

(c) Proposed WiLiConnect: parallel CSI feedback via Li-Fi uplinks.

Figure 7.2: CSI feedback comparison: Wi-Fi-only (a), hybrid but unutilized Li-Fi (b), and proposed WiLiConnect (c).

CSI Sharing Model: In conventional Wi-Fi, CSI feedback involves sequential NDP transmission, polling, and user response (Fig. 7.2(a)), which limits scalability. Li-Fi, however, can assist by carrying CSI feedback via its infrared uplink to a Li-Fi AP, which then relays it to the Wi-Fi AP over a wired connection (Ethernet). This method enables parallel, interference-free CSI reporting (Fig. 7.2(b)), reducing latency and overhead.

7.4 Proposed WiLiConnect Framework

The proposed **WiLiConnect** framework mitigates CSI feedback overhead by enabling users to transmit CSI via the nearest AP, either Wi-Fi or Li-Fi, depending on channel strength and SINR, as depicted in Fig. 7.3. Each Li-Fi AP acts as a feedback relay, collecting CSI over optical uplinks and forwarding it to the corresponding Wi-Fi AP through a high-speed wired backhaul via central controller. This distributed and parallelized approach significantly reduces CSI feedback delay, uplink congestion, and associated bandwidth waste.

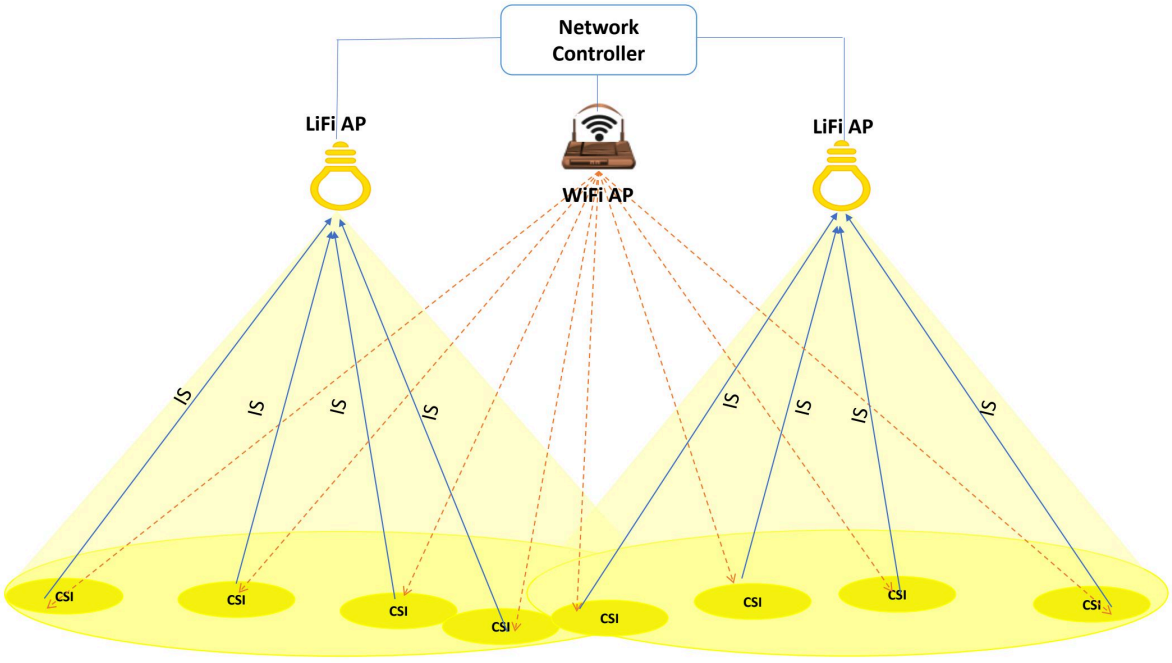

Figure 7.3: Illustration of CSI feedback sharing.

Key operational steps of WiLiConnect:

1. Wi-Fi AP broadcasts the NDP for channel estimation.

2. Users within Li-Fi coverage send CSI via Li-Fi uplinks (CSI_L); others use Wi-Fi uplink (CSI_W).

3. Li-Fi APs forward the received CSI to the Wi-Fi AP via the central controller.

4. The Wi-Fi AP updates MU-MIMO precoding based on CSI received via LiFi or WiFi AP.

This parallel CSI sharing mechanism allows Wi-Fi to maintain high downlink efficiency without compromising feedback latency or spatial multiplexing performance.

7.4.1 System Model

We consider a hybrid Li-Fi/Wi-Fi network consisting of m users, n Wi-Fi APs, and p Li-Fi APs deployed in an indoor environment of known dimensions. All APs are mounted on the ceiling, and each user device is equipped with both Wi-Fi and Li-Fi interfaces. A central controller, connected to all APs via a high-speed wired backhaul, manages user associations and CSI collection scheduling based on real-time channel conditions.

Each Wi-Fi AP is equipped with n_t transmitting antennas, while each user device has n_r receiving antennas. Wi-Fi APs operate according to IEEE 802.11ac (Wi-Fi 5) or 802.11ax (Wi-Fi 6) standards, both supporting spatial multiplexing. Hence, multiple users can be served simultaneously via MU-MIMO if the AP has accurate CSI and multiple uncorrelated channels.

7.4.2 User Association and Resource Allocation

User association in the hybrid network is dynamically determined based on the received SINR. Each user is connected to the AP either Wi-Fi or Li-Fi, which provides the maximum instantaneous SINR. This association strategy ensures load balancing between technologies and optimizes link utilization.

The CC follows a two-step resource management process:

1. **SINR Thresholding:** Users whose SINR falls below a minimum threshold are excluded to maintain QoS stability.

2. **Round-Robin Scheduling:** Among the eligible users, a round-robin algorithm distributes CSI feedback load evenly across APs, preventing congestion.

Each AP allocates its available bandwidth equally among associated users. Although simple, this *equal allocation policy* ensures fairness and isolates the effect of CSI feedback on throughput performance. More sophisticated strategies (e.g., proportional fair or QoS-aware scheduling) may further enhance performance and can be explored in future work.

7.4.3 Blockage Model

Blockages in Li-Fi are modeled as cylindrical objects with height H_b and radius r_b. They obstruct the LoS path between Li-Fi APs and users, forming shadow regions that impact CSI transfer efficiency.

The geometric similarity principle, shown in Fig. 4.1, is used to calculate the shadow length:

$$d_x = \frac{H_b - H_u}{H_r - H_u} \cdot d_T, \tag{7.1}$$

where H_r is room height, H_u is user receiver height, and d_T is the horizontal distance from AP projection to the user.

Diffraction and scattering are neglected, consistent with standard Li-Fi modeling [94], as visible and infrared light exhibit minimal bending. This model offers tractable and realistic blockage estimation for CSI feedback link evaluation.

7.4.4 CSI Feedback Mechanism and Problem Definition

In conventional Wi-Fi systems, CSI acquisition involves three stages:

1. Transmission of a Null Data Packet (NDP) ,

2. Polling of individual users, and

3. CSI feedback from each user sequentially.

This procedure introduces significant delay T_d since no data transmission occurs during CSI collection:

$$T_d = T_n + T_p + T_c, \tag{7.2}$$

where T_n, T_p, and T_c denote the durations of NDP transmission, polling, and CSI feedback respectively.

To mitigate this overhead, **WiLiConnect** utilizes both Wi-Fi and Li-Fi APs for parallel CSI feedback. Let N_j represent the set of users sharing CSI through AP j, where:

$$N_j \cap N_k = \varnothing, \quad \forall j,k \in \{1,\ldots,w+l\}. \tag{7.3}$$

Then, the total feedback delay becomes:

$$T_d = T_n + \max_{j=1,\ldots,w+l} \sum_{u_i \in N_j} [t_p^i + t_c^i], \tag{7.4}$$

where t_p^i and t_c^i are the polling and CSI transmission times for user i.

Each user selects one AP for CSI sharing based on link availability:

$$\sum_{j=1}^{w+l} x_{ij} = 1, \quad x_{ij} \leq S_{ij}, \tag{7.5}$$

where $x_{ij} \in \{0,1\}$ indicates if user i sends CSI to AP j, and $S_{ij} = 1$ only if RSSI permits CSI transfer.

Algorithm 3 Algorithm to share information across Li-Fi APs

INPUT: Set of users N_w that want to utilize Wi-Fi,
set of users connected to each Li-Fi AP j,
set of APs A, set of users covered by a Li-Fi j, M_j, number of antennas n_t
OUTPUT: Set of users N_j which utilize information sharing via AP j

$T_p^j \leftarrow 0, \forall j$
$T_c^j \leftarrow 0, \forall j$
$N_j \leftarrow \phi$
while $|\bigcup_j N_j| \leq n_t$ or $A \neq \phi$ **do**
    $l \leftarrow \arg\min_j T_p^j + T_c^j$
    $k \leftarrow \arg\max_{i \in M_j} SINR(i, j)$
    if $SINR(k,l) > t$ **then**
        $T_p^l = T_p^l + t_p^k$
        $T_c^l = T_c^l + t_c^k$
        $M_j \leftarrow M_j \setminus \{u_i\}, \forall j$
    else
        $A \leftarrow A \setminus \{u_l\}$
    end if
end while

The CSI transmission time depends on the number of user antennas and uplink rate:

$$t_c^i = \frac{n_r^i \times s}{R_u^{ij}} + t_p^i, \tag{7.6}$$

where s is CSI size per antenna (bits) and R_u^{ij} is the uplink rate. Thus, total delay is minimized as:

$$\min \sum_{t=1}^{T} T_d^t. \tag{7.7}$$

This problem is NP-hard, equivalent to the number partitioning problem [95]. Hence, we propose an efficient round-robin algorithm for practical analysis.

This algorithm balances load across APs, minimizing total CSI overhead. Its complexity is $O(nl \log l)$, ensuring real-time applicability for typical small-cell deployments.

7.5 WiLiConnect-Opt with Optimization Techniques

While WiLiConnect efficiently reduces CSI feedback overhead, its performance can degrade under Li-Fi link blockages as illustrated in Fig. 7.4. To address this, we extend WiLiConnect

Table 7.1: Notation Used in CSI Sharing Formulation

Symbol	Description
u_i	i^{th} user
w, l	Number of Wi-Fi and Li-Fi APs
x_{ij}	1 if u_i sends CSI to AP j
S_{ij}	CSI feasibility indicator (RSSI threshold)
t_p^i, t_c^i	Polling and CSI transmission times
T_d	Total CSI feedback delay
R_u^{ij}	Uplink data rate between u_i and AP j
n_r^i	Number of receive antennas for u_i
s	CSI size per antenna (bits)
N_j	Set of users assigned to AP j
n_t	Number of transmit antennas (MU-MIMO streams)

to **WiLiConnect-Opt**, which integrates blockage awareness and Pareto-optimized CSI routing to maintain reliability under non-line-of-sight (NLoS) or dynamic user conditions.

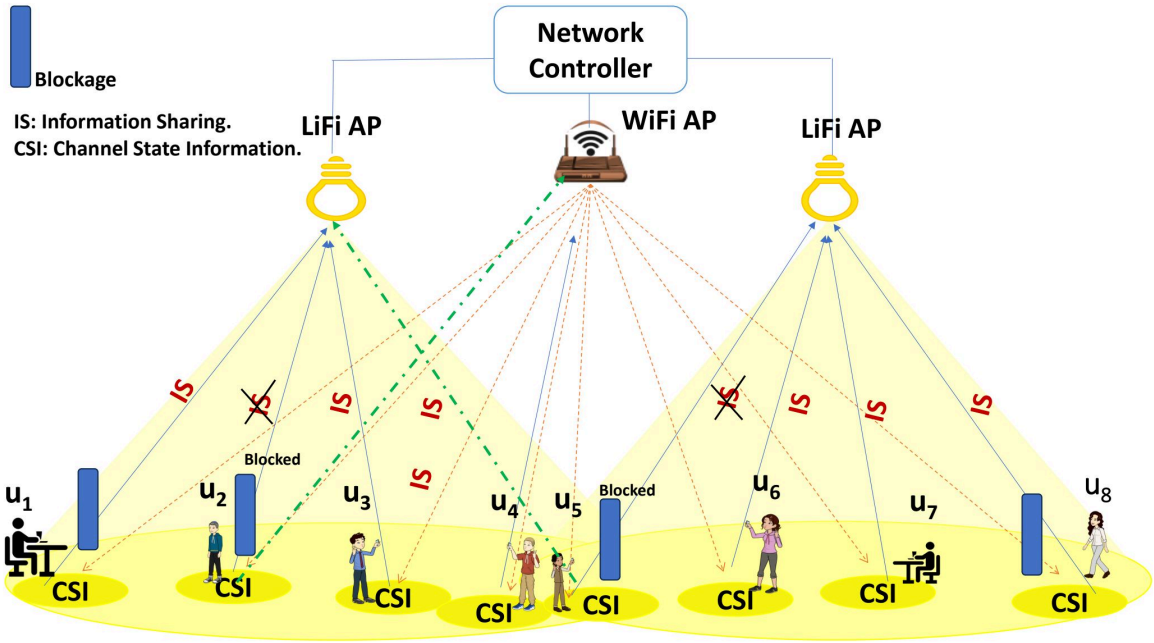

Figure 7.4: Illustration of CSI feedback sharing in presence of blockage effect.

Cross-Technology Synchronization and Scheduling: To enable efficient cooperation between Li-Fi and Wi-Fi networks in the proposed WiLiConnect-Opt framework, a centralized network controller is employed to coordinate timing and resource allocation across both technologies.

The controller maintains a global view of network conditions, including CSI, user association, and traffic demand. Synchronization between Li-Fi and Wi-Fi systems is achieved through time-slotted coordination, where the controller aligns transmission intervals using a common reference clock. This can be realized through software-defined networking (SDN)-based control or centralized coordination at the access point level.

In particular, the controller schedules Li-Fi and Wi-Fi transmissions in a complementary manner. Li-Fi links are primarily utilized for CSI feedback transmission due to their high data rate and low interference characteristics, while Wi-Fi is reserved for downlink data communication. The controller assigns dedicated time slots for CSI feedback over Li-Fi to avoid contention with Wi-Fi transmissions.

To ensure seamless operation, guard intervals and scheduling offsets are introduced to accommodate differences in propagation delay and processing time between Li-Fi and Wi-Fi systems. This coordinated scheduling mechanism minimizes interference and ensures timely CSI updates, thereby improving overall system efficiency.

Thus, the proposed synchronization and scheduling framework enables effective cross-technology cooperation by aligning transmission timing and optimizing resource utilization across Li-Fi and Wi-Fi networks.

7.5.1 Optimization Formulation

The objective is to jointly maximize CSI throughput and minimize blockage-induced failures. The optimization is expressed as:

$$\textbf{Maximize} \quad \sum_{i=1}^{k} \sum_{j=1}^{l} B_{ij} \log_2(1+\gamma_{ij}), \tag{7.8}$$

$$\textbf{Minimize} \quad \sum_{i=1}^{k} \sum_{j=1}^{l} p_{ij} x_{ij}, \tag{7.9}$$

subject to bandwidth constraints:

$$\sum_{i=1} x_{ij} B_{ij} \leq B_{Li-Fi}, \quad \forall j, \tag{7.10}$$

$$B_{ij} \leq B_{Li-Fi} x_{ij}, \quad \forall i, j. \tag{7.11}$$

Here, γ_{ij} denotes SINR between user i and AP j, p_{ij} is blockage probability, and B_{Li-Fi} is total Li-Fi bandwidth. Eq. (7.8) ensures maximum CSI throughput, while Eq. (7.9) penalizes blocked links.

To achieve Pareto efficiency, the blockage term is converted into a constraint:

$$\sum_{i=1}^{k} \sum_{j=1}^{l} p_{ij} x_{ij} \leq M, \tag{7.12}$$

where M denotes the system's tolerance to blockage. This results in a standard integer linear program (ILP) , solved through relaxation and rounding of decision variables.

WiLiConnect-Opt adaptively allocates CSI feedback channels to minimize delay while ensuring robustness under varying blockage and SINR conditions. This optimization enables a dynamic, environment-aware feedback process, significantly improving hybrid network reliability and spectral efficiency.

7.6 Performance Evaluation and Discussion

This section presents a detailed performance evaluation of the proposed **WiLiConnect** and **WiLiConnect-Opt** frameworks for hybrid LiFi/WiFi networks. The objective is to quantify their effectiveness in reducing CSI feedback overhead, improving network throughput, and ensuring robust performance under dynamic indoor conditions such as user mobility and line-of-sight blockages. Comprehensive simulations are conducted using a realistic indoor topology, comparing the proposed schemes against conventional WiFi-based feedback mechanisms and

the idealized ORACLE benchmark. The results highlight the significant gains in sum rate, scalability, and blockage resilience achieved through distributed CSI sharing and Pareto-based optimization in the hybrid architecture.

7.6.1 Simulation Settings

We consider an indoor environment of dimensions $5 \times 5 \times 3$ m^3 to evaluate the proposed hybrid Wi-Fi/Li-Fi network, as illustrated in Fig. 7.5. Four Li-Fi APs are symmetrically placed on the ceiling, while a single WiFi AP is positioned at the geometric center. Users are uniformly distributed across the room floor, each equipped with both Wi-Fi and Li-Fi transceivers. Key simulation parameters are summarized in Table 7.2.

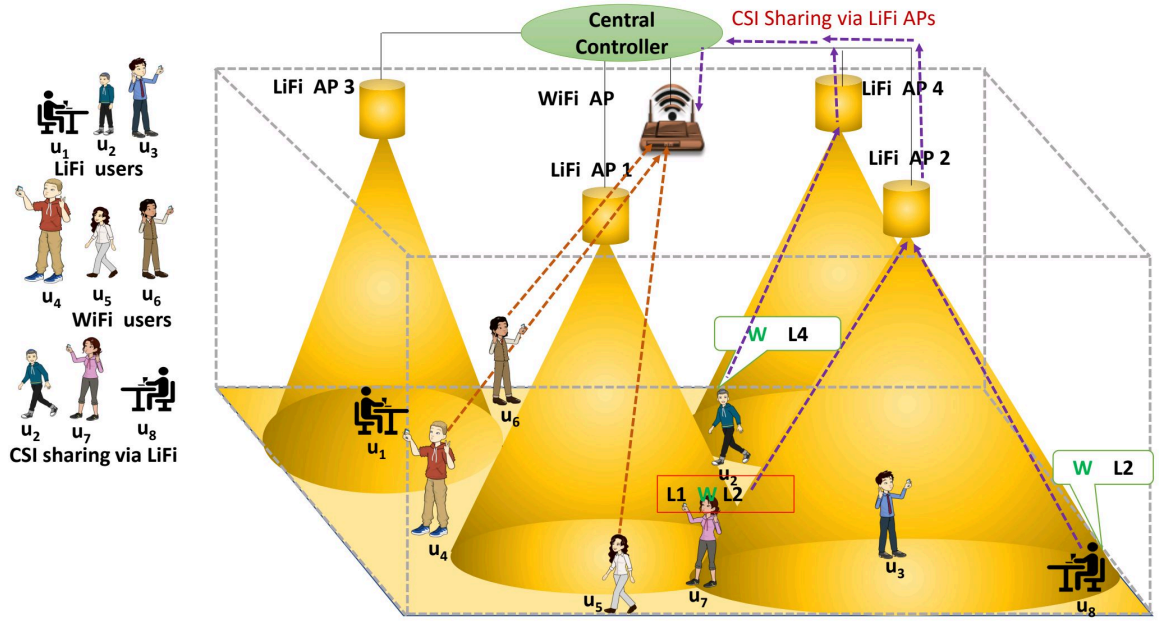

Figure 7.5: Hybrid WiFi/LiFi indoor network illustration used for evaluating CSI sharing strategies.

User association is determined dynamically based on the received SINR. Each user connects to the AP (Wi-Fi or Li-Fi) that provides the highest SINR given its current position and instantaneous channel condition. Both Wi-Fi and Li-Fi APs use CSMA/CA-based access for association and employ RTS/CTS handshaking for uplink contention management.

Resource allocation:

- The Wi-Fi AP supports MU-MIMO and OFDMA (orthogonal frequency division multiple access) . It spatially multiplexes up to four users via MU-MIMO while allocating additional users orthogonal time–frequency resources using OFDMA.
- Each LiFi AP employs OFDMA to allocate non-overlapping subcarriers among its users under an IM/DD-based SISO configuration.

A centralized controller coordinates all APs, aggregates CSI feedback, and performs AP–user assignment based on SINR thresholds and round-robin scheduling for load balancing. Unless otherwise stated, the Wi-Fi AP has four antennas, following IEEE 802.11ac/ax standards. It broadcasts a NDP for channel estimation, after which users transmit CSI feedback either through the Wi-Fi uplink or via the nearest Li-Fi AP. Feedback collected by Li-Fi APs is relayed through Ethernet to the central controller and then to the Wi-Fi AP. This process enables WiLiConnect to reduce uplink burden by intelligently distributing CSI transmission among APs.

The Wi-Fi channel coherence time is assumed to be 15 ms, necessitating periodic CSI updates [54]. The available Wi-Fi bandwidth (B_{WiFi}) is divided between MU-MIMO and OFDMA users as:

$$B_u = \frac{B_{Wi-Fi}}{\max(1, N_w - N_m + 1)}, \tag{7.13}$$

where N_w and N_m denote the number of Wi-Fi users and MU-MIMO streams, respectively.

The achievable data rate for the i^{th} Wi-Fi user is:

$$R^i_{u,w} = B_u \log_2(1 + \gamma_{i,w}), \tag{7.14}$$

where $\gamma_{i,w}$ is the received SNR between user i and the Wi-Fi AP. Similarly, the LiFi user rate is modeled as [86]:

$$R^i_{u,l} = \frac{B_{Li-Fi}}{2} \log_2\left(1 + \frac{6}{\pi e}\gamma_{i,l}\right), \tag{7.15}$$

Table 7.2: Simulation Parameters [8, 15]

LiFi Parameters		**WiFi Parameters**	
Height from user plane	2.15 m	Carrier frequency (f_c)	2.4 GHz
PD area (A_{PD})	1 cm^2	Transmit power (P_{WiFi})	20 dBm
Optical filter gain (g_{f})	1	Bandwidth (B_{WiFi})	20 MHz
FOV	60°	Noise PSD (N_{WiFi})	-174 dBm/Hz
Optical to electrical conversion (K)	3	WiFi AP antennas (n_t)	4, 8
Responsivity (R_{PD})	0.53 A/W	User antennas (n_r)	1
Optical transmit power (P_{opt})	3 W	NDP time (T_{NDP})	80 μs
Bandwidth (B_{LiFi})	40 MHz	Polling time per user (T_p)	52 μs
Noise PSD (N_{LiFi})	-210 dBm/MHz	CSI feedback per user (T_c)	258 μs
–	–	Channel coherence time (τ_c)	15 ms

where $B_{\text{Li}-\text{Fi}}$ is the Li-Fi bandwidth and $\gamma_{i,l}$ represents the SINR between user i and its associated Li-Fi AP.

The total hybrid network throughput is obtained as:

$$R_u = \sum_{u_i \in W} R^i_{u,w} + \sum_{u_i \in L} R^i_{u,l}, \tag{7.16}$$

where w and l denote the sets of Wi-Fi and Li-Fi associated users, respectively.

During CSI feedback, Wi-Fi temporarily suspends data transmission, while Li-Fi continues due to its duplex nature (infrared uplink, visible-light downlink). For consistency, all APs are normalized to a 40 MHz bandwidth, following [96].

7.6.2 Effect of Blockage on CSI Sharing Overhead

Blockages can disrupt Li-Fi-based CSI feedback, increasing overhead and reducing overall efficiency. Fig. 7.6a compares CSI sharing overhead across four schemes without blockage. Feedback through Wi-Fi alone leads to substantial overhead (median $\approx$12%), while Li-Fi-assisted schemes progressively reduce it. WiLiConnect-Lite achieves $\approx$ 4%, and WiLiConnect further stabilizes the variance across cases.

Although CSI feedback adds minimal control load to Li-Fi uplink channels, its impact on throughput is negligible because Li-Fi operates in full duplex infrared uplink and visible down-

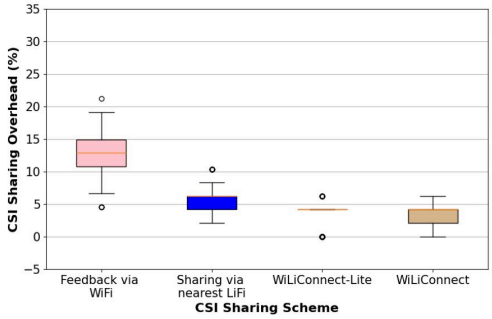

(a) CSI feedback overhead under no blockage ($n_t = 4$).

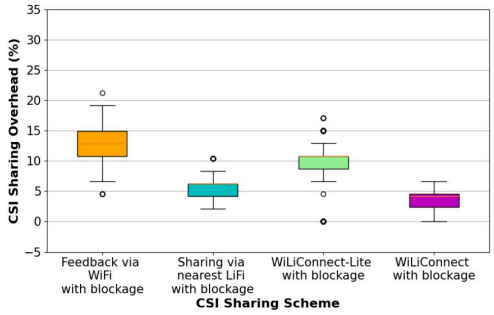

(b) CSI feedback overhead under blockage ($n_t = 4$).

Figure 7.6: Comparison of CSI feedback overhead in hybrid Wi-Fi/Li-Fi networks: (a) under no blockage and (b) under blockage for $n_t = 4$.

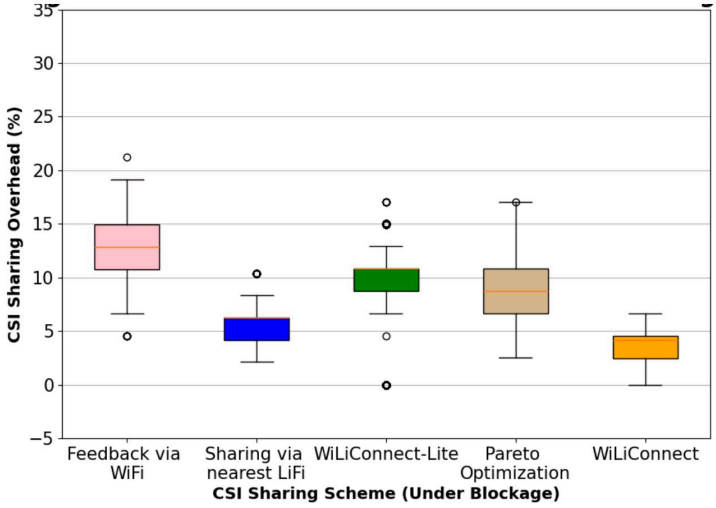

Figure 7.7: CSI overhead comparison for WiLiConnect, WiLiConnect-Lite, and optimized WiLiConnect-Opt.

link, allowing parallel transmissions without RF interference. Moreover, WiLiConnect-Opt optimizes CSI routing based on SINR and blockage probability, ensuring efficient utilization of Li-Fi bandwidth and robustness under NLoS conditions.

When blockage occurs, as shown in Fig. 7.6b, some CSI links are rerouted through alternate APs, slightly increasing overhead. WiLiConnect's distributed feedback mitigates this rise effectively. Further optimization via the Pareto-based WiLiConnect-Opt reduces CSI overhead by approximately 27%, as demonstrated in Fig. 7.7.

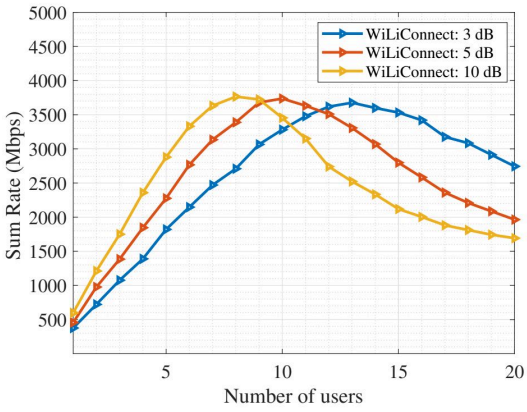

(a) Sum rate performance under varying SINR thresholds with blockage.

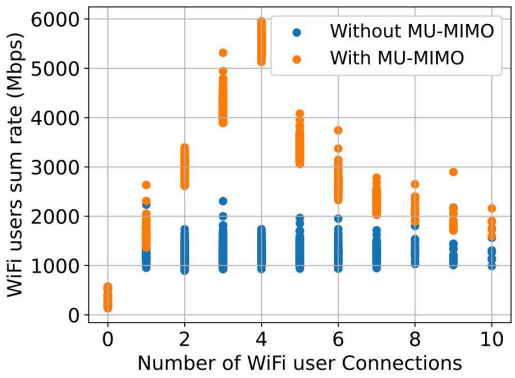

(b) WiFi connection count versus sum rate for $n_t = 4$.

Figure 7.8: Sum rate analysis of the hybrid Wi-Fi/Li-Fi network: (a) effect of varying SINR thresholds under blockage conditions, and (b) relationship between Wi-Fi connection count and achievable sum rate ($n_t = 4$).

7.6.3 SINR Threshold-Based Analysis

7.6.3.1 Sum Rate Analysis

Fig. 7.8a shows the network sum rate variation with SINR threshold. At low thresholds (3 dB), more users associate with Li-Fi APs, maximizing utilization and throughput. At higher thresholds (5 to 10 dB), fewer users qualify for Li-Fi, increasing Wi-Fi load and slightly reducing sum rate. For $n_t = 4$, Wi-Fi achieves maximum efficiency with up to four spatially multiplexed users; beyond this, performance saturates (Fig. 7.8b).

7.6.3.2 CSI Sharing Overhead

The CSI overhead exhibits an inverse trend: higher SINR thresholds reduce Li-Fi participation and shift load to Wi-Fi, increasing feedback overhead. As shown in Fig. 7.9a, for 20 users, the median overhead rises from 3.2% (3 dB) to 5.8% (10 dB).

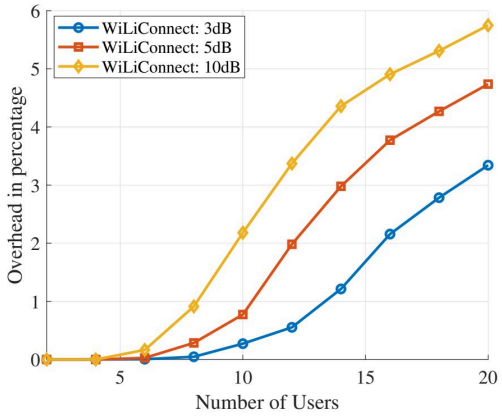

(a) CSI overhead variation with SINR threshold under blockage.

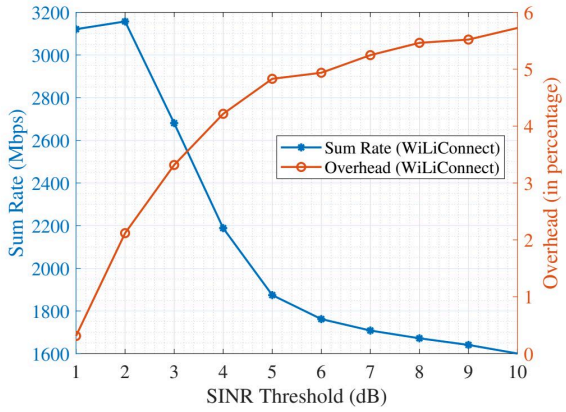

(b) Trade-off between sum rate and CSI overhead for different SINR thresholds.

Figure 7.9: Performance comparison of CSI feedback mechanisms in hybrid WiFi/LiFi networks: (a) variation of CSI overhead with SINR threshold under blockage, and (b) trade-off analysis between achievable sum rate and CSI overhead across SINR thresholds.

7.6.3.3 Trade-Off Between Sum Rate and CSI Overhead

Fig. 7.9b highlights the trade-off between throughput and overhead as SINR threshold increases. The 3 dB threshold achieves the most balanced operation, maximizing sum rate while maintaining manageable CSI overhead.

7.6.3.4 Downlink Sum Rate Analysis

Fig. 7.10 compares downlink sum rate under blockage and non-blockage conditions. Disabling spatial multiplexing reduces performance by $\sim$3.4$\times$ for $n_t = 4$ and $N = 13$. WiLiConnect achieves near-ideal performance, maintaining sum rates within 11% of ORACLE for 20 users, validating the efficiency of distributed CSI feedback.

WiLiConnect-Opt further improves robustness under blockage, while conventional WiFi and OFDMA feedback schemes exhibit higher latency and CSI congestion, confirming the advantage of LiFi-assisted CSI offloading.

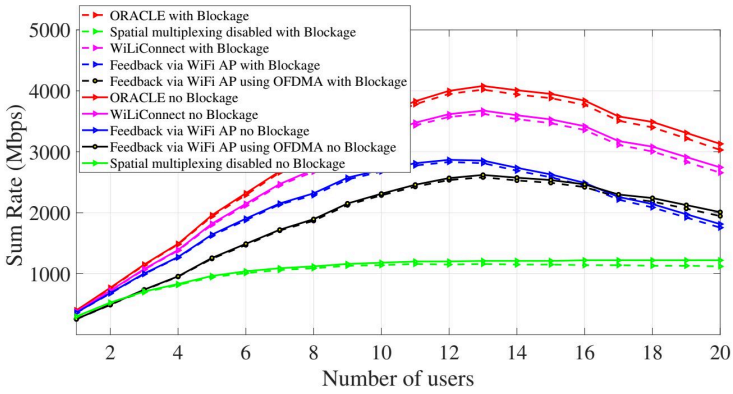

Figure 7.10: Downlink sum rate versus number of users (with and without blockage).

7.7 Summary

This chapter addressed the inherent limitation of Wi-Fi-based multi-user MIMO systems, where the extensive CSI feedback required for spatial multiplexing introduces significant overhead and latency, ultimately degrading the performance of hybrid LiFi/WiFi networks. To overcome this, we proposed *WiLiConnect*, a CSI feedback offloading framework that utilizes the high-capacity Li-Fi uplink to reduce Wi-Fi congestion and feedback delay while maintaining load balance through SINR-based user association and a round-robin scheduling algorithm. Furthermore, an enhanced version, *WiLiConnect-Opt*, was developed to account for Li-Fi specific limitations such as LoS blockages and SINR variations, employing Pareto-based optimization to jointly minimize blockage effects and feedback delay while maximizing sum rate. While these frameworks effectively mitigate CSI overhead and enhance throughput, increasing demands from high-bandwidth applications such as AR/VR motivate the need for more robust hybrid connectivity. Hence, **Chapter 8** explores link aggregation and outage analysis in HLWNs to further improve network capacity, reliability, and continuity under dynamic indoor conditions.

It is further observed that the performance of the proposed WiLiConnect frameworks is strongly influenced by CSI feedback overhead, user density, and Li-Fi link quality. As the number of users increases, CSI overhead becomes a major bottleneck in Wi-Fi systems, reduc-

ing spectral efficiency and increasing latency. Offloading CSI through Li-Fi links effectively mitigates this limitation, improving overall throughput. However, the effectiveness of this approach depends on Li-Fi link conditions, which are affected by LoS availability and SINR variations. These insights emphasize the importance of adaptive cross-technology coordination in hybrid networks.

Chapter 8

Link Aggregation in HLWNs

The previous chapter addressed the CSI feedback overhead in HLWNs through the proposed *WiLiConnect* and *WiLiConnect-Opt* frameworks, which significantly improved feedback efficiency and reduced latency. However, even with optimized CSI sharing, the overall throughput and reliability of HLWNs remain limited by single-link operation, where each user connects to either a Li-Fi or a Wi-Fi AP at a time. Such an approach leads to underutilization of available spectrum resources and degraded performance during blockage or mobility, particularly for bandwidth-intensive applications such as AR/VR and UHD streaming.

To overcome these limitations, this chapter investigates **link aggregation (LA)** as a means to enable simultaneous data transmission over both Li-Fi and Wi-Fi links. By leveraging the complementary characteristics of the two technologies, Li-Fi's high-capacity optical channel and Wi-Fi's robust coverage, LA enhances throughput, reliability, and user fairness in dynamic indoor environments. The chapter presents three LA-based algorithms, namely *LA-SINR*, *LA-EQoS*, and *FLADA*, along with an analytical model for outage probability in LA-enabled HLWNs. These frameworks collectively aim to maximize data rate, maintain QoS under blockage, and quantify reliability improvements achieved through aggregation.

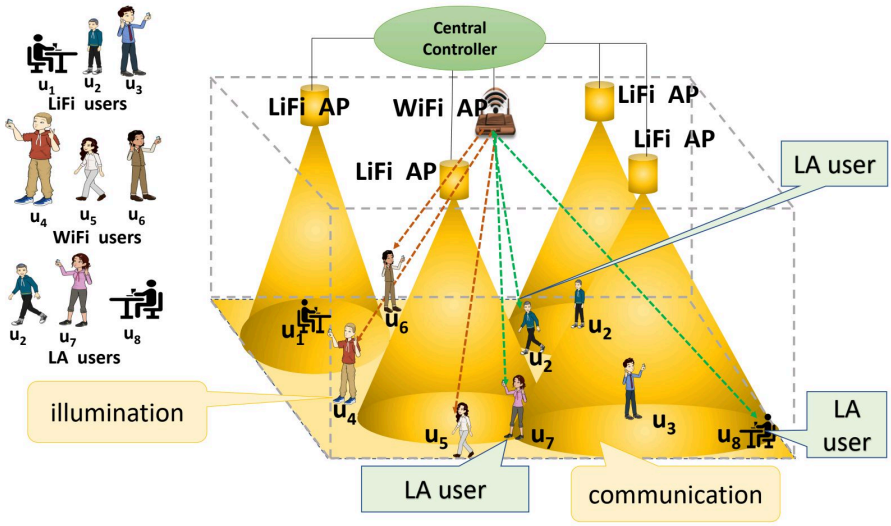

Figure 8.1: Conceptual illustration of link aggregation in hybrid Li-Fi/Wi-Fi networks.

8.1 Need for Link Aggregation in HLWNs

Conventional hybrid Li-Fi/Wi-Fi networks typically rely on RSS or SINR-based association, where each user connects to a single AP — either Li-Fi or Wi-Fi. While this strategy simplifies resource allocation, it results in suboptimal network utilization, particularly under uneven traffic loads or dynamic user mobility conditions. The shorter range and LoS dependency of LiFi often cause frequent disconnections, forcing users to rely on WiFi alone. This, in turn, leads to uplink congestion and reduced throughput, as observed in [8, 9].

To overcome these limitations, *link aggregation* enables simultaneous connectivity to both Li-Fi and Wi-Fi APs, allowing a user to receive and transmit data concurrently over both channels. This dual connectivity improves throughput, load balancing, and handover resilience by combining Li-Fi's high-capacity optical channel with Wi-Fi's wide coverage and robustness. Figure 8.1 conceptually illustrates this dual-link operation, where aggregated flow-based scheduling enhances both reliability and user quality of experience.

The following sections discuss three LA algorithms—LA-SINR, LA-EQoS, and FLADA—and analyze outage modeling and performance comparisons.

8.2 Proposed Link Aggregation Algorithms

To enable efficient utilization of both Li-Fi and Wi-Fi links in HLWNs, two heuristic Link Aggregation algorithms are proposed in this section *LA-SINR* and *LA-EQoS*. These algorithms aim to exploit the complementary strengths of Li-Fi and Wi-Fi to enhance the overall system throughput, user QoS, and network coverage while reducing the outage probability. However, as shown through analysis and simulation, their performance and scalability vary depending on user density and link conditions.

8.2.1 LA-SINR Algorithm

The first heuristic, termed *LA-SINR*, aggregates both Li-Fi and Wi-Fi connections for every user. Each user associates with the Li-Fi AP offering the highest SINR, ensuring strong optical connectivity, while simultaneously receiving data from the Wi-Fi AP. The overall data rate of user u is given by:

$$R_{u,\text{LA-SINR}} = \beta_{ov} \times \left(R_{u,\text{LiFi}} + R_{u,\text{WiFi}}\right), \tag{8.1}$$

where β_{ov} denotes the link aggregation overhead, considered as $\beta_{ov} = 0.2$ based on [97]. The aggregation overhead factor β_{ov} accounts for practical inefficiencies arising from multi-link operation across Li-Fi and Wi-Fi interfaces. A key contributor to this overhead is packet reordering at the receiver, since packets transmitted over different links may experience varying delays and arrival times.

In addition, factors such as buffering, synchronization, and control signaling between heterogeneous interfaces further contribute to performance degradation. To incorporate these effects in a simplified manner, a constant overhead factor β_{ov} is used.

In this work, β_{ov} is set to 0.2 based on [97], representing typical overhead levels in multi-interface wireless systems.

Advantages: LA-SINR ensures all users benefit from dual connectivity and achieves significantly higher average data rates than standalone or hybrid (non-aggregated) networks,

particularly in low-to-moderate user densities. The approach guarantees that even users in Li-Fi coverage holes maintain connectivity through Wi-Fi backup, leading to lower outage probabilities.

Limitations: However, since every user undergoes aggregation, the Wi-Fi AP becomes heavily overloaded as the number of users increases. This leads to a degradation of per-user throughput and inefficient utilization of Wi-Fi resources. Furthermore, the equal treatment of all users neglects fairness and does not prioritize those who truly need assistance due to poor LiFi QoS.

8.2.2 Outage and Coverage Probability Analysis

In this work, the QoS requirement is defined in terms of a minimum data rate threshold, denoted by Γ_0. A user is considered to be in outage if its achieved data rate R_u is less than Γ_0.

Accordingly, the outage probability is computed as:

$$\Phi_0 = \frac{\sum_{u=1}^{U} \mathbb{I}(R_u < \Gamma_0)}{U}, \tag{8.2}$$

where U is the total number of users and $\mathbb{I}(\cdot)$ is the indicator function, which equals 1 if the condition is true and 0 otherwise.

The achievable data rate R_u is obtained using the rate expressions defined earlier for LiFi, WiFi, and hybrid link aggregation schemes. These rates depend on channel gain, user association, and the applied aggregation strategy.

The results are generated using Monte Carlo simulations over 10,000 iterations, where user locations and channel conditions are varied. The outage probability is averaged across all realizations for different QoS (data rate) thresholds.

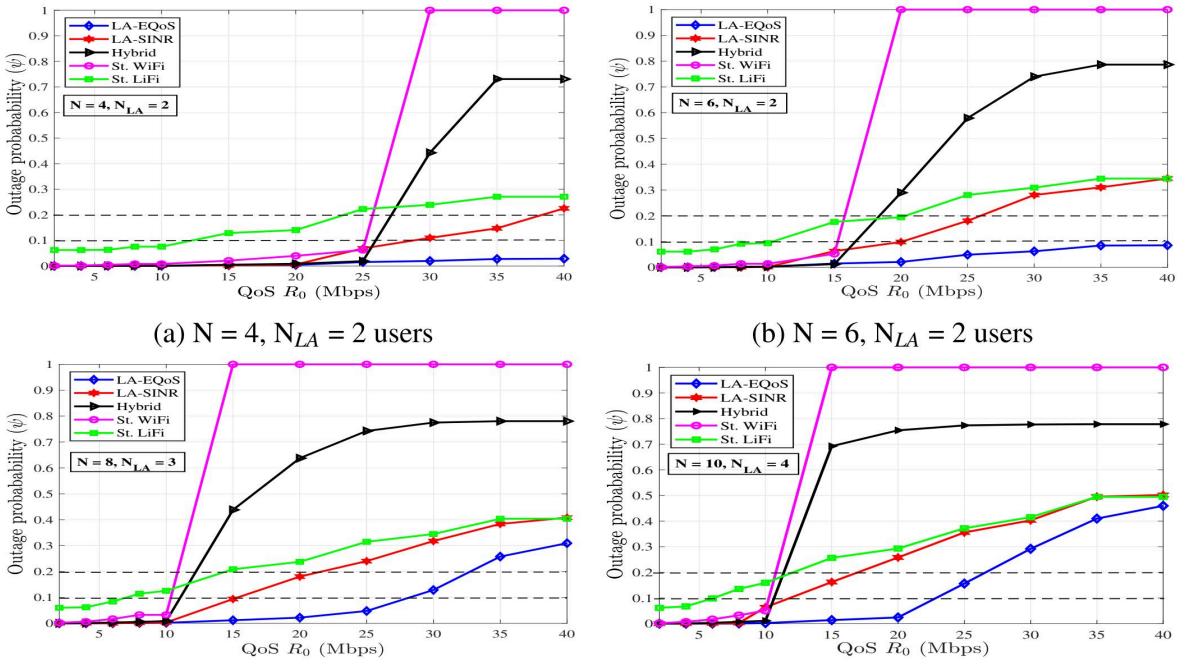

(a) N = 4, N_{LA} = 2 users

(b) N = 6, N_{LA} = 2 users

(c) N = 8, N_{LA} = 3 users

(d) N = 10, N_{LA} = 4 users

Figure 8.2: Outage probability plots for different N-N_{LA} user pairs

The coverage probability is defined as the complement of outage probability, representing the fraction of users achieving the required QoS:

$$P_{\text{cov}} = \Pr(R_u \geq \Gamma_0) = 1 - \Phi_0. \tag{8.3}$$

Simulation results (Fig. 8.2 and Fig. 8.3b) confirm that LA-SINR improves average data rate and coverage probability compared to standalone and hybrid networks but fails to scale efficiently beyond $N > 8$ users. While it maintains 100% coverage up to $N = 4$, the coverage drops below 80% for larger user sets as the WiFi AP saturates. Similarly, outage probability increases sharply for higher QoS thresholds (above 25–30 Mbps), indicating the need for selective aggregation rather than full aggregation.

8.2.3 LA-EQoS Algorithm

To overcome the inefficiency of aggregating all users, a selective aggregation heuristic termed *LA-EQoS* (Link Aggregation for Enhanced QoS) is proposed. In this approach, only users experiencing low LiFi QoS are supplemented with additional WiFi links, thereby maintaining load balance and improving fairness. The number of aggregation users is denoted as N_{LA}, selected from the total user set N.

The rate for each user μ under LA-EQoS is expressed as:

$$R_{u,\text{LA-EQoS}} = \begin{cases} \beta_{ov} \times \left(R_{u,\text{LiFi}} + R_{u,\text{WiFi}}\right), & u \in \mathbb{U}_{LA}, \\ R_{\mu,\text{LiFi}}, & \text{otherwise}, \end{cases} \tag{8.4}$$

where $\mathbb{U}_{LA}$ denotes the set of users selected for aggregation based on lowest QoS.

Algorithm Behavior and Heuristic Insights: The parameter N_{LA} plays a critical role in determining network performance. When $N_{LA} = 0$, LA-EQoS reduces to a standalone LiFi system, leading to high outage due to coverage holes. Conversely, when $N_{LA} = N$, the algorithm behaves like LA-SINR, overloading WiFi and reducing throughput. Hence, an optimal N_{LA} must balance these extremes.

Simulation analysis (Fig. 8.3a) demonstrates that for $N = 10$ users, an optimal value of $N_{LA} = 3$ to 4 maximizes average throughput while minimizing outage probability. Increasing N_{LA} beyond this point yields diminishing returns, as Wi-Fi bandwidth becomes the bottleneck. This trade-off indicates that heuristic selection of N_{LA} can provide near-optimal operation without exhaustive search if guided by SINR-based thresholds or target QoS levels.

Performance Discussion: As shown in Figs. 8.2 and 8.3b, the LA-EQoS algorithm outperforms LA-SINR, hybrid, and standalone networks in both outage and coverage performance. For an outage probability constraint of 10%, LA-EQoS achieves up to 1.5$\times$ higher QoS compared to other networks, while maintaining 100% coverage for up to $N = 10$ users. Even under stricter outage constraints (20%), LA-EQoS provides robust QoS ($\simeq$ 40 Mbps) compared to

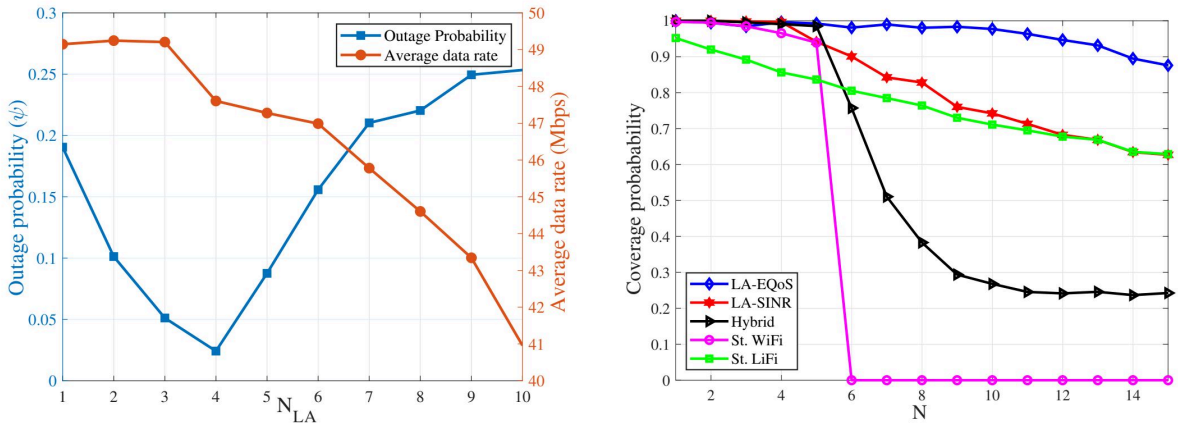

(a) Optimal N_{LA} analysis.

(b) Coverage for predefined QoS $R_0 = 20$ Mbps.

Figure 8.3: Performance comparison of heuristic LA algorithms: (a) optimal number of LA users (N_{LA}) for throughput–outage trade-off, and (b) coverage probability versus number of users under a fixed QoS requirement.

only $\simeq 25$ Mbps for hybrid and Wi-Fi-only networks. These results demonstrate that selective aggregation efficiently utilizes Wi-Fi resources while maintaining fairness and high throughput.

Limitations and Motivation for Next Analysis: Despite its advantages, LA-EQoS still depends on an exhaustive search to determine N_{LA} and does not capture multi-dimensional dependencies between SINR, AP load, and backhaul constraints. Moreover, it lacks a formal mechanism for fairness or dynamic adaptation to traffic variations. These limitations motivate the development of a more systematic and near-optimal approach *Flow-based Algorithm for Data Allocation (FLADA)* which models LA as a constrained optimization problem to achieve efficient, fair, and scalable aggregation decisions across users.

8.2.4 FLADA

Despite the significant improvements achieved using LA-SINR and LA-EQoS algorithms, both methods rely on heuristic user–AP association strategies. These heuristic approaches, although effective in reducing outage probability and enhancing average data rates, lack the adaptability to handle dynamic traffic load variations and interdependent link constraints in LA-HLWNs. Specifically, LA-SINR associates users purely based on received SINR, leading

to unnecessary Wi-Fi overloading when all users undergo link aggregation. On the other hand, LA-EQoS improves system efficiency by selectively assigning link aggregation to users with low LiFi QoS; however, it still determines the optimal number of LA users (N_{LA}) through exhaustive search, which becomes computationally expensive with larger user populations. Furthermore, both algorithms fail to incorporate key network constraints such as backhaul limitations, fairness among users, and aggregated link overheads within a unified analytical framework.

To overcome these limitations, we propose a near-optimal algorithm termed **FLADA** . The FLADA framework models the joint problem of AP selection and data rate allocation as a *multi-dimensional commodity flow optimization problem*. Unlike heuristic techniques, FLADA captures all major network constraints, including link capacity, user QoS requirements, AP backhaul capacity, and fairness, within a single mathematical formulation. This unified formulation enables a systematic optimization of the data rate distribution across Li-Fi and Wi-Fi access points, ensuring efficient utilization of network resources and avoiding AP overloading.

In link aggregation-enabled LA-HLWNs, as illustrated in Fig. 8.1, users can receive data concurrently from both Li-Fi and Wi-Fi APs [61]. This concurrent transmission enhances the achievable throughput and user satisfaction by minimizing handovers between Li-Fi and Wi-Fi links. However, since Wi-Fi APs have a larger coverage area, they tend to get overloaded unless the data rate demands of users are intelligently allocated. Hence, efficient AP selection and rate allocation are critical to balance the overall system performance and fairness.

To this end, the data rate allocation problem is formulated as a **multi-dimensional commodity flow problem** [98–100], where each flow represents the data rate assignment between users and APs under multiple constraints. The formulation jointly considers the user demand, signal quality, AP backhaul capacity, and fairness criteria. The resulting optimization problem is shown to be **NP-Hard** [101], implying that finding the exact optimal solution within polynomial time is computationally intractable.

Therefore, we develop **FLADA**, a near-optimal solution framework that efficiently approximates the optimal allocation. FLADA first formulates the data rate allocation as an *ILP* problem and then relaxes it into a *LP* model to reduce complexity. The LP solution is refined using a rounding mechanism to obtain feasible integer values for AP-user associations. Any data rate released due to rounding is reallocated iteratively to under-served users without violating fairness constraints. Through theoretical analysis, it is proven that FLADA guarantees a performance bound of at least **0.5× the optimal sum rate** (see Theorem 3, Section 8.2.4.4).

Fig. 8.4 presents the flow-graph-based system representation that forms the basis of FLADA, where each edge represents a possible data rate flow between users and APs across Li-Fi and Wi-Fi channels. This structure enables a unified and scalable framework for near-optimal link aggregation decisions in LA-HLWNs.

8.2.4.1 System Representation and Concept of Flow Graph

We consider an HLWN comprising m users, n Wi-Fi APs, and p Li-Fi APs in a typical indoor environment. Each user can associate with one Wi-Fi AP, or one Li-Fi AP, or both simultaneously via link aggregation. The central controller coordinates these associations based on channel quality, user demand, and AP backhaul capacity.

Unlike conventional optimization-based methods, FLADA introduces a unique **two-dimensional flow graph model** to represent the HLWN. In this graph, both the *rate flow* and *association flow* are modeled simultaneously, enabling precise mapping between user demands and multi-link capacities.

As illustrated in Fig. 8.4, the flow graph consists of five hierarchical layers of nodes:

1. The **source node** s, representing the collective application demand of all users.
2. **User nodes** f_i, corresponding to individual users.
3. Intermediate nodes f_i^w and f_i^l that capture the potential usage of WiFi and LiFi links by user i.

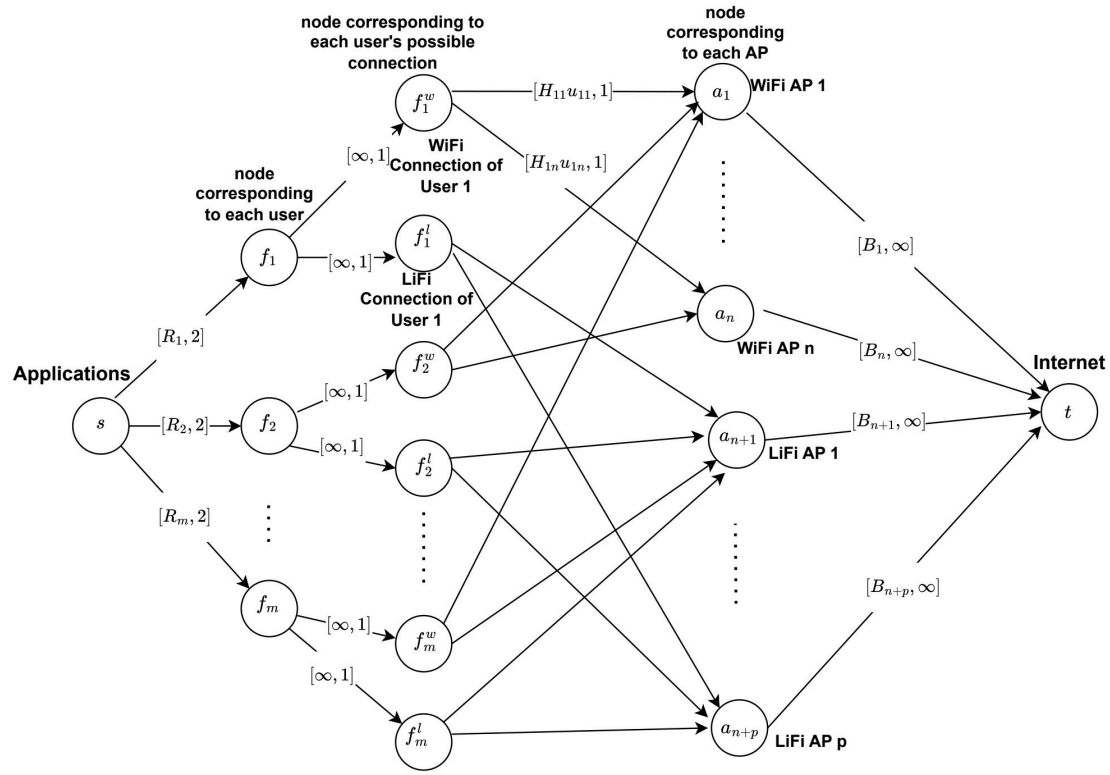

(a) Flow graph structure showing interconnection between users and APs.

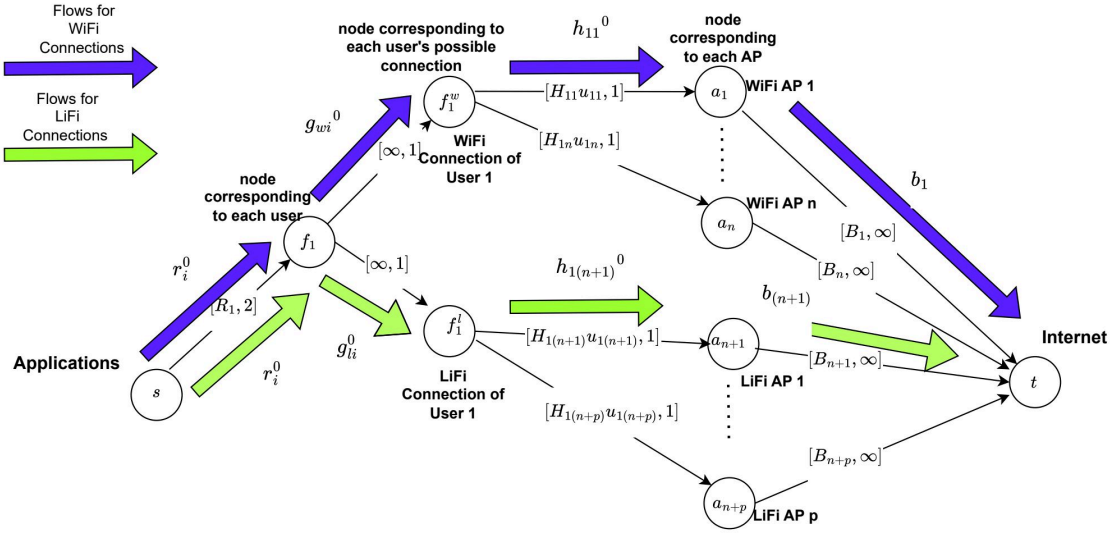

(b) Illustration of user-specific rate flows via LiFi and WiFi channels.

Figure 8.4: Flow-graph-based system representation for the proposed FLADA algorithm. Each edge carries dual information data rate and connection usage, forming the basis of the two-dimensional mixed max-flow (2DMMF) problem.

4. **AP nodes** a_j representing both WiFi and LiFi APs.

5. The **sink node** t, representing the Internet gateway or backhaul.

Each edge in this flow graph is assigned a capacity in the form of a two-dimensional vector $[x, y]$, where the first component represents the *data rate capacity*, and the second denotes the *connection capacity* (the number of allowable AP associations). For example: - Edge $\langle s, f_i \rangle$ has capacity $[R_i, 2]$, meaning user i can receive up to R_i Mbps and connect to at most two APs. - Edge $\langle f_i, f_i^w \rangle$ has capacity $[\infty, 1]$, restricting each user to only one WiFi AP. - Similar constraints apply for LiFi connections ($\langle f_i, f_i^l \rangle$).

The data rate flow from users to APs is denoted as h_{ij}^0, while the binary connection indicator is h_{ij}^1. This dual representation enables FLADA to capture both bandwidth allocation and link selection decisions in a unified mathematical model a key novelty compared to heuristic aggregation algorithms.

8.2.4.2 Problem Formulation and Solution

Building upon the flow-graph model illustrated in Fig. 8.4, we formally represent the data rate allocation problem in link aggregation-enabled hybrid LiFi/WiFi networks as a mixed integer-linear programming (MILP) problem. The objective is to maximize the total data rate delivered to users while ensuring fairness, respecting access point (AP) capacity limits, and accounting for link aggregation overhead.

Let r_i^q, h_{ij}^q, and b_j denote the user rate, flow from AP j to user i, and the total data transmitted by AP j, respectively; where $q \in \{0, 1\}$ corresponds to rate and association flows. The formulation aims to optimize these variables under realistic system constraints, as expressed in (8.5)–(8.16). This results in a multi-dimensional max-flow structure, herein referred to as the two-dimensional mixed max-flow (2DMMF) problem.

The complete set of equations and constraints is summarized as follows:

Objective Function: The optimization goal is:

$$\textbf{Maximize} \sum_{i=1}^{m} r_i^0 \tag{8.5}$$

which represents the maximization of the total data rate delivered to all users. subject to flow conservation, AP capacity, backhaul limits, fairness constraints, and the link aggregation overhead β_{ov}. The resulting problem is NP-Hard [101], making exact solutions computationally impractical for real-time operation. To address this, we introduce the proposed algorithm FLADA that provides an efficient, near-optimal solution for the 2DMMF problem.

Flow Conservation Constraints: To ensure that no intermediate node (user or AP) stores any data, flow conservation must hold throughout the network:

$$r_i^q = g_{wi}^q + g_{li}^q, \quad \forall i = 1,\ldots,m,\ q \in \{0,1\}, \tag{8.6}$$

$$g_{wi}^q = \sum_{j=1}^{n} h_{ij}^q, \quad g_{li}^q = \sum_{j=n+1}^{n+p} h_{ij}^q, \tag{8.7}$$

$$\sum_{i=1}^{m} h_{ij}^0 = b_j, \quad \forall j = 1,\ldots,n+p. \tag{8.8}$$

Capacity and Connectivity Constraints: Each link and node in the flow graph is subject to capacity limits, represented as:

$$r_i^0 \leq R_i, \quad \text{(user } i \text{ cannot exceed its demand)} \tag{8.9}$$

$$h_{ij}^0 \leq H_{ij} u_{ij}, \quad \text{(rate} \leq \text{capacity} \times \text{allocated RUs)} \tag{8.10}$$

$$b_j \leq B_j, \quad \text{(backhaul limit for AP } j\text{)} \tag{8.11}$$

$$r_i^1 \leq 2, \quad \text{(each user can connect to max two APs)} \tag{8.12}$$

Additionally, an AP can only allocate data to a user if a connection exists:

$$h_{ij}^1 > \lceil u_{ij}/U_j \rceil \tag{8.13}$$

Aggregation Overhead and Fairness Constraints: To model practical aggregation, an overhead factor β $(0 < \beta < 1)$ is included:

$$r_i^0 \leq \beta(g_{wi}^0 + g_{li}^0) + M(1 - g_{wi}^1) + M(1 - g_{li}^1), \tag{8.14}$$

where M is a sufficiently large constant ensuring constraint activation only for aggregated users.

A relaxed max–min fairness constraint is also introduced to ensure equitable data distribution:

$$r_i^0 \geq \gamma r_j^0, \quad \forall i, j \in \{1, \ldots, m\} \tag{8.15}$$

where γ $(0 < \gamma \leq 1)$ defines the fairness coefficient among users.

Finally, the bandwidth constraint for each AP ensures that the allocated resource units (RUs) do not exceed availability:

$$\sum_{i=1}^{m} u_{ij} \leq U_j, \quad \forall j = 1, \ldots, n + p \tag{8.16}$$

Variable Definitions:

- $r_i^0, g_{wi}^0, g_{li}^0, h_{ij}^0, b_j \in \mathbb{R}$ data rate and flow variables.
- $g_{wi}^1, g_{li}^1, h_{ij}^1 \in \{0, 1\}$ binary AP connection indicators.
- $r_i^1 \in \{0, 1, 2\}$ number of APs connected to user i.
- $u_{ij} \in \mathbb{Z}_{\geq 0}$ integer resource units allocated from AP j to user i.

8.2.4.3 Problem Complexity and NP-Hardness

Equations (8.5)–(8.16) define the complete MILP formulation, referred to as the **Two-Dimensional Mixed Max-Flow (2DMMF)** problem.

Since the problem combines integer allocation, backhaul limits, and fairness constraints, it is computationally intractable for real-time deployment. The following theorem establishes its NP-Hardness.

Theorem 8.2.1. *The 2DMMF problem is NP-Hard.*

Proof. We reduce the 2DMMF problem to the well-known 0–1 multiple knapsack problem. Considering a simplified case with only Li-Fi APs ($n = 0$), unlimited user demand ($R_i = \infty$), and no fairness constraint ($\gamma = 0$), the objective reduces to:

$$\textbf{Maximize} \sum_{i=1}^{m} \sum_{j=1}^{p} H_{ij} u_{ij}, \tag{8.17}$$

subject to:

$$\sum_{i=1}^{m} u_{ij} \leq U_j, \quad \forall j = 1, \ldots, p, \tag{8.18}$$

$$\sum_{j=1}^{p} \lceil u_{ij}/U_j \rceil \leq 1, \quad \forall i = 1, \ldots, m. \tag{8.19}$$

This formulation matches the 0–1 multiple knapsack problem, thereby proving NP-Hardness. □

Since solving this MILP optimally requires exponential time, we design a near-optimal, polynomial-time approximation of the proposed FLADA algorithm to obtain practical, high-quality solutions efficiently.

8.2.4.4 Solution Framework: FLADA

The complete FLADA procedure (illustrated in Fig. 8.5) comprises three major components:

1) LP Relaxation and Rounding (Algorithm 4): The MILP is relaxed into a Linear Programming (LP) problem (LPP), allowing continuous variables. After solving the LP optimally, the results are rounded to integers by retaining only the highest-rate APs (one

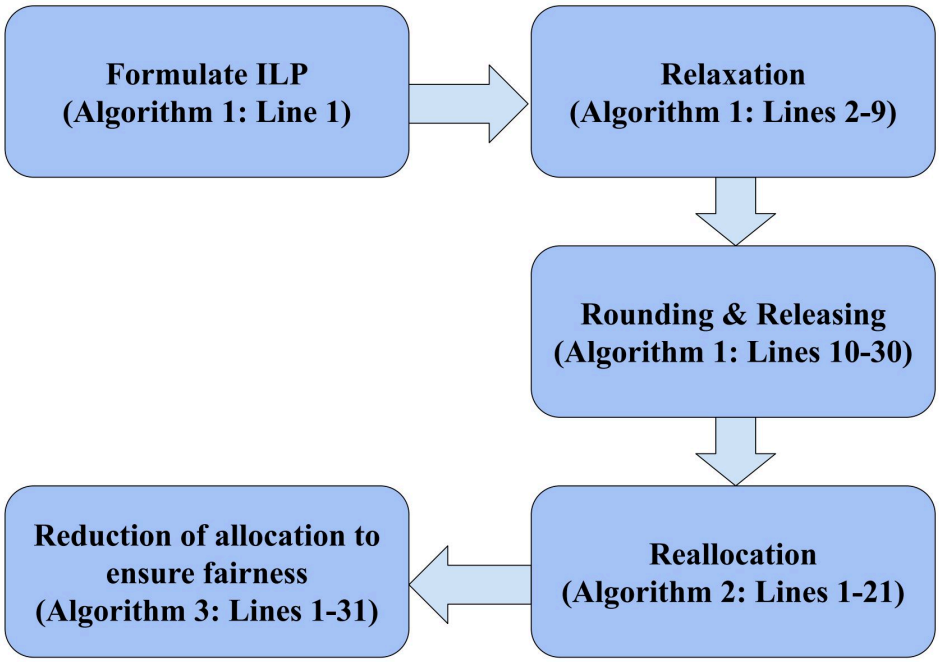

Figure 8.5: Overall flow of the proposed FLADA algorithm.

Li-Fi and one Wi-Fi) for each user. This ensures computational feasibility while maintaining near-optimal flow allocations.

2) Reallocation (Algorithm 5): Residual capacities released during rounding are redistributed to users with unsatisfied demands. This reallocation ensures improved bandwidth utilization without violating capacity or backhaul constraints.

3) Fairness Adjustment (Algorithm 6): To satisfy the fairness constraint, excessive allocations are proportionally reduced from over-served users based on the fairness coefficient γ. The final result ensures both throughput efficiency and equitable user distribution.

8.2.4.5 Approximation Guarantee and Feasibility

FLADA provides a constant-factor approximation with a theoretical lower bound of 0.5 of the optimal MILP solution.

Theorem 8.2.2. *LP-rounding followed by reallocation and fairness adjustment yields a feasible solution satisfying all flow, capacity, and fairness constraints of the 2DMMF problem.*

Algorithm 4 Generation of Feasible Result using LPP Solver and Rounding

Require: $R_i, H_{ij}^0, B_j, \forall i = 1,\ldots,m,\ j = 1,\ldots,n+p$
Ensure: Values $r_i^q, h_{ij}^q, b_j, \forall i = 1,\ldots,m,\ j = 1,\ldots,n+p,\ q \in \{0,1\}$
Formulate the ILP as described in Expressions (8.5)–(8.15)
Use LPP solver to solve the relaxed version of ILP
for all $i \in [1,\ldots,m]$ **do**
    $a_w \leftarrow \arg\max_{j=1}^{n} h_{ij}^0$
    $a_l \leftarrow \arg\max_{j=n+1}^{n+p} h_{ij}^0$
    $h_{ij}^q \leftarrow 0$, $u_{ij} = 0$, for all $j = n,\ldots,n+p$, $j \notin \{a_l, a_w\}$, and $q \in \{0,1\}$
    $g_{wi}^0 \leftarrow h_{ij}^0$ where $j = a_w$
    $g_{li}^0 \leftarrow h_{ij}^0$ where $j = a_l$
end for
for all $i \in [1,\ldots,m]$ **do**
    if $r_i^1 = 2$ **then** ▷ Check overhead and release weaker AP if needed
        if $(g_{wi}^0 + g_{li}^0) \times \beta < g_{li}^0$ **then**
            $a_w \leftarrow \arg\max_{j=1}^{n} g_{wi}^0$
            $b_j \leftarrow b_j - g_{wi}^0$ where $j = a_w$
            $u_{ij} \leftarrow 0$ where $j = a_w$
            $g_{wi}^q \leftarrow 0$ for all $q \in \{0,1\}$
            $r_i^0 \leftarrow g_{li}^0$
            $r_i^1 \leftarrow 1$
        else if $(g_{wi}^0 + g_{li}^0) \times \beta < g_{wi}^0$ **then**
            $a_l \leftarrow \arg\max_{j=n+1}^{n+p} g_{li}^0$
            $b_j \leftarrow b_j - g_{li}^0$ where $j = a_l$
            $u_{ij} \leftarrow 0$ where $j = a_l$
            $g_{li}^q \leftarrow 0$ for all $q \in \{0,1\}$
            $r_i^0 \leftarrow g_{wi}^0$
            $r_i^1 \leftarrow 1$
        end if
    end if
end for
return $\{r, g, h, u, b\}$

Lemma 8.2.3. *The LP-relaxation-based rounding guarantees that the total rate achieved by FLADA is at least* 0.5 *times that of the optimal ILP solution:*

$$O_r \geq 0.5 O^* \tag{8.20}$$

where O_r and O^* denote the achieved and optimal total rates, respectively.

Proof. Since each user connects to at most two APs, rounding may at most eliminate half of the allocated flow from the LP solution. Hence, the feasible rate achieved after rounding

Algorithm 5 Reallocation to Increase the Data Rate

Require: $R_i, H_{ij}^0, B_j, \forall i = 1,\ldots,m;\ j = 1,\ldots,n+p$
Ensure: Updated values $r_i^q, h_{ij}^q, b_j, \forall i = 1,\ldots,m;\ j = 1,\ldots,n+p;\ q \in \{0,1\}$

Sort users L in ascending order of $(R_i - r_i^0)$
for all $i \in [1,\ldots,m]$ **do**
  $a \leftarrow \max_{i=1}^{m}(R_i - r_i^0)$
  $i \leftarrow L[0]$ ▷ User with smallest remaining rate demand
  $a_w \leftarrow \arg\max_{j=1,\ldots,n} h_{ij}^0$
  $a_l \leftarrow \arg\max_{j=n+1,\ldots,n+p} h_{ij}^0$
  if $a_w > 0$ **then**
    $j \leftarrow a_w$
    $v_{ij} \leftarrow \min\left(R_i - r_i^0, H_{ij}U_{ij} - h_{ij}^0, B_j - b_j, a/\gamma\right)$
    $h_{ij}^0 \leftarrow h_{ij}^0 + v_{ij}$
    $g_{wi}^0 \leftarrow g_{wi}^0 + v_{ij}$
    $b_j \leftarrow b_j + v_{ij}$
  end if
  if $a_l > 0$ **then**
    $j \leftarrow a_l$
    $v_{ij} \leftarrow \min\left(R_i - r_i^0, H_{ij}U_{ij} - h_{ij}^0, B_j - b_j, a/\gamma\right)$
    $h_{ij}^0 \leftarrow h_{ij}^0 + v_{ij}$
    $g_{li}^0 \leftarrow g_{li}^0 + v_{ij}$
    $b_j \leftarrow b_j + v_{ij}$
  end if
end for
return r

satisfies:

$$O_r \geq 0.5 O_{LPP} \geq 0.5 O^*. \tag{8.21}$$

□

8.2.4.6 Performance Evaluation of FLADA

We first compare the proposed FLADA algorithm with three benchmark techniques: (i) Greedy, which connects each user to the AP providing the highest instantaneous data rate, (ii) Base-FLADA, which employs only LP rounding without reallocation or fairness correction, and (iii) the optimal ILP solution. Each simulation is averaged over 10,000 random user placements to ensure statistical reliability.

1) Sum Rate, Approximation Ratio, and Fairness: Figure 8.6 presents the overall performance comparison of FLADA against baseline schemes. Subfigures (a)–(b) show that FLADA

Algorithm 6 Release of data rates to satisfy fairness constraint.

INPUT: $R_i, H_{ij}^0, B_j, \forall i = 1,\ldots,m, j = 1,\ldots,n+p,$

OUTPUT: Values $r_i^q, h_{ij}^q, b_j, \forall i = 1,\ldots,m, j = 1,\ldots,n+p, q = \{0,1\},$

$L \leftarrow$ sorted users in descending order of $R_i - r_i^0$
for all $i \in L$ **do**
  $b' \leftarrow r_i^0 - a/\gamma$
  /*Reduce allocation to u_i by b' */
  if $b' < 0$ **then return** r
  end if
  /*Reduce WiFi allocation by w_r to x_{ij}*/
  $x_{ij} \leftarrow \min(b', g_{wi}^0)$
  $r_i^0 \leftarrow r_i^0 - x_{ij}$
  $g_{wi}^0 \leftarrow g_{wi}^0 - x_{ij}$
  for all $j \in [1,\ldots,n]$ **do**
    if $h_{ij}^0 > 0$ **then**
      $v_{ij} \leftarrow \max(0, h_{ij}^0 - x_{ij})$
      $h_{ij}^0 \leftarrow v$
      $b_j \leftarrow b_j - v$
      $x_{ij} \leftarrow x_{ij} - v$
      $r_i^0 \leftarrow r_i^0 - v$
    end if
  end for
  /*Reduce LiFi allocation by x_{ij} to u_i*/
  $x_{ij} \leftarrow b' - w_r$
  $g_{li}^0 \leftarrow g_{li}^0 - x_{ij}$
  for all $j \in [n+1,\ldots,n+p]$ **do**
    if $r_{ij}^0 > x_{ij}$ **then**
      $g_{li}^0 \leftarrow \max(0, g_{li}^0 - x_{ij})$
      $b_j \leftarrow b_j - x_{ij}$
      $r_i^0 \leftarrow r_i^0 - x_{ij}$
    end if
  end for
end forreturn r

consistently achieves near-optimal sum rates (up to 82% of ILP) for both small and large indoor setups. The approximation ratios in subfigure (c) validate that FLADA always meets the guaranteed bound of at least 0.5× optimal. Subfigure (d) shows Jain's fairness index, confirming that FLADA achieves higher fairness levels compared to Greedy and Base-FLADA for increasing γ, with a balanced trade-off between throughput and fairness.

2) Impact of Blockage and Computational Efficiency: Figure 8.7 illustrates the resilience of FLADA under blockage conditions and its computational scalability. In subfigure 8.7a, we observe that the sum rate decreases in the presence of Li-Fi blockage, but FLADA efficiently reallocates user demand across Wi-Fi links, resulting in only 14%–24% degradation. Subfig-

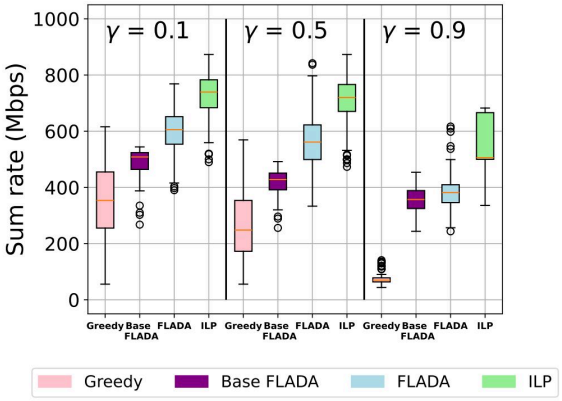

(a) Small room: $5 \times 5 \times 3$ m^3

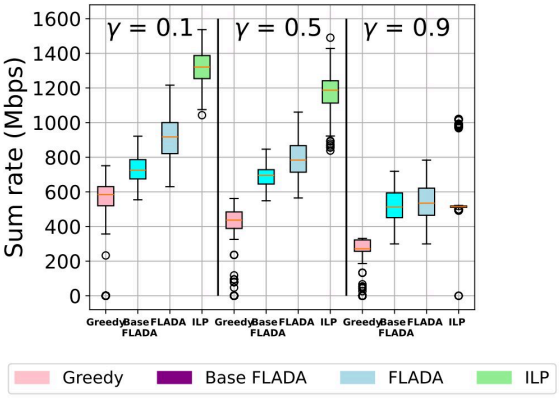

(b) Large room: $15 \times 5 \times 3$ m^3

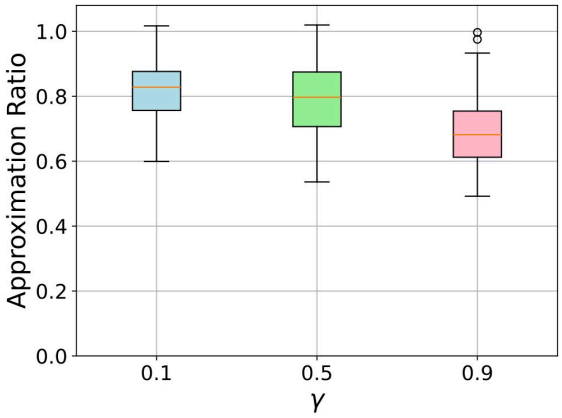

(c) Approximation ratio (FLADA/ILP)

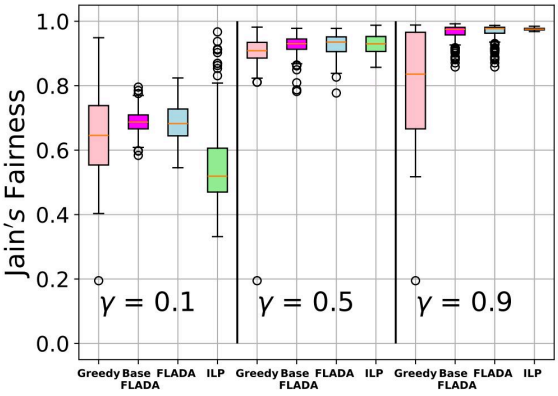

(d) Jain's fairness index

Figure 8.6: Performance comparison of FLADA with baseline algorithms. (a)–(b) Sum rate in small and large rooms, (c) approximation ratio validating the 0.5× theoretical bound, and (d) fairness variation with γ.

ure 8.7b shows that FLADA executes within 4–50 ms for small to large networks over 35× and 1200× faster than ILP, enabling real-time operation.

3) Effect of Link Aggregation and User Density: Figure 8.8 highlights the benefits of link aggregation and scalability with increasing user density. Subfigure 8.8a shows that enabling link aggregation yields a gain of approximately 149 Mbps at $\gamma = 0.5$. Subfigure 8.8b depicts that as the number of users increases, the per-user rate decreases due to fixed backhaul capacity, while fairness controls the rate distribution across users.

4) Access Point Contribution, User Satisfaction, and Energy Efficiency: The detailed insight analysis in Fig. 8.9 shows system-level efficiency metrics. Subfigure 8.7 reveals that

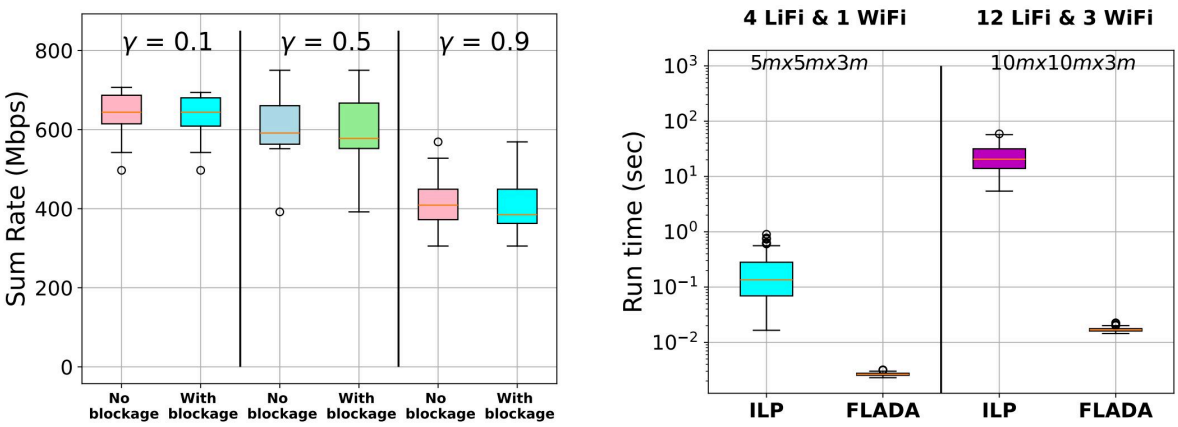

(a) Sum rate under blockage/non-blockage

(b) Runtime comparison (FLADA vs ILP)

Figure 8.7: Impact of blockage and computational efficiency. (a) FLADA shows robustness to LiFi blockage via dynamic reallocation. (b) Runtime comparison showing FLADA's fast convergence relative to ILP.

Li-Fi APs dominate throughput for low user counts, while Wi-Fi balances load as users increase. Subfigure 8.9b illustrates the user satisfaction ratio, where FLADA achieves near-optimal satisfaction for moderate fairness levels ($\gamma = 0.5$). Subfigure (c) demonstrates that link aggregation significantly enhances energy efficiency by reusing static AP power budgets for dual-link communication.

8.2.4.7 Key Takeaways

The FLADA algorithm offers a scalable, fairness-aware, and computationally efficient framework for link aggregation in HLWNs. By integrating flow conservation, aggregation overhead, and fairness constraints into a unified model, FLADA achieves near-optimal data rate allocation with provable performance guarantees, bridging the gap between theoretical optimality and real-time feasibility.

This stepwise approach ensures that the resulting allocations are feasible, fair, and computationally efficient. The LP-based relaxation guarantees at least 50% of the optimal achievable sum rate, while simulations confirm that the practical performance exceeds 85–88% of the ILP optimum on average.

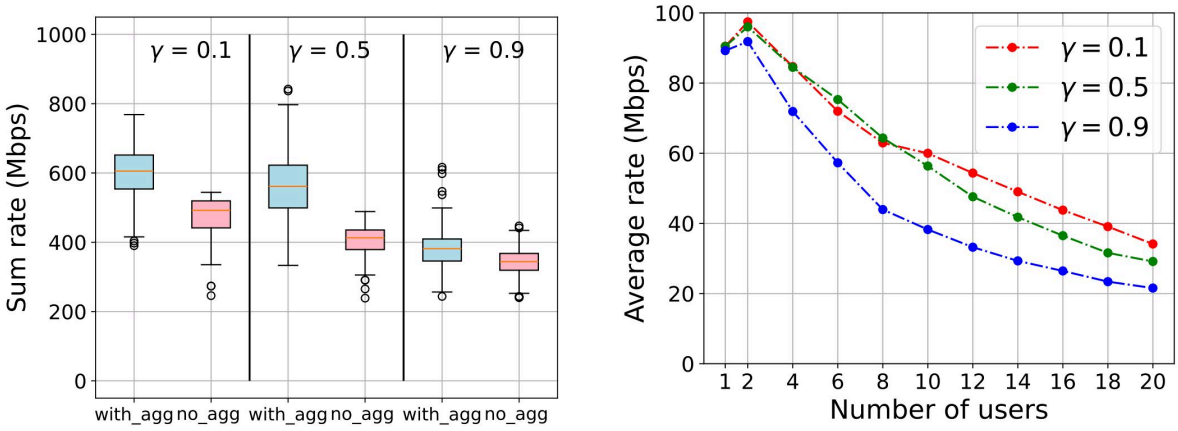

(a) With and without link aggregation

(b) Average rate vs. number of users

Figure 8.8: Impact of link aggregation and user density on system throughput. (a) Link aggregation yields significant sum rate gain. (b) Average user rate decreases with user count due to limited capacity.

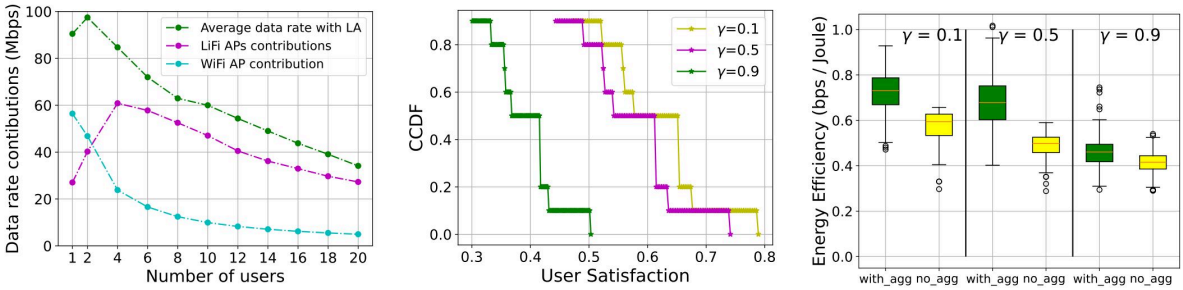

(a) LiFi/WiFi contribution

(b) User satisfaction

(c) Energy efficiency

Figure 8.9: Detailed performance metrics of FLADA: (a) AP contribution to total throughput, (b) user satisfaction under different fairness values, and (c) energy efficiency comparison for aggregated and non-aggregated links.

8.2.5 Practical Considerations for Global Information and Scalable Implementation

The proposed optimization framework for link aggregation assumes the availability of global network information, including user traffic demand, channel conditions (SINR), and AP load. In practical deployments, such information can be collected through a centralized network controller, which periodically gathers measurements from Li-Fi and Wi-Fi access points as well as user devices. This can be implemented using software-defined networking (SDN)-based architectures or centralized coordination units within hybrid access networks.

However, maintaining an accurate global view becomes challenging in highly dynamic environments with mobile users, where channel conditions and user associations change rapidly. Frequent updates of global information may introduce significant signaling overhead and latency, thereby limiting scalability.

To address these challenges, lightweight and distributed approaches can be employed. For instance, local decision-making strategies can be adopted, where users or APs make link selection and rate allocation decisions based on partial or locally available information, such as instantaneous SINR or queue length. Additionally, hybrid approaches combining periodic global optimization with real-time local adaptation can strike a balance between performance optimality and computational complexity.

These considerations highlight that while the proposed optimization framework provides a theoretical upper bound on performance, practical implementations can leverage hierarchical or distributed control mechanisms to enable scalable and efficient link aggregation in dynamic hybrid Li-Fi/Wi-Fi networks.

8.3 Summary

This chapter addressed the need for link aggregation in hybrid LiFi/WiFi networks to overcome the limitations of single-link association and LA-induced overhead. Three algorithms—LA-SINR, LA-EQoS, and FLADA—were proposed to achieve trade-offs between throughput, fairness, and computational efficiency. The results confirm that link aggregation improves network throughput, reduces outage probability, and supports high-demand applications such as AR/VR and ultra-HD streaming. Building on these outcomes, the subsequent chapter explores cross-layer aggregation, scheduling, and reliability optimization for next-generation multi-link hybrid systems.

While this chapter primarily addressed link aggregation for static or quasi-static users, real-world deployments inevitably involve user mobility and dynamic handover events. These

factors significantly influence network stability, throughput, and fairness, particularly when users traverse overlapping Li-Fi attocells. To address these challenges, the next chapter introduces mobility-aware link aggregation and access point selection frameworks that integrate predictive user movement modeling with dynamic optimization.

It is further observed that the performance of link aggregation in hybrid LiFi/WiFi networks is strongly influenced by the SINR conditions of LiFi and WiFi links, aggregation overhead, and traffic distribution strategies. Higher SINR improves achievable data rates and enhances aggregation gains, while practical overheads such as packet reordering and synchronization reduce effective throughput. Moreover, efficient allocation of traffic across multiple links plays a key role in balancing throughput and fairness. These insights emphasize the importance of overhead-aware and adaptive link aggregation mechanisms.

Chapter 9

Mobility-Aware Rate Allocation and Handover Optimization in LA-enabled HLWNs

Hybrid Li-Fi/Wi-Fi networks have shown significant potential for delivering high-capacity and low-latency indoor wireless connectivity. The previous chapter addressed static network optimization through the FLADA framework, which efficiently managed link aggregation and rate allocation among users to enhance throughput and fairness. However, such approaches assume stationary or quasi-static users, whereas real-world indoor environments are inherently dynamic.

User mobility introduces frequent transitions across Li-Fi attocell and Wi-Fi coverage zones, resulting in link fluctuations, blockages, and handover delays. These effects degrade throughput and user experience, especially when Li-Fi links are intermittently obstructed or Wi-Fi becomes overloaded. Hence, mobility-aware mechanisms are essential to ensure seamless service continuity and efficient utilization of hybrid network resources.

To address these challenges, this chapter presents the **Mobility-Aware Probabilistic Selection (MAPS)** framework, which dynamically optimizes AP selection and data rate

allocation by integrating user mobility prediction, probabilistic association, and load-aware optimization. Two variants are introduced *MAPS-LP* (Linear Programming-based) and *MAPS-GP* (Greedy Programming-based) that balance analytical tractability with system efficiency. The proposed framework minimizes handover frequency, mitigates link outages, and sustains high aggregate throughput under user movement.

9.1 Resource Allocation Challenges in Hybrid Networks

In HLWNs, efficient resource allocation plays a crucial role in maintaining system performance, particularly under user mobility. While static optimization schemes such as FLADA provide high throughput and fairness for stationary users, these solutions are less effective when users move dynamically across Li-Fi attocells and WiFi zones. User movement causes frequent variations in received signal strength, leading to fluctuating link quality, unbalanced load distribution, and an increased number of handovers.

Li-Fi APs offer high data rates but are sensitive to LoS conditions, user orientation, and blockage. Even minor movement can disrupt an optical link, forcing a transition to WiFi for continuity. Conversely, Wi-Fi access points provide wider coverage but may suffer from congestion due to many users sharing the same bandwidth. Hence, an optimal solution must jointly consider mobility, link reliability, load balancing, and backhaul constraints.

Conventional association methods that rely solely on instantaneous received signal strength or SINR lead to premature or unnecessary handovers. Therefore, an adaptive and probabilistic strategy that integrates mobility prediction, fairness, and link reliability is necessary. The proposed MAPS framework addresses these requirements through a unified optimization approach.

9.2 System Model and Design

9.2.1 Description of the System

We consider an indoor environment containing m users, n Wi-Fi APs, and p LiFi APs deployed within a known area. All APs are ceiling-mounted to provide full coverage, and a CC coordinates dynamic user–AP associations based on channel quality and demand. Each user i has a data rate demand R_i corresponding to the throughput required for its application (e.g., $\sim$7.4 Mbps for 1080p video streaming).

The actual rate allocated to user i at time t is denoted by r_i^t, bounded by network resources and user demand. Each user may connect to one Wi-Fi AP, or one Li-Fi AP, or both concurrently. When both are used, link aggregation enables data reception from both links simultaneously.

Bandwidth allocation follows modern WiFi standards (IEEE 802.11ax/be) using OFDMA RUs. Each 20 MHz channel can be subdivided into multiple RUs, with adaptive modulation and coding schemes (MCS) ranging from BPSK to 4096-QAM according to SINR conditions.

9.2.2 Constraint on User Data Rates

Link aggregation introduces a reordering overhead, quantified by β $(0 \leq \beta \leq 1)$, where (β) represents the packet reorder overhead in case of link aggregation. Thus, user i's achievable rate is constrained as

$$r_i^t \leq \min(R_i, \sum_{j=1}^{n+p} \beta_i B_{ij}^t c_{ij}^t), \tag{9.1}$$

where B_{ij}^t is the allocated bandwidth and c_{ij}^t denotes bits/Hz based on modulation. $\beta_i = 0.2$ for aggregated links and 1 otherwise. Each AP j has a fixed backhaul capacity B_j defined by its wired connection.

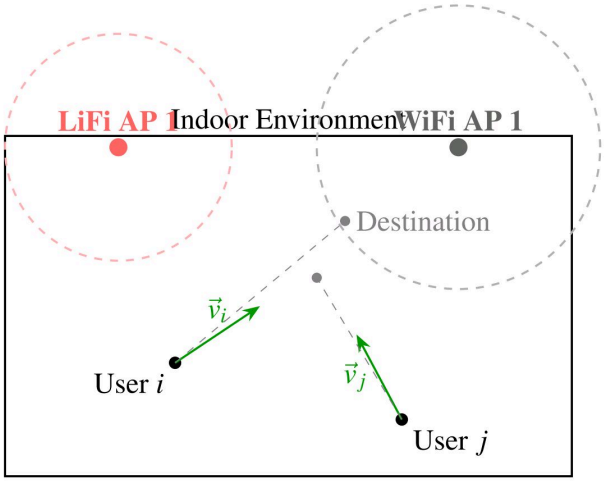

Figure 9.1: User mobility under the Random Waypoint (RWP) model showing current positions, velocity vectors, and destinations.

9.2.3 User Mobility Model

User positions evolve according to the RWP model, suitable for bounded indoor spaces [102, 103]. Each user randomly selects a destination and moves with velocity $\vec{v}_i(t) \in [v_{\min}, v_{\max}]$. The position update is

$$l_i(t+\Delta t) = l_i(t) + \vec{v}_i(t) \cdot \Delta t. \tag{9.2}$$

After reaching a destination, the user pauses briefly before selecting a new waypoint. Figure 9.1 illustrates this motion.

9.3 Problem Formulation and Solution

9.3.1 Objective Function

The primary objective is to maximize the overall throughput of all users in the HLWNs. However, this throughput is affected by mobility-induced handovers. Whenever a user moves from one AP to another between consecutive time intervals $(t, t+\Delta t)$, a temporary reduction

in data rate occurs due to the handover overhead. Hence, the number of handovers H_t at time t is defined as the number of users whose AP association changes during Δt:

$$H_t = 1(B_{ij}^t) - 1(B_{ij}^{t+\Delta t}), \tag{9.3}$$

where $1(\cdot)$ denotes an indicator function that equals 1 when the bandwidth allocation is non-zero and 0 otherwise.

Accordingly, the overall network utility U over a time horizon of $k\Delta t$ is expressed as:

$$U = \sum_{t=T}^{T+k\Delta t} \sum_{i=1}^{m} r_i^t - \alpha H_t, \tag{9.4}$$

where α represents the penalty incurred due to a handover. Since both r_i^t and H_t depend on the user's position, which is inherently stochastic, the goal is to maximize the expected utility:

$$\textbf{Maximize: } E_D[U] = E_D\left[\sum_{t=T}^{T+k\Delta t} \sum_{i=1}^{m} r_i^t - \alpha H_t\right], \tag{9.5}$$

where the expectation $E_D[\cdot]$ is taken over all possible user movement directions and speeds as dictated by the mobility model.

Equations (9.2)–(9.5) together formulate an integer programming problem aimed at optimizing AP association and bandwidth allocation. However, solving this integer problem at every time instant is computationally expensive. Therefore, a relaxed and scalable approach is required that can efficiently update associations in near-real time.

9.3.2 Scalable AP Assignment via Linear Programming

A practical way to approximate the solution of the above problem is to relax the integer variables and solve a LPP at each update interval. The LPP determines the optimal association and bandwidth distribution that maximizes the expected throughput for the next step while accounting for potential handover costs.

Algorithm 7 Scalable AP Assignment via Selective Optimization (LPP-Based Approach)

Input: User positions, velocities, current AP associations
Output: Optimal AP and bandwidth assignment
while network is active **do**
    Estimate expected utility E_D assuming users follow current velocities
    Identify mobile users located near AP coverage boundaries
    Generate feasible AP assignment permutations for these boundary users
    for each permutation p of boundary AP assignments **do**
        Solve the LPP to compute corresponding utility $U(p)$
    end for
    Select the optimal configuration: $\text{AP}^* = \arg\max_p U(p)$
    Solve the final LPP to obtain B_{ij}^t for the selected assignment
end while

The procedure, outlined in Algorithm 7, executes periodically, predicting user positions based on current velocities and optimizing only for those users near AP coverage boundaries where handovers are most probable.

9.3.3 Mobility-Aware Probabilistic Selection (MAPS) Algorithm

Although the LPP-based method effectively estimates near-optimal associations, it must be repeatedly solved for every potential user movement pattern, which becomes computationally intensive. To address this, we propose a *Mobility-Aware Probabilistic Selection (MAPS)* framework that employs intelligent pruning and probability-based optimization to reduce complexity.

Maximum Probability Estimation

In realistic mobility models such as RWP, users predominantly continue in their current direction until reaching a waypoint. Hence, the likelihood of abrupt direction changes is relatively low. Leveraging this observation, MAPS considers only the most probable next-step movement (i.e., a single-step prediction with $\Delta t = 1$). This approximation yields a practical estimate of the expected utility, denoted as U_a, without evaluating all stochastic trajectories.

Search Space Pruning

To further reduce computational load, MAPS employs two pruning strategies:

1. **Mobility-based pruning:** Only users near AP boundaries are considered for reassignment, as others are unlikely to change associations.

2. **AP-selection pruning:** For each user, only the two strongest APs (in terms of received SINR or achievable rate) are retained for consideration, reducing n to 2 per user.

Together, these constraints significantly reduce the search space, transforming the original exhaustive complexity of $\mathcal{O}((n+p)^m)$ into a manageable form suitable for real-time operation.

MAPS-LP Variant

In the first variant, **MAPS-LP**, the expected user positions at $t = t_0 + 1$ are used to solve the LPP for each candidate AP configuration. The algorithm then selects the configuration that maximizes the cumulative utility U over the considered time steps, incorporating handover penalties.

MAPS-GP Variant

While MAPS-LP yields high accuracy, solving multiple LPPs remains resource-intensive. Therefore, a second variant, **MAPS-GP**, replaces the LPP evaluation step with a lightweight greedy algorithm that approximates utility using instantaneous rate estimates. Once the optimal configuration is identified through this greedy evaluation, final allocations are refined using a single LPP step for precision.

Although MAPS-GP sacrifices some optimality, it achieves a substantial reduction in runtime, nearly 50% compared to MAPS-LP while maintaining close performance, with an average utility degradation of less than 30%.

9.3.4 Performance Analysis of the MAPS Algorithm

Let the optimal expected utility be E_D^o, and the utility achieved by MAPS be E_D^c. Since the algorithm prioritizes the APs offering the highest or second-highest data rates, sub-optimality occurs only when the cumulative benefit of alternate associations outweighs the chosen configuration. This behavior is characterized by the following lemmas.

Lemma 9.3.1. *The MAPS algorithm is non-optimal only if:*

$$E_D^c(i,j) \geq E_D^c(i,k), \quad \textit{and} \tag{9.6}$$

$$E_D^c(i,j) \leq \sum_{i'} E_D^c(i',j), \tag{9.7}$$

where $E_D^c(i,j)$ denotes the utility of user i associated with AP j, and k represents another potential AP.

Lemma 9.3.2. *The loss incurred by user i, denoted by L_i, is given by:*

$$L_i = \sum_{i'} [E_D^c(i',j) - E_D^c(i',k)] - [E_D^c(i,j) - E_D^c(i,j')], \tag{9.8}$$

where AP k is an alternate AP previously used by user i', and j' is an AP weaker than j.

Lemma 9.3.3. *The total expected loss L across all users is expressed as:*

$$L = \sum_{i=1}^{m} E[L_i] = P(m_j) \sum_{i=2}^{m} \frac{L_i}{R_i}, \tag{9.9}$$

where m_j is the number of users within the coverage area of AP j, and $P(m_j)$ is the probability of that occupancy.

For a typical scenario with 10 users and 4 Li-Fi APs in a small indoor environment, the probability distribution of users across APs follows a binomial model with parameters $(N, 1/m)$. Numerical evaluation shows that $L = 0.45D$, indicating that the MAPS algorithm achieves at

least 55% of the optimal utility on average, while operating at a fraction of the computational cost.

9.4 Performance Evaluation and Discussion

This section presents the performance evaluation of the proposed MAPS-LP and MAPS-GP algorithms, compared with the benchmark schemes Linear Programming-based and Greedy allocation. The simulation environment, user mobility model, and channel characteristics follow the configurations defined in Chapters 6 and 8.

9.4.1 Simulation Setup Overview

We consider two indoor hybrid Li-Fi/Wi-Fi scenarios: (i) a small room of $5 \times 5 \times 3$ m^3 and (ii) a large room of $10 \times 5 \times 3$ m^3, with multiple Li-Fi APs and Wi-Fi APs as shown previously in Fig. 8.1. Users move according to the RWP model, and link aggregation is applied to enable concurrent LiFi–WiFi data reception. The aggregation overhead factor $\beta = 0.2$ accounts for reordering and synchronization costs, consistent with [97]. All simulation and channel parameters remain identical to those listed in Table 6.2 and Table 6.3 (see Chapter 6).

9.4.2 Performance Evaluation of the Proposed Algorithms

9.4.2.1 Sum Rate Comparison

Figs. 9.2(a) and (b) present the sum rate performance of MAPS-LP, MAPS-GP, LPP, and Greedy algorithms across fairness coefficients $\gamma \in \{0.1, 0.5, 0.9\}$ for the small and large room configurations (10 and 20 users).

As fairness constraints become stricter (γ increases), the overall sum rate decreases since resources are distributed more evenly among users. MAPS-LP consistently achieves the highest throughput in both environments, attaining nearly 950 Mbps at $\gamma = 0.1$ in the large room, while

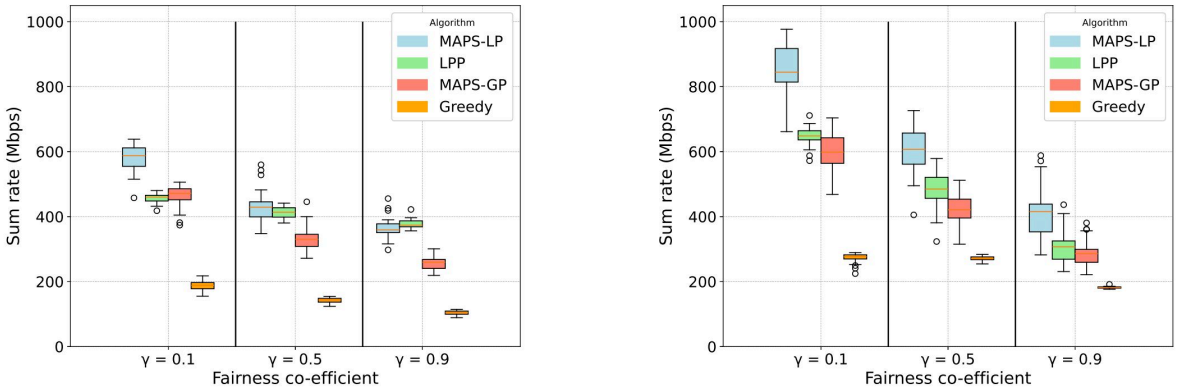

(a) Small room ($5 \times 5 \times 3$ m^3) with 10 users.

(b) Large room ($10 \times 5 \times 3$ m^3) with 20 users.

Figure 9.2: Sum rate performance comparison for the proposed MAPS-LP and MAPS-GP with baseline algorithms (LPP and Greedy) under varying fairness coefficients γ.

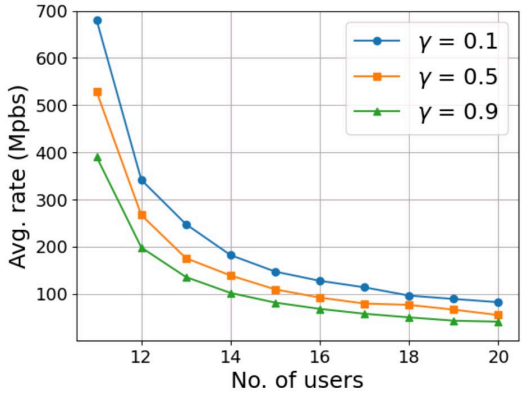

Figure 9.3: Average user rate achieved by MAPS-LP under varying fairness coefficients in the large room configuration.

MAPS-GP closely follows with $\sim$ 700 Mbps. Both methods outperform LPP and Greedy across all fairness levels, demonstrating robustness and scalability under varying user densities.

9.4.2.2 Average User Rate

The variation of average user data rate with increasing user count is shown in Fig. 9.3. The average rate decreases as the number of users grows, primarily due to bandwidth sharing. At $\gamma = 0.1$, the network prioritizes throughput maximization, achieving the highest average rates, while higher γ values (0.5 and 0.9) yield more uniform but reduced rates due to fairness constraints.

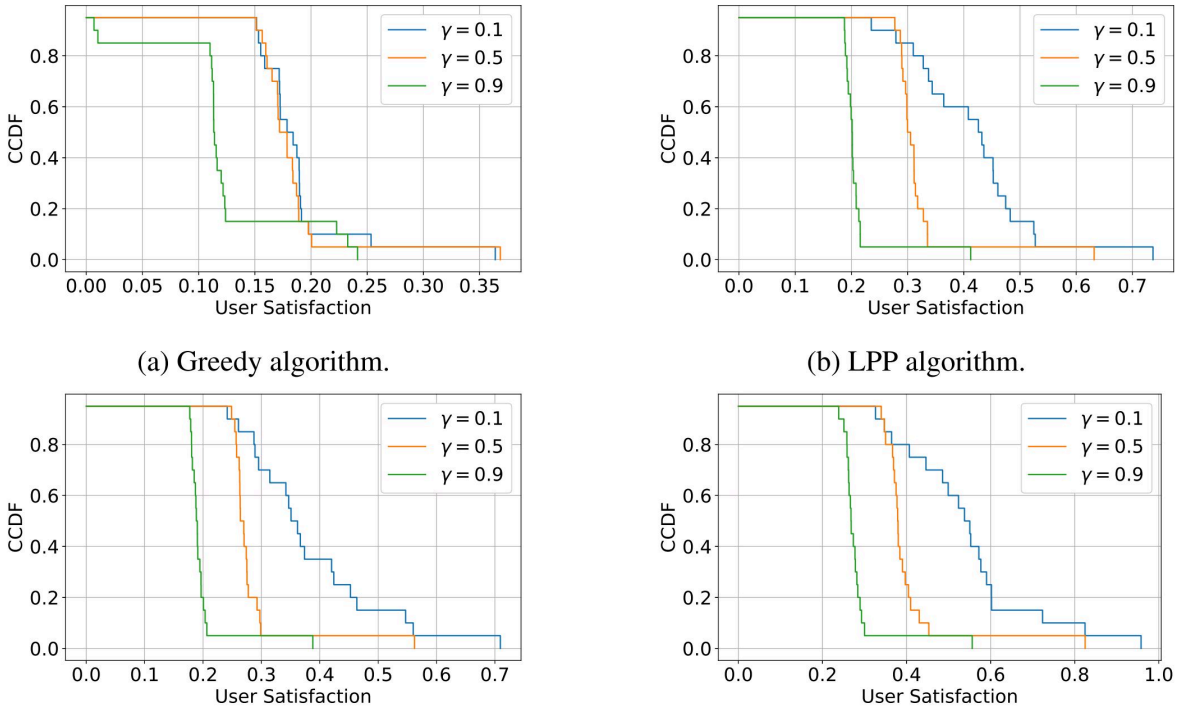

(a) Greedy algorithm.

(b) LPP algorithm.

(c) Proposed MAPS-GP.

(d) Proposed MAPS-LP.

Figure 9.4: Comparison of user satisfaction (CCDF) for all algorithms under different fairness coefficients γ.

9.4.2.3 User Satisfaction Analysis

User satisfaction $S = r_i^t / R_i$ quantifies the ratio of achieved to requested rate. Fig. 9.4 compares the complementary cumulative distribution function (CCDF) of satisfaction across all algorithms.

The proposed MAPS-LP achieves the highest satisfaction levels, with a peak of 0.83 at $\gamma = 0.5$, followed by MAPS-GP at 0.56. Both significantly outperform the baselines, which exhibit lower satisfaction (LPP: 0.64, Greedy: 0.36). The right-shifted CCDF curves of MAPS-LP indicate that more users meet their data rate requirements even in mobility conditions.

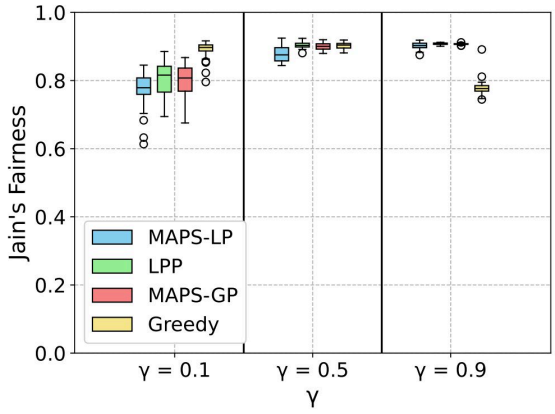

Figure 9.5: Fairness comparison across algorithms via Jain's index under different γ values.

9.4.2.4 Fairness Evaluation via Jain's Index

Fairness is evaluated using Jain's index, given by:

$$J = \frac{(\sum_{i=1}^{m} r_i^t)^2}{m \sum_{i=1}^{m} (r_i^t)^2}. \tag{9.10}$$

Fig. 9.5 shows that at low γ (0.1), MAPS-LP and MAPS-GP achieve $J \approx 0.8$, as the system prioritizes throughput. As fairness enforcement increases ($\gamma = 0.9$), both algorithms converge to near-perfect fairness ($J > 0.95$), outperforming LPP and Greedy, which show higher variability.

9.4.2.5 Handover Rate Analysis

To quantify the stability of user–AP association, Fig. 9.6 compares the average handover rate across algorithms. MAPS-GP achieves the lowest handover rate, reflecting its steady greedy-based assignment strategy. MAPS-LP balances slightly higher handovers with superior throughput, while LPP and Greedy both exhibit high rates due to reactive and unstable reassignment policies.

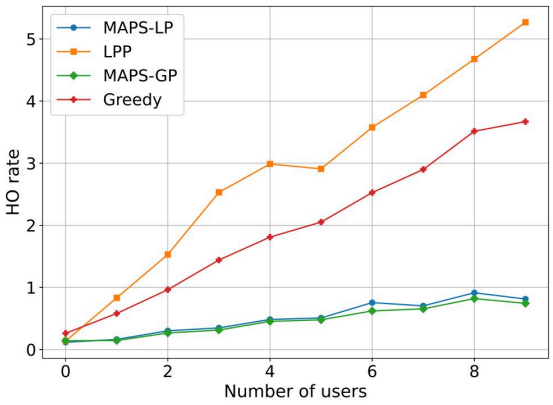

Figure 9.6: Comparison of handover rate for MAPS-LP, MAPS-GP, and baseline algorithms.

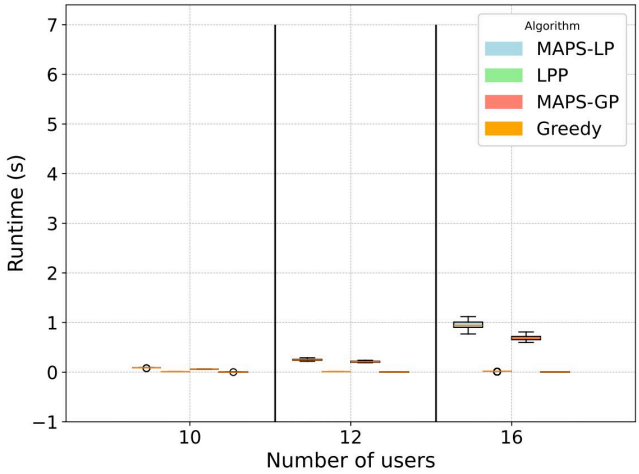

Figure 9.7: Runtime comparison of all algorithms with increasing number of users.

9.4.2.6 Runtime Performance

The runtime scalability of the proposed algorithms is illustrated in Fig. 9.7. MAPS-GP executes in under 0.5 s for up to 20 users, achieving near-real-time responsiveness, whereas MAPS-LP requires about 1 s per iteration reasonable for fairness-critical applications. In both cases, runtime growth is sublinear with user count, confirming computational efficiency through probabilistic pruning and limited AP reassignment.

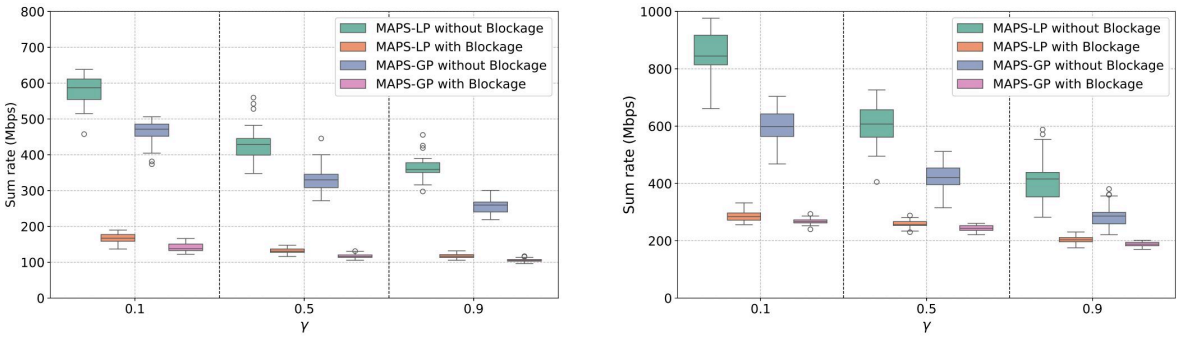

(a) Small room ($5 \times 5 \times 3$ m^3), 10 users.

(b) Large room ($10 \times 5 \times 3$ m^3), 20 users.

Figure 9.8: Sum rate comparison for MAPS-LP and MAPS-GP under blockage and no-blockage scenarios.

9.4.2.7 Impact of LiFi Blockage

The impact of human blockage on Li-Fi throughput is evaluated in Fig. 9.8. In both room sizes, blockage leads to significant rate reductions, particularly for low fairness values ($\gamma = 0.1$), where throughput maximization dominates. MAPS-LP retains the highest throughput under both blockage and no-blockage conditions, while MAPS-GP remains computationally efficient with acceptable degradation.

9.4.2.8 Comparative Summary

Table 9.1 summarizes the performance comparison across all algorithms. MAPS-LP achieves the highest throughput and fairness at moderate computation cost, whereas MAPS-GP offers a near-optimal balance between performance and runtime. Both outperform the baseline LPP and Greedy algorithms across all metrics.

9.5 Summary

This chapter presented a mobility-aware optimization framework for LA-enabled HLWNs. Two algorithms **MAPS-LP** and **MAPS-GP** are proposed to jointly optimize user data rate allocation and handover reduction under mobility and fairness constraints.

Table 9.1: Comparative Performance Summary of MAPS-LP, MAPS-GP, LPP, and Greedy Algorithms

Metric	**MAPS-LP**	**MAPS-GP**	**LPP**	**Greedy**
Sum Rate (10 Users)	Highest ($\sim$650 Mbps at $\gamma = 0.1$)	Slightly lower than MAPS-LP	Moderate; drops sharply with increasing γ	Lowest; not fairness-aware
Sum Rate (20 Users)	Peak $\sim$950 Mbps at $\gamma = 0.1$	Close to MAPS-LP ($\sim$700 Mbps)	Moderate ($\sim$500 Mbps)	Poor performance ($<$300 Mbps)
User Satisfaction (CCDF)	Up to 0.83 at $\gamma = 0.5$; high satisfaction under all γ	Peaks at 0.56; improves over LPP	Moderate (peak $\sim$0.64)	Poor (peak $\sim$0.36)
Jain's Fairness Index	Near 1.0 at $\gamma = 0.9$; consistent across γ	Near 1.0 at $\gamma = 0.9$; stable	Fair but with higher variability	Lowest fairness under low γ
Handover Rate (Fig. 9.6)	Low; gradually increases with users	Lowest HO rate across all user counts	Highest (exceeds 5 at 9 users)	Moderate; grows with user density
Runtime (Fig. 9.7)	Moderate ($\sim$1 s at 16 users); highest among all	Low ($\sim$0.4 s); $\sim$50% lower than MAPS-LP	Low and grows with user count	Minimal due to greedy nature

By modeling user mobility with the RWP approach and applying probabilistic pruning, the proposed methods effectively reduced computational complexity while maintaining high system utility. MAPS-LP achieved the highest throughput and fairness, while MAPS-GP provided comparable performance with lower runtime, demonstrating suitability for real-time operation.

Extensive simulations showed that the MAPS-based algorithms significantly outperform baseline methods in terms of throughput, fairness, and handover rate, even under Li-Fi blockage conditions. Overall, this chapter established that incorporating mobility awareness and probabilistic decision-making substantially enhances performance in hybrid Li-Fi/Wi-Fi systems. The next chapter concludes the thesis and discusses potential future extensions.

Practical Deployment Considerations: The two proposed algorithms, MAPS-LP and MAPS-GP, differ significantly in terms of computational complexity and suitability for practical deployment scenarios. MAPS-LP, based on linear programming, provides near-optimal per-

formance in terms of throughput and fairness, but requires a global view of the network and incurs higher computational overhead. Therefore, it is more suitable for small to medium-scale networks or semi-static environments, such as enterprise or office deployments, where user mobility is limited and centralized control is feasible.

In contrast, MAPS-GP adopts a heuristic approach with reduced computational complexity, making it more suitable for large-scale and highly dynamic environments with mobile users. Due to its lower runtime and reliance on simplified decision-making, MAPS-GP can be effectively deployed in real-time systems, such as dense indoor public spaces or IoT-driven environments, where fast adaptation is required.

Thus, MAPS-LP is preferred for performance-critical scenarios with manageable network size, while MAPS-GP is better suited for scalable, real-time implementations in dynamic hybrid Li-Fi/Wi-Fi networks.

It is further observed that the performance of mobility-aware link aggregation in HLWNs is strongly influenced by user mobility patterns, access point load distribution, and handover strategies. Increased mobility leads to frequent handovers, which can degrade throughput and increase latency if not efficiently managed. Furthermore, the effectiveness of rate allocation depends on channel conditions and load balancing across LiFi and WiFi links. The choice of pruning and probabilistic decision mechanisms also impacts the trade-off between computational complexity and system performance. These insights emphasize the importance of mobility-aware optimization and efficient handover management in hybrid networks.

Chapter 10

Conclusion and Future Work

This dissertation presented a comprehensive investigation into the design, modeling, and optimization of **Hybrid Li-Fi/Wi-Fi Networks (HLWNs)** for high-performance indoor wireless communication. Motivated by the increasing data demands of emerging applications and the limitations of conventional RF-based networks, this research aimed to develop practical solutions that combine the strengths of Li-Fi and Wi-Fi while overcoming their individual shortcomings. Through analytical modeling, algorithmic design, and experimental validation, the thesis provides a unified framework that spans MAC-layer enhancement, physical modeling, hybrid integration, and mobility-aware resource management.

10.1 Summary of Contributions

The main contributions of this dissertation can be summarized as follows:

- The initial part of the research established the foundation for hybrid networking by identifying critical limitations in conventional RF-based systems and highlighting Li-Fi as a complementary technology capable of providing vast unlicensed bandwidth, enhanced security, and energy-efficient operation. To improve medium access in Li-Fi environments, a hybrid CSMA/CA–HCCA-based MAC protocol was developed that dynamically adapts access mechanisms based on traffic and network load. This protocol

significantly improved throughput, reduced collisions, and minimized latency under heterogeneous traffic scenarios, thereby enhancing the efficiency of Li-Fi uplinks.

- A major contribution of this work lies in the analytical modeling of Li-Fi channel behavior under practical deployment conditions. Two realistic models were introduced: the Fixed Obstruction Model (FixOM) for static obstacles and the Shadowing-Aware Model (SAM) for dynamic and partial blockage conditions. These models accurately capture the effects of human movement, furniture, and environmental dynamics on Li-Fi performance, forming a critical basis for system-level optimization and deployment planning. Furthermore, to address the impact of user device orientation and movement, an orientation-aware multi-AP Li-Fi framework (OAM-LiFiNet) was developed. By leveraging real-time SINR feedback and adaptive AP association, this framework ensured stable connectivity and improved data throughput even under frequent user motion.

- The dissertation further introduced and experimentally validated a hybrid Li-Fi/Wi-Fi system architecture that seamlessly integrates both technologies. The prototype implementation demonstrated substantial gains in throughput, handover smoothness, and service continuity compared to standalone Li-Fi or Wi-Fi systems, thereby confirming the practical feasibility and benefits of hybrid integration. Complementing this, novel frameworks WiLiConnect and WiLiConnect-Opt were proposed to offload Wi-Fi CSI feedback through LiFi links. This approach effectively reduced CSI overhead, improved spectral efficiency, and enhanced MU-MIMO Wi-Fi performance in dense indoor environments.

- Another key contribution of this research is the development of advanced link aggregation algorithms for hybrid networks. The proposed Flow-based Algorithm for Data Allocation (FLADA) formulated the rate allocation problem as a linear programming model, incorporating fairness and backhaul constraints to balance load across Li-Fi and Wi-Fi links. FLADA achieved near-optimal data allocation performance, maintaining fairness while minimizing access point overload. Building upon this, two mobility-aware

probabilistic algorithms MAPS-LP (using linear programming) and MAPS-GP (a greedy variant) were introduced to address the dynamic nature of user mobility. These algorithms employed selective pruning strategies to efficiently handle AP re-association and rate allocation, significantly improving throughput, fairness, and handover efficiency under user mobility without incurring high computational overhead.

- Overall, the research outcomes demonstrate that hybrid Li-Fi/Wi-Fi networks can effectively combine the complementary strengths of both technologies to deliver high-capacity, reliable, and adaptive indoor connectivity. The analytical and simulation models (FixOM, SAM, and OAM-LiFiNet) provide realistic tools for performance prediction, while the algorithmic frameworks (FLADA, MAPS-LP, and MAPS-GP) offer scalable and fairness-aware solutions for dynamic resource management. Experimental validations through simulations further confirm the feasibility and efficiency of the proposed approaches, achieving significant gains in throughput, fairness, and service continuity compared to conventional methods.

- The key findings of this dissertation can be summarized as follows. The hybrid frameworks effectively harness the unique advantages of Li-Fi and Wi-Fi, delivering enhanced network capacity and stability. The FLADA algorithm achieves near-optimal data allocation while maintaining fairness and minimizing backhaul congestion. The MAPS-LP and MAPS-GP algorithms enable scalable, mobility-aware resource allocation that reduces unnecessary handovers and improves user satisfaction. Experimental evaluations confirm the theoretical insights, demonstrating consistent performance improvements under realistic scenarios. Finally, the developed analytical and algorithmic foundations serve as a valuable platform for future research and deployment of next-generation hybrid wireless networks.

Collectively, these dissertation presents a holistic approach to designing and optimizing HLWNs from fundamental channel modeling and MAC enhancements to system-level hybrid integration and mobility-driven optimization.

Research Impact and Significance: The outcomes of this research contribute significantly to the advancement of next-generation indoor wireless communication systems. By addressing key challenges such as MAC-layer inefficiencies, blockage and shadowing effects, user mobility, and heterogeneous network integration, this work provides a comprehensive framework for designing robust and high-capacity hybrid Li-Fi/Wi-Fi networks.

From a theoretical perspective, the proposed models and optimization frameworks offer new insights into multi-layer system design, resource allocation, and mobility-aware communication. From a practical standpoint, the integration of Li-Fi and Wi-Fi technologies enables efficient utilization of the unlicensed optical spectrum while maintaining the reliability and coverage of RF systems. These contributions are particularly relevant for emerging applications such as smart homes, offices, AR/VR environments, and IoT-driven indoor networks, where high data rates, low latency, and seamless connectivity are essential.

Overall, this research bridges the gap between theoretical modeling and practical deployment, paving the way for scalable, efficient, and reliable indoor wireless communication systems in future 6G and beyond networks.

10.2 Future Research Directions

Building upon the foundations established in this dissertation, several promising research directions can be pursued:

10.2.1 AI/ML for Hybrid Networks

Future extensions could leverage **artificial intelligence (AI)** and **machine learning (ML)** methods, such as deep reinforcement learning, to enable self-learning resource allocation and

predictive handover control. These methods can dynamically adapt to non-stationary user behavior, varying traffic demands, and environmental dynamics without explicit mathematical modeling. Integrating federated or edge learning paradigms could further enhance scalability, privacy, and distributed intelligence in large-scale deployments.

10.2.2 ISAC-based Hybrid Networks

The integration of **Integrated Sensing and Communication (ISAC)** technologies into HLWNs offers a new paradigm where Li-Fi and Wi-Fi can simultaneously sense and communicate. ISAC-based hybrid networks could predict user motion, detect human presence or blockage, and proactively adjust resource allocations. This direction will strengthen mobility prediction, network reliability, and energy efficiency in dense indoor environments.

10.2.3 OIRS-Assisted Hybrid Networks

One of the fundamental limitations of LiFi systems is their susceptibility to blockage, as the visible light signal cannot penetrate opaque obstacles. To address this challenge, a promising direction for future research is the integration of *Optical Intelligent Reflecting Surfaces (OIRS)* within hybrid Li-Fi/Wi-Fi networks. OIRS can dynamically control the reflection and redirection of optical signals to maintain LoS communication, thereby mitigating signal degradation due to blockages. The future work will focus on the design, modeling, and prototyping of OIRS-assisted HLWN architectures, enabling adaptive beam steering and improved link resilience. Such intelligent reflection mechanisms are expected to enhance coverage continuity and reliability, paving the way for robust and efficient HLWNs.

10.2.4 Real-Time Prototyping and Deployment

Future work should also focus on developing **real-time hardware testbeds** that integrate both Li-Fi and Wi-Fi access points equipped with adaptive controllers implementing FLADA

and MAPS algorithms. Such practical validation will enable quantitative assessment of delay, scalability, and end-user experience. This step is crucial for transitioning from simulation-driven research to deployable hybrid systems suitable for smart buildings, industrial automation, and beyond-5G wireless infrastructures.

In conclusion, this thesis presents a unified framework that advances the theoretical modeling and practical optimization of hybrid Li-Fi/Wi-Fi systems. By combining fairness-aware link aggregation, flow-based allocation, and mobility-aware optimization, the proposed methodologies provide a foundation for the development of intelligent, high-throughput, and reliable indoor wireless networks aligned with the vision of future 6G ecosystems.

Appendix A

Author's Publications

Patents

1. **Saswati Paramita**, Arani Bhattacharya, Anand Srivastava, Vivek Ashok Bohara. "Utilizing Li-Fi for sending channel feedback in a hybrid Wi-Fi/Li-Fi network". Indian Patent Application Number: 202311061031. **[Granted: Januay 20, 2026]**

2. Ankit Pal, Rahul, Saswati Paramita, Vivek Ashok Bohara, "AN OPTICAL INTELLIGENT REFLECTING SURFACE SYSTEM AND A METHOD THEREOF", (November 12, 2025), application Number: 202511089632, Indian Patent.

Journals (Published)

1. **S. Paramita**, A. Rawat, M. Daderwal and V. A. Bohara, "FixOM-SAM: Blockage Analysis in Indoor Li-Fi Networks," in IEEE Open Journal of the Communications Society, vol. 6, pp. 5746-5758, 2025, doi: 10.1109/OJCOMS.2025.3585614.

2. **S. Paramita**, A. Bhattacharya, R. Ahmad, V. A. Bohara and A. Srivastava, "Flow-Based Rate Maximization for Link Aggregation Enabled Hybrid LiFi-WiFi Network," in IEEE Transactions on Vehicular Technology, vol. 74, no. 2, pp. 3269-3282, Feb. 2025, doi: 10.1109/TVT.2024.3477310.

3. **Saswati Paramita**, Arani Bhattacharya, Anand Srivastava, Vivek Ashok Bohara, Hybrid CSMA/CA and HCCA uplink medium access control protocol for VLC based heterogeneous users, Computer Communications, Volume 225, 2024, Pages 54-64, ISSN 0140-3664, https://doi.org/10.1016/j.comcom.2024.06.017.

4. **S. Paramita**, V. A. Bohara, A. Bhattacharya and A. Srivastava, "Outage Probability Analysis for Link Aggregation-Enabled Hybrid LiFi-WiFi Network," in IEEE Communications Letters, doi: 10.1109/LCOMM.2026.3674993.

5. **S. Paramita**, A. Rawat and V. A. Bohara, "Adaptive Link Selection and Handover in Orientation-Aware Hybrid Li-Fi/Wi-Fi Networks," in IEEE Networking Letters, doi: 10.1109/LNET.2026.3670370.

Journals (Under Submission)

1. Saswati Paramita, A. Bhattacharya, V. A. Bohara, A. Srivastava, “Optimizing CSI Overhead in Hybrid WiFi/LiFi Networks Using LiFi-Assisted Feedback", Journal of Optical Communications and Networking (JOCN).

2. Saswati Paramita, R.Mondal, A. Bhattacharya, V. A. Bohara, A. Srivastava, “Optimizing Handover and Throughput in Heterogeneous LiFi-WiFi Network with User Mobility", IEEE Transactions on Mobile Computing.

Conferences: (Published)

1. **S. Paramita**, Y Garg, Vivek A Bohara, “Learning-Enabled Throughput–Handover Trade-Offs in Hybrid LiFi/WiFi Networks," 2025 IEEE International Conference on Advanced Networks and Telecommunications Systems (ANTS), Delhi, India, 2025, pp. 1-6, doi: 10.1109/ANTS66931.2025.11429769.

2. **S. Paramita** ,etal. “OAM-LiFiNet: Orientation Aware Multi-AP Li-Fi Network with user mobility”,2025 IEEE Future Networks World Forum (FNWF), Bangalore, India, 2025, pp. 1-6, doi: 10.1109/FNWF66845.2025.11317169.

3. **S. Paramita**, etal., "A Practical Demo of Mirror-Assisted NLOS Li-Fi for Overcoming LoS Limitations", 2026 18th International Conference on COMmunication Systems and NETworks (COMSNETS), Bengaluru, India, 2026, pp. 1282-1284, doi: 10.1109/COMSNETS67989.2026.11418169.

4. **S. Paramita**, R. Mondal, A. Bhattacharya, V. A. Bohara and A. Srivastava, “MARM-HyLiWi: Mobility-Aware Rate Maximization in Link Aggregation Enabled Hybrid Li-Fi/Wi-Fi Networks," 2025 17th International Conference on COMmunication Systems and NETworks (COMSNETS), Bengaluru, India, 2025, pp. 891-894, doi: 10.1109/COMSNETS63942.2025.10885587.

5. **S. Paramita**, A. Bhattacharya, V. A. Bohara and A. Srivastava, “WiLiConnect: A Novel CSI Sharing Technique in Hybrid WiFi/LiFi Networks," 2024 IEEE 99th Vehicular Technology Conference (VTC2024-Spring), Singapore, Singapore, 2024, pp. 1-5, doi: 10.1109/VTC2024-Spring62846.2024.10683067.

6. **S. Paramita**, A. Bhattacharya, A. Srivastava, V. A. Bohara, K. Joshi and D. Solanki, “Usage of P2P Li-Fi Transceivers for Establishing Backhaul Connectivity," 2024 16th International Conference on COMmunication Systems & NETworkS (COMSNETS), Bengaluru, India, 2024, pp. 333-335, doi: 10.1109/COMSNETS59351.2024.10427237.

7. **S. Paramita** et al., “A Proof-of-Concept Demonstration of Hybrid Li-Fi/Wi-Fi Network on a Prototype Testbed," 2023 IEEE International Conference on Advanced Networks and Telecommunications Systems (ANTS), Jaipur, India, 2023, pp. 509-514, doi: 10.1109/ANTS59832.2023.10468742.

8. **S. Paramita** et al., “Demo of Hybrid LiFi/WiFi Network for an Indoor Environment," 2023 15th International Conference on COMmunication Systems & NETworkS (COMSNETS), Bangalore, India, 2023, pp. 213-215, doi:10.1109/COMSNETS56262.2023.10041414.

9. N. M. Karoti, S. Paramita, R. Ahmad, V. A. Bohara and A. Srivastava, “Improving the performance of Heterogeneous LiFi-WiFi network using a novel Link Aggregation Framework," 2022 IEEE Wireless Communications and Networking Conference (WCNC), Austin, TX, USA, 2022, pp. 2322-2327, doi: 10.1109/WCNC51071.2022.9771553.

Conferences: (Under Submission)

1. **S. Paramita**, V. A. Bohara, Peter Han Joo Chong, “ISAC-Enabled Hybrid LiFi/WiFi Networks for Localization-Aware AP Association", 2026 IEEE 37th International Symposium on Personal, Indoor and Mobile Radio Communications (PIMRC).

References

[1] S. Paramita, A. Bhattacharya, A. Srivastava, and V. A. Bohara, "Hybrid CSMA/CA and HCCA uplink medium access control protocol for VLC based heterogeneous users," *Computer Communications*, vol. 225, pp. 54–64, 2024.

[2] S. Paramita, A. Rawat, and V. A. Bohara, "Oam-lifinet: Orientation aware multi-ap li-fi network with user mobility," in *2025 IEEE Future Networks World Forum (FNWF)*, 2025, pp. 1–6.

[3] S. Paramita, A. Rawat, M. Daderwal, and V. A. Bohara, "FixOM-SAM: Blockage analysis in indoor Li-Fi networks," *IEEE Open Journal of the Communications Society*, vol. 6, pp. 5746–5758, 2025.

[4] S. Paramita *et al.*, "A proof-of-concept demonstration of Hybrid Li-Fi/Wi-Fi Network on a prototype testbed," in *2023 IEEE International Conference on Advanced Networks and Telecommunications Systems (ANTS)*, 2023, pp. 509–514.

[5] S. Paramita and et al., "Demo of Hybrid LiFi/WiFi Network for an indoor environment," in *2023 15th International Conference on Communication Systems & Networks (COMSNETS)*, 2023, pp. 213–215.

[6] S. Paramita, A. Bhattacharya, V. A. Bohara, and A. Srivastava, "Wiliconnect: A novel CSI sharing technique in Hybrid WiFi/LiFi Networks," in *2024 IEEE 99th Vehicular Technology Conference (VTC2024-Spring)*, 2024, pp. 1–5.

[7] S. Paramita, A. Bhattacharya, V. A. Bohara, and A. Srivastava., "Optimizing CSI overhead in Hybrid WiFi/LiFi networks using LiFi-assisted feedback," *Journal of Optical Communications and Networking (JOCN)*, 2025, (Submitted).

[8] N. M. Karoti, S. Paramita, R. Ahmad, V. A. Bohara, and A. Srivastava, "Improving the performance of Heterogeneous LiFi-WiFi network using a novel link aggregation framework," in *2022 IEEE Wireless Communications and Networking Conference (WCNC)*, 2022, pp. 2322–2327.

[9] S. Paramita, A. Bhattacharya, R. Ahmad, V. A. Bohara, and A. Srivastava, "Flow-based rate maximization for link aggregation enabled Hybrid LiFi-WiFi Network," *IEEE Transactions on Vehicular Technology*, vol. 74, no. 2, pp. 3269–3282, Feb. 2025.

[10] S. Paramita, R. Mondal, A. Bhattacharya, V. A. Bohara, and A. Srivastava, "Optimizing handover and throughput in Heterogeneous LiFi-WiFi Network with user mobility," *IEEE Transactions on Mobile Computing*, 2025, (Submitted).

[11] S. Paramita, V. A. Bohara, A. Bhattacharya, and A. Srivastava, "Outage probability analysis for link aggregation-enabled hybrid lifi-wifi network," *IEEE Communications Letters*, vol. 30, pp. 1588–1591, 2026.

[12] S. Paramita, A. Rawat, and V. A. Bohara, "Adaptive link selection and handover in orientation-aware hybrid li-fi/wi-fi networks," *IEEE Networking Letters*, pp. 1–1, 2026.

[13] Y. Wang, D. A. Basnayaka, X. Wu, and H. Haas, "Optimization of load balancing in hybrid LiFi/RF networks," *IEEE Transactions on Communications*, vol. 65, no. 4, pp. 1708–1720, 2017.

[14] X. Wu, M. Safari, and H. Haas, "Access point selection for hybrid Li-Fi and Wi-Fi networks," *IEEE Transactions on Communications*, vol. 65, no. 12, pp. 5375–5385, 2017.

[15] H. Yu and T. Kim, "Beamforming transmission in IEEE 802.11 ac under time-varying channels," *the scientific world journal*, vol. 2014, 2014.

[16] P. Jeevitha, R. Anitha, and S. Janakiraman, "Exploitation of spectrum white spaces and traffic congestion: Spectrum efficiency in cognitive radio networks," *Wireless Personal Communications*, 2025.

[17] M. Abdolkhani, O. Abbasi, H. Khodakarami, and C. Nour, "Deep reinforcement learning for eh-enabled Cognitive-IoT under jamming attacks," *IEEE Internet of Things Journal*, vol. 11, no. 19, pp. 30 988–30 999, 2024.

[18] Z. Liang, X. Wang, L. Liu, and Y. Zhao, "An extended kalman filtering based secure transmission scheme for IRS-Aided SWIPT networks," *Journal of Electronics & Information Technology*, vol. 47, no. 2, pp. 533–541, 2025.

[19] N. Ahuja, "Design and reliable framework for mobile Adhoc network," Ph.D. dissertation, Shodhganga: INFLIBNET Centre, 2024. [Online]. Available: http://shodhganga.inflibnet.ac.in/handle/10603/623389

[20] M. Prasad, M. Jayaram *et al.*, "Multimedia data transmission in underwater wireless sensor network," in *Proceedings of the Conference on Recent Advances in Communication*. IEEE, 2024.

[21] R. Kashif, *Hybrid Communication Systems for Future 6G and Beyond: Visible Light Communication & Radio Over Fiber Technology*. Springer, 2024.

[22] K. Gupta, R. Kumar *et al.*, "A vision towards optical wireless communication for 6g," *IEEE Access*, vol. 11, pp. 121 560–121 577, 2023.

[23] T. Komine and M. Nakagawa, "Fundamental analysis for visible-light communication system using LED lights," *IEEE Transactions on Consumer Electronics*, vol. 50, no. 1, pp. 100–107, 2004.

[24] P. H. Pathak, X. Feng, P. Hu, and P. Mohapatra, "Visible light communication, networking, and sensing: A survey, potential and challenges," *IEEE Communications Surveys & Tutorials*, vol. 17, no. 4, pp. 2047–2077, 2015.

[25] F. Zafar, N. Khan *et al.*, "Survey on hybrid LiFi and WiFi networks: Key issues, challenges and future research directions," *Physical Communication*, vol. 50, p. 101559, 2022.

[26] X. Wu, M. D. Soltani, L. Zhou, M. Safari, and H. Haas, "Hybrid LiFi and WiFi networks: A survey," *IEEE Communications Surveys & Tutorials*, vol. 23, no. 2, pp. 1398–1420, 2021.

[27] H. Haas, L. Yin, C. Chen, S. Videv, D. Parol, E. Poves, H. Alshaer, and M. S. Islim, "Introduction to indoor networking concepts and challenges in LiFi," *Journal of Optical Communications and Networking*, vol. 12, no. 2, pp. A190–A203, 2020.

[28] P. Shams, M. Erol-Kantarci, and M. Uysal, "MAC layer performance of the IEEE 802.15. 7 visible light communication standard," *Transactions on Emerging Telecommunications Technologies*, vol. 27, no. 5, pp. 662–674, 2016.

[29] P. P. Játiva, C. A. Azurdia-Meza, I. Sánchez, F. Seguel, D. Zabala-Blanco, A. D. Firoozabadi, C. A. Gutiérrez, and I. Soto, "A VLC channel model for underground mining environments with scattering and shadowing," *IEEE Access*, vol. 8, pp. 185 445–185 464, 2020.

[30] T. Pal, A. Singh, V. A. Bohara, and A. Srivastava, "Impact of time-varying dynamic human blockages on indoor visible light communication system," *IEEE Transactions on Wireless Communications*, vol. 23, no. 9, pp. 10 562–10 574, 2024.

[31] M. D. Soltani, A. A. Purwita, I. Tavakkolnia, H. Haas, and M. Safari, "Impact of device orientation on error performance of LiFi systems," *IEEE Access*, vol. 7, pp. 41 690–41 701, 2019.

[32] M. D. Soltani, Z. Zeng, I. Tavakkolnia, H. Haas, and M. Safari, "Random receiver orientation effect on channel gain in LiFi systems," in *2019 IEEE Wireless Communications and Networking Conference (WCNC)*, 2019, pp. 1–6.

[33] X. Wu and H. Haas, "Mobility-aware load balancing for hybrid LiFi and WiFi networks," *Journal of Optical Communications and Networking*, vol. 11, no. 12, pp. 588–597, 2019.

[34] X. Rao and V. K. N. Lau, "Minimization of CSI feedback dimension for interference alignment in MIMO interference multicast networks," *IEEE Transactions on Information Theory*, vol. 61, no. 3, pp. 1218–1246, 2015.

[35] J. Guo, C.-K. Wen, and S. Jin, "Eliminating CSI feedback overhead via deep learning-based data hiding," *IEEE Journal on Selected Areas in Communications*, vol. 40, no. 8, pp. 2267–2281, 2022.

[36] A. Zubow, P. Gawłowicz, K. L. Bober, V. Jungnickel, K. Habel, and F. Dressler, "Hy-Fi: Aggregation of LiFi and WiFi using MIMO in IEEE 802.11," in *2021 IEEE 22nd International Symposium on a World of Wireless, Mobile and Multimedia Networks (WoWMoM)*, 2021.

[37] S. Paramita, R. Mondal, A. Bhattacharya, V. A. Bohara, and A. Srivastava, "MARM-HyLiWi: Mobility-aware rate maximization in link aggregation enabled Hybrid Li-Fi/Wi-Fi Networks," in *2025 17th International Conference on Communication Systems and Networks (COMSNETS)*, 2025, pp. 891–894.

[38] H. Haas, L. Yin, Y. Wang, and C. Chen, "What is lifi?" *Journal of Lightwave Technology*, vol. 34, no. 6, pp. 1533–1544, 2016.

[39] J. Armstrong, "OFDM for optical communications," *Journal of Lightwave Technology*, vol. 27, no. 3, pp. 189–204, 2009.

[40] Z. Ghassemlooy, W. Popoola, and S. Rajbhandari, *Optical Wireless Communications: System and Channel Modelling with MATLAB®*, 2nd ed. Boca Raton, FL, USA: CRC Press, 2017.

[41] M. D. Soltani, X. Wu, M. Safari, and H. Haas, "Bidirectional user throughput maximization based on feedback reduction in LiFi networks," *IEEE Transactions on Communications*, vol. 66, no. 7, pp. 3172–3186, 2018.

[42] Z. Nan and X. Chi, "Research on an uplink carrier sense multiple access algorithm of large indoor visible light communication networks based on an optical hard core point process," *Applied optics*, vol. 55, no. 36, pp. 10 392–10 399, 2016.

[43] M. A. Arfaoui, M. D. Soltani, I. Tavakkolnia, A. Ghrayeb, C. M. Assi, M. Safari, and H. Haas, "Measurements-based channel models for indoor LiFi systems," *IEEE Transactions on Wireless Communications*, vol. 20, no. 2, pp. 827–842, 2021.

[44] A. A. Purwita, M. D. Soltani, M. Safari, and H. Haas, "Terminal orientation in OFDM-Based LiFi systems," *IEEE Transactions on Wireless Communications*, vol. 18, no. 8, pp. 4003–4016, 2019.

[45] T. Nguyen, A. Yesilkaya, C. Chen, and H. Haas, "A novel mobile multi-user lifi system," in *ICC 2022 - IEEE International Conference on Communications*, 2022, pp. 589–594.

[46] X. Wu, "Performance analysis of visible light communications with channel blockage caused by human bodies," in *ICC 2023 - IEEE International Conference on Communications*, 2023, pp. 6541–6545.

[47] N. A. Amran, M. D. Soltani, and M. Safari, "Link blockage analysis for indoor optical wireless communications," in *GLOBECOM 2023 - 2023 IEEE Global Communications Conference*, 2023, pp. 5568–5573.

[48] A. Singh, H. B. Salameh, M. Ayyash, and H. Elgala, "Performance analysis of oirs-aided indoor VLC systems under dynamic human blockages and random UE orientation," *IEEE Internet of Things Journal*, vol. 11, no. 20, pp. 33 110–33 119, 2024.

[49] X. Wu and H. Haas, "Access point assignment in hybrid lifi and wifi networks in consideration of lifi channel blockage," in *2017 IEEE 18th International Workshop on Signal Processing Advances in Wireless Communications (SPAWC)*, 2017, pp. 1–5.

[50] Y. Wang, X. Wu, and H. Haas, "Analysis of area data rate with shadowing effects in li-fi and rf hybrid network," in *2016 IEEE International Conference on Communications (ICC)*, 2016, pp. 1–5.

[51] X. Wu, C. Chen, and H. Haas, "Mobility management for hybrid lifi and wifi networks in the presence of light-path blockage," in *2018 IEEE 88th Vehicular Technology Conference (VTC-Fall)*, 2018, pp. 1–5.

[52] Y. Wang and H. Haas, "Dynamic load balancing with handover in hybrid Li-Fi and Wi-Fi networks," *Journal of Light-wave Technology*, vol. 33, no. 22, pp. 4671–4682, 2015.

[53] F. Jin, R. Zhang, and L. Hanzo, "Resource allocation under delay-guarantee constraints for heterogeneous visible-light and RF femtocell," *IEEE Transactions on Wireless Communications*, vol. 14, no. 2, 2014.

[54] X. Xie, X. Zhang, and K. Sundaresan, "Adaptive feedback compression for MIMO networks," in *Proceedings of the 19th annual international conference on Mobile computing & networking*, 2013, pp. 477–488.

[55] K.-H. Lee, "Using OFDMA for MU-MIMO user selection in 802.11 ax-based Wi-Fi networks," *IEEE Access*, vol. 7, 2019.

[56] X. Xie and X. Zhang, "Scalable user selection for MU-MIMO networks," in *IEEE INFOCOM 2014-IEEE Conference on Computer Communications*. IEEE, 2014, pp. 808–816.

[57] C. Wen, W. Shih, and S. Jin, "Deep learning for CSI feedback in massive MIMO systems," *IEEE Wireless Communications Letters*, vol. 7, no. 5, pp. 748–751, 2018.

[58] A. Anastasopoulos and A. Goldsmith, "Deepcmc: Deep learning-based joint compression of channel state information and data," *IEEE Trans. Wireless Communications*, 2020.

[59] Y. Li and H. Haas, "Hybrid RF/VLC CSI estimation and feedback for multi-user MIMO systems," in *IEEE Globecom*, 2022.

[60] X. Li, R. Zhang, and L. Hanzo, "Cooperative load balancing in hybrid visible light communications and WiFi," *IEEE Transactions on Communications*, vol. 63, no. 4, pp. 1319–1329, 2015.

[61] M. Kashef, M. Ismail, M. Abdallah, K. A. Qaraqe, and E. Serpedin, "Energy efficient resource allocation for mixed RF/VLC heterogeneous wireless networks," *IEEE Journal on Selected Areas in Communications*, vol. 34, no. 4, pp. 883–893, 2016.

[62] M. Ayyash, H. Elgala, A. Khreishah, V. Jungnickel, T. Little, S. Shao, M. Rahaim, D. Schulz, J. Hilt, and R. Freund, "Coexistence of WiFi and LiFi toward 5G: concepts, opportunities, and challenges," *IEEE Communications Magazine*, vol. 54, no. 2, pp. 64–71, 2016.

[63] W. Zhang, L. Chen, X. Chen, Z. Yu, Z. Li, and W. Wang, "Design and realization of indoor VLC-Wi-Fi hybrid network," *Journal of Communications and Information Networks*, vol. 2, no. 4, pp. 75–87, 2017.

[64] A. Zubow, P. Gawowicz, C. Brunn, K. L. Bober, V. Jungnickel, K. Habel, and F. Dressler, "Hybrid-Fidelity: Utilizing IEEE 802.11 MIMO for practical aggregation of LiFi and WiFi," *IEEE Transactions on Mobile Computing*, pp. 1–1, 2022.

[65] S. Shao, A. Khreishah, M. Ayyash, M. B. Rahaim, H. Elgala, V. Jungnickel, D. Schulz, T. D. Little, J. Hilt, and R. Freund, "Design and analysis of a visible-light-communication enhanced WiFi system," *Journal of Optical Communications and Networking*, vol. 7, no. 10, pp. 960–973, 2015.

[66] Y. S. M. Pratama and K. W. Choi, "Bandwidth aggregation protocol and throughput-optimal scheduler for hybrid RF and visible light communication systems," *IEEE Access*, vol. 6, pp. 32 173–32 187, 2018.

[67] A. Zubow, P. Gawłowicz, K. L. Bober, V. Jungnickel, K. Habel, and F. Dressler, "Hy-Fi: Aggregation of LiFi and WiFi using MIMO in IEEE 802.11," in *22nd International Symposium on a World of Wireless, Mobile and Multimedia Networks (WoWMoM)*, 2021, pp. 100–108.

[68] W. Wu, F. Zhou, and Q. Yang, "Adaptive network resource optimization for heterogeneous vlc/rf wireless networks," *IEEE Transactions on Communications*, vol. 66, no. 11, pp. 5568–5581, 2018.

[69] H. Yang, A. Alphones, W.-D. Zhong, C. Chen, and X. Xie, "Learning-based energy-efficient resource management by heterogeneous rf/vlc for ultra-reliable low-latency industrial iot networks," *IEEE Transactions on Industrial Informatics*, vol. 16, no. 8, pp. 5565–5576, 2020.

[70] J. Kong, Z.-Y. Wu, M. Ismail, E. Serpedin, and K. A. Qaraqe, "Q-learning based two-timescale power allocation for multi-homing hybrid rf/vlc networks," *IEEE Wireless Communications Letters*, vol. 9, no. 4, pp. 443–447, 2020.

[71] R. Ahmad, M. D. Soltani, M. Safari, and A. Srivastava, "Reinforcement learning-based near-optimal load balancing for heterogeneous LiFi WiFi network," *IEEE Systems Journal*, vol. 16, no. 2, pp. 3084–3095, 2022.

[72] J. Ghimire and C. Rosenberg, "Resource allocation, transmission coordination and user association in heterogeneous networks: A flow-based unified approach," *IEEE Transactions on Wireless Communications*, vol. 12, no. 3, pp. 1340–1351, 2013.

[73] F. Wang, W. Chen, H. Tang, and Q. Wu, "Joint optimization of user association, subchannel allocation, and power allocation in multi-cell multi-association OFDMA heterogeneous networks," *IEEE Transactions on Communications*, vol. 65, no. 6, pp. 2672–2684, 2017.

[74] Y. Chen, J. Li, W. Chen, Z. Lin, and B. Vucetic, "Joint user association and resource allocation in the downlink of heterogeneous networks," *IEEE Transactions on Vehicular Technology*, vol. 65, no. 7, pp. 5701–5706, 2016.

[75] S. Gopalam, S. V. Hanly, and P. Whiting, "Distributed user association and resource allocation algorithms for three tier HetNets," *IEEE Transactions on Wireless Communications*, vol. 19, no. 12, pp. 7913–7926, 2020.

[76] X. Ge, L. Pan, S. Tu, H.-H. Chen, and C.-X. Wang, "Wireless backhaul capacity of 5g ultra-dense cellular networks," in *IEEE 84th Vehicular Technology Conference (VTC-Fall)*, 2016, pp. 1–6.

[77] H. Vijayaraghavan and W. Kellerer, "Mobifi: Mobility-aware reactive and proactive wireless resource management in lifi-wifi networks," *IEEE Transactions on Network and Service Management*, vol. 21, no. 6, pp. 6597–6613, 2024.

[78] G. Bianchi, "Performance analysis of the IEEE 802.11 distributed coordination function," *IEEE Journal on Selected Areas in Communications*, vol. 18, no. 3, pp. 535–547, 2000.

[79] M. D. Soltani, M. Safari, and H. Haas, "Analysis of random orientation and user mobility in LiFi networks," Ph.D. dissertation.

[80] M. A. Al-Maqri, M. Othman, B. M. Ali, and Z. M. Hanapi, "Adaptive multi-polling scheduler for QoS support of video transmission in IEEE 802.11 e wlans," *Telecommunication systems*, vol. 61, no. 4, pp. 773–791, 2016.

[81] Y.-S. Chen, Y.-W. Lee, and J. H. Park, "Enhanced HCCA mechanism for multimedia traffics with QoS support in IEEE 802.11 e networks," *Journal of Network and Computer Applications*, vol. 34, no. 5, pp. 1566–1571, 2011.

[82] E. W. Weisstein, "Point-line distance," https://mathworld.wolfram.com/Point-LineDistance2-Dimensional.html, accessed: 2026.

[83] Z. Ghassemlooy, W. Popoola, and S. Rajbhandari, *Optical Wireless Communications: System and Channel Modelling with MATLAB*. CRC Press, 2015.

[84] H. Haas, "Visible light communication: Tutorial," 2015, pp. 1–72.

[85] G. M. Insights, "Li-Fi market size by component."

[86] R. Ahmad, M. D. Soltani, M. Safari, and A. Srivastava, "Load balancing of hybrid LiFi WiFi networks using reinforcement learning," in *2020 IEEE 31st Annual International Symposium on Personal, Indoor and Mobile Radio Communications*. IEEE, 2020, pp. 1–6.

[87] D. A. Basnayaka and H. Haas, "Hybrid rf and vlc systems: Improving user data rate performance of vlc systems," in *2015 IEEE 81st vehicular technology conference (VTC Spring)*. IEEE, 2015, pp. 1–5.

[88] W. Zhang, L. Chen, X. Chen, Z. Yu, Z. Li, and W. Wang, "Design and realization of indoor VLC-Wi-Fi hybrid network," *Journal of Communications and Information Networks*, vol. 2, no. 4, 2017.

[89] S. Paramita, A. Bhattacharya, R. Ahmad, V. A. Bohara, and A. Srivastava, "Flow-based rate maximization for link aggregation enabled Hybrid LiFi-WiFi Network," *IEEE Transactions on Vehicular Technology*, pp. 1–13, 2024.

[90] SeedScientific, "How much data is created every day? +27 staggering stats," https://seedscientific.com/how-much-data-is-created-every-day/.

[91] T. C. Models, "Ieee standard 802.11-03/940r4," *IEEE P802*, vol. 11, 2004.

[92] X. Wu, M. D. Soltani, L. Zhou, M. Safari, and H. Haas, "Hybrid LiFi and WiFi networks: A survey," *IEEE Communications Surveys and Tutorials*, vol. 23, no. 2, pp. 1398–1420, 2021.

[93] Y. Daldoul, D.-E. Meddour, and A. Ksentini, "Performance evaluation of OFDMA and MU-MIMO in 802.11ax networks," *Computer Networks*, vol. 182, p. 107477, 2020.

[94] S. Paramita, A. Rawat, and M. Daderwal, "FixOM-SAM: Blockage analysis in indoor Li-Fi networks," *IEEE Open Journal of the Communications Society*, 2025.

[95] M. R. Garey and D. S. Johnson, *Computers and intractability*. freeman San Francisco, 1979, vol. 174.

[96] H. Haas, L. Yin, C. Chen, S. Videv, D. Parol, E. Poves, H. Alshaer, and M. S. Islim, "Introduction to indoor networking concepts and challenges in LiFi," *J. Opt. Commun. Netw.*, vol. 12, no. 2, Feb 2020.

[97] C. Zeng and S. Licardie, "Systems and methods for performing layer one link aggregation over wireless links," Sep. 1 2015, uS Patent 9,125,084.

[98] C. Cheng, "A approximation algorithm to solve the maximum multicommodity flow problem with local dominant," in *3rd International Conference on Electronic Information Technology and Computer Engineering (EITCE)*, 2019, pp. 988–992.

[99] A. F. Zantuti, "Linear capacity algorithms for multicommodity flow problems in computer wan," in *25th International Conference on Systems Engineering (ICSEng)*, 2017, pp. 263–267.

[100] A. Moitra, "Approximation algorithms for multicommodity-type problems with guarantees independent of the graph size," in *50th Annual IEEE Symposium on Foundations of Computer Science*, 2009, pp. 3–12.

[101] M. R. Garey and D. S. Johnson, *Computers and Intractability: A Guide to the Theory of NP-Completeness (Series of Books in the Mathematical Sciences)*. W. H. Freeman, 1979.

[102] F. T. Al Rabee, A. Al-Rimawi, and R. D. Gitlin, "Channel capacity in a dynamic random waypoint mobility model," in *2018 9th IEEE Annual Ubiquitous Computing, Electronics & Mobile Communication Conference (UEMCON)*, 2018, pp. 711–715.

[103] T. Tang, L. Shi, and Q. Li, "Mobility analysis of visible light communications with orientation-based random waypoint model," in *2024 5th Information Communication Technologies Conference (ICTC)*, 2024, pp. 194–198.